CRYSTAL STRUCTURE AND MAGNETIC PROPERTIES OF GEOMETRICALLY FRUSTRATED FACE CENTERED CUBIC (f.c.c.) DOUBLE PEROVSKITES,

La_2LiMO_6 and Ba_2YMO_6 (M= Mo, Re and Ru)

CRYSTAL STRUCTURE AND MAGNETIC PROPERTIES OF GEOMETRICALLY FRUSTRATED FACE CENTERED CUBIC (f.c.c.) DOUBLE PEROVSKITES,

La_2LiMO_6 and Ba_2YMO_6 (M= Mo, Re and Ru)

BY

TOMOKO AHAREN, B. Sc., M. Sc.

A Thesis

Submitted to the School of Graduate Studies

in Partial Fulfillment of the Requirements

for the Degree

Doctor of Philosophy

McMaster University

DOCTOR OH PHILOSOPHY (2010) McMaster University

(Chemistry) Hamilton, Ontario

TITLE: CRYSTAL STRUCTURE AND MAGNETIC PROPERTIES OF GEOMETRICALLY FRUSTRATED FACE CENTERED CUBIC (f.c.c.) DOUBLE PEROVSKITES,La_2LiMO_6 and Ba_2YMO_6 (M= Mo, Re and Ru)

AUTHOR: TOMOKO AHAREN. B. Sc., M. Sc., (Keio University)

SUPERVISOR: Doctor John E. Greedan

NUMBER OF PAGES: xv,180

Abstract

This thesis reports a systematic study of geometrically frustrated f.c.c. double perovskites with both monoclinic ($P2_1/n$) La_2LiMO_6 and cubic (Fm3m) Ba_2YMO_6 symmetries, where M=Mo (S=1/2), Re (S=1) and Ru (S=3/2). The roles of both the spin quantum number, i.e. quantum spin fluctuations, and the local site symmetry, i.e. orbital ordering, on the determination of the ground magnetic state were studied. All the compounds were prepared by solid state reaction and the structural information and magnetic properties of the compounds were collected using diffraction techniques (X-ray and neutron), dc susceptibility, heat capacity, muon spin relaxation (μSR) and solid state NMR.

The S=3/2 materials, La_2LiRuO_6 and Ba_2YRuO_6, while highly frustrated with frustration indices f ~ 16 and 8, respectively, both show antiferromagnetic (AF) long range ordering at 24K and 37K, respectively. The Neel temperature of the latter compound was determined for the first time by the heat capacity and neutron diffraction. This compound shows an unusual AF transition as two broader peaks were observed in the susceptibility while La_2LiRuO_6 shows a typical AF behavior. There is about 1% of Y/Ru site mixing observed by ^{89}Y MAS NMR in Ba_2YRuO_6.

For the S=1 materials, monoclinic La_2LiReO_6 shows collective singlet like behavior as zero magnetization was observed in the ZFC susceptibility and a static and diluted spin system was indicated by μSR. On the other hand, the cubic phase, Ba_2YReO_6 surprisingly shows a spin glass behavior confirmed by μSR while no Y/Re site mixing was observed by MAS NMR. It is also a surprising observation that this compound retains cubic symmetry down to 3K where it would have a structure transition subject to the Jahn-Teller theorem.

Finally, the S=1/2 compounds, La_2LiMoO_6 and Ba_2YMoO_6, show quite different magnetic behavior. Monoclinic La_2LiMoO_6 shows the presence of at least short range order achieved at 18K according to the heat capacity and μSR measurements. Ba_2YMoO_6 retains cubic symmetry down to 3K and no Jahn-Teller distortion was observed at the limit of the resolution of neutron diffraction. This compound surprisingly appears to remain paramagnetic down to 2K, yet evidence for a collective singlet state was observed by a paramagnetic Knight shift measurement in NMR. This is consistent with an existing theoretical prediction.

An extended study on other S=1/2 Mo analogues, Ba_2LuMoO_6 and Ba_2ScMoO_6 is also presented. Both compounds show cubic structure confirmed by X-ray diffraction and paramagnetic behavior down to 2K in the susceptibility.

Acknowledgement

I would like to thank to my supervisor, Dr. Greedan to give me opportunities to do researches here at McMaster. It was very nice to have a lot of chances to explore in magnetism of compounds with various techniques. His knowledge and insight into subjects inspires me and encouraged to pursue profound studies. I really appreciate that he also gave me a friendly and helpful working environment since the transition from industry to academia was not easy. I also appreciate my committee members, Dr. Gillian Goward and Dr. Bruce Gaulin for their supports for my Ph.D. study. I am grateful to BIMR staffs, Dr. Paul Dube, Mr. Jim Garret and Mr. Frank Gibbs for their assistance for material preparation and characterization. To Greedan's past and present members, Heather, Athena, Diego, Tetsu, Craig, Shahab, Jonathan, Farshid, Andrew, and Dr. Mozharivskij's group, Volodia, Peng, Janice, Scott and Jinlei, I have big thanks for very cheerful and supportive environment we have. To Dr. Luke and his group members, Adam, Jose, Greg, thanks for everything on μSR. I would not have had wonderful experience without you in TRIUMF. I would like to thank to Dr. Imai and Fanlong for the NMR measurements and useful suggestions. Much appreciation goes to Dr. Gaulin's students, Jacob, Pat and Sarah for their useful discussion. To Dr. Hanna Dabkowska and Dr. Antoni Dabkowski, I have millions of thanks to you for not only research aspects but also family-like support to stay better in Hamilton.

My friends at McMaster and chemistry department, I cannot count up one by one now since I got a lot of friendships here and I special thanks to all of you. I am very happy to have kind and helpful friends here and this makes my McMaster life much better!

Soko and Rastko, your friendships and supports are precious.

Faraz, I am thankful to you for so many interesting/fun times we have shared and your friendship. You always inspire me for something, which I really like and valuable. I can say that the life without your friendship would be much less wonderful. Çok teşekkűr ederim!

Last but not the least, I have special thanks to my family to help and support me always, anytime, anywhere. It was a surprising for you that I decided to study abroad. Having your support always cheers me up in any situation and I would not be able to complete this study without you.

Table of Contents

List of Figures

List of Tables

Chapter One

Introduction

Outline of this thesis

Transition metal oxides are widely known for their applications in electronics such as ferroelectric $BaTiO_3$[1] and $LiCoO_2$ in Li-ion batteries [2], and potentialities for new technologies and their applications to daily life. Focusing on the fundamental research on transition metal oxides has been essential to seek further capability to invent useful devices or concepts for further creation and innovation.

Among fundamental researches, geometrically frustrated materials have attracted great interest in condensed matter science due to their unusual/unexpected behaviours originating in quantum phenomena. Geometrically frustrated materials usually possess triangles as a motif of the magnetic ion arrangement. B-site ordered double perovskite (face centered cubic symmetry) possesses one version of a three-dimensional framework of a frustrated geometry. Although this structure type allows a great versatility for chemical substitution, which enables researchers to conduct systematic studies, B-site ordered double perovskite compounds, $A_2BB'O_6$, have not attracted much attention intensively compared to other geometrically frustrated compounds such as the Pyrochlore titanates $Tb_2Ti_2O_7$ [3] or $Dy_2Ti_2O_7$[4].

Thus a systematic study of face-center-cubic double perovskites, particularly a series of B site ordered double perovskite, $A_2BB'O_6$, where A=La or Ba, B=Li or Y and B= Mo, Re and Ru, was initiated to investigate the importance of quantum fluctuations on the determination of the magnetic ground states of f.c.c. frustrated materials. The crystal structure dependence of magnetic ground states was also included in this investigation. Appropriate magnetic ions of the 4d and 5d transition metal elements have been chosen depending on the target spin quantum number, S=3/2 to S=1/2.

The structure of this thesis is as follows; Chapter one will give an introduction to geometric frustration and face centered cubic double perovskites. In chapter two, the theories of the experimental techniques involved in this project are presented. From Chapter three to Chapter five, the systematic study (S=1/2 Mo^{5+} analogues, S=1 Re^{5+} analogues and S=3/2 Ru^{5+} analogues) of the magnetic ground state of B-site ordered double perovskites are presented, which have been accepted/published in Physical

Review B. In chapter six, the analogues of *S*=1/2 Mo compounds were synthesized and the results are presented, followed by a conclusion.

Basics of Magnetism

When a compound is placed in a magnetic field, generally the field within the compound is different from that without any field. The new field will be described as follows,

$$B = H + 4\pi I \qquad (1.1)$$

where B is a magnetic induction and H is the applied field and I is the induced magnetization.

The equation is converted into,

$$B/H = 1 + 4\pi(I/H) = 1 + 4\pi\kappa = 1 + 4\pi(\rho/\mathrm{M_w})\chi_{\mathrm{mol}} \quad (1.2)$$

where ρ is the density of a compound, $\mathrm{M_w}$ is the molar weight of the compound and χ_{mol} is a molar susceptibility of the compound.

Normally, the response of a compound to an applied field is observed as (1) attracted to the field (paramagnetism) or (2) repelled against the field (diamagnetism). This difference in the response originates in whether a compound contains unpaired electrons (paramagnet) or not (diamagnet). A phenomenon treated in this thesis, geometric magnetic frustration, which is introduced later in this chapter, is a subject of unpaired electrons and the influence of diamagnetism on the compounds involved in this thesis is negligible therefore only paramagnetism shall be introduced here.

Origin of Paramagnetism

As mentioned earlier, paramagnetism has its origin in the interaction of unpaired electrons (spins), of a compound with an applied field. Microscopically, it is also described as a thermally weighted sum of the magnetic moments from all accessible states in the applied field and the population of the spins in the resulting energy levels according to the Boltzmann distribution. Generally, a paramagnetic behaviour is described with the Van Vleck equation. E_i^0 is the energy of the level in absence of field, $E_i^{(1)}$ is the first order Zeeman coefficient of ith level and $E_i^{(2)}$ is the second order Zeeman coefficient of ith level[5].

$$\chi = \frac{N\sum_i\left(\frac{E_i^{(1)^2}}{kT} - 2E_i^{(2)}\right)\exp\left(-\frac{E_i^0}{kT}\right)}{\sum_i \exp\left(-\frac{E_i^0}{kT}\right)} \qquad (1.3)$$

When there is only one energy level in a zero field and this is degenerate, the equation above yields the Curie law and the Curie constant, C [5],

$$\chi = C/T \qquad (1.4)$$

When there is a singlet ground state and at least one degenerate excited state with energy >>kT, the equation yields [5]

$\chi = N\alpha$, T.I.P (temperature independent paramagnetism) (1.5)

When the ground state is degenerate and all excited states are >>kT above, the susceptibility is the sum of two cases shown earlier, then the yield is[5],

$$\chi = \frac{C}{T} + N\alpha \qquad (1.6)$$

In general, the Curie constant C is expressed as [6, 7],

$$C = \frac{Ng^2\beta^2J(J+1)}{3k} \qquad (1.7)$$

In this equation, g is Lande's g factor, β is Bohr magneton, J is the total angular momentum spin quantum number and k is Boltzmann constant.

The effective magnetic moment per atom μ_{eff} is defined as follows. L is the orbital angular momentum quantum number and S is spin angular momentum quantum number.

$$\mu_{eff} = [L(L+1) + 4S(S+1)]^{1/2} \qquad (1.8)$$

When spin-orbit coupling is included, the equation above is converted to that below with taking account for Lande's splitting factor g,

$$\mu_{eff} = g[J(J+1)]^{1/2} \qquad (1.9)$$

where,

$$g = \frac{3}{2} + \frac{S(S+1)-L(L+1)}{2J(J+1)} \qquad (1.10)$$

Therefore, it can be converted into the following term using the Curie constant, C,

$$\mu_{eff} = \left(\frac{3k}{N\beta^2}\right)^{1/2} C^{1/2} \approx \sqrt{8C} \qquad (1.11)$$

When orbital contribution is quenched, the effective magnetic moment (spin-only) ($g \approx 2$) is

$$\mu_{eff}\,(s.o.) = [4S(S+1)]^{1/2} \qquad (1.12)$$

The Curie constant of a compound is obtainable experimentally and is indicative of the interaction between spin and orbital angular momentum in the compound.

Magnetic ordering

There are special states of paramagnetism when spins in a compound fall into an ordered state. They are mainly ferromagnets and antiferromagnets. The temperature dependences of the susceptibility of these compounds show critical temperatures (Tc, for ferromagnets) or Neel temperatures (T_N, for antiferromagnets) therefore the modification of the Curie law was defined as the Curie-Weiss law,

$$\chi = \frac{C}{T-\theta} \qquad (1.13)$$

Below a critical temperature or a Neel temperature, a magnetic ordering occurs in these compounds. When spins align parallel, the compound is a ferromagnetic and if antiparallel, an antiferromagnetic. Experimentally both states are generally distinguishable by the Weiss constant, θ, which is calculated from the fitting of inverse susceptibility against temperature with the Curie-Weiss law. A ferromagnet yields a positive Weiss constant and an antiferromagnet yields a negative one. Then, the Hamiltonian of the interaction between any spins is expressed by using an exchange constant J and spin operators of ith spin S_i,

$$\mathcal{H} = -\sum_{i,j} J_{ij} S_i \cdot S_j \qquad (1.14)$$

The exchange constant, *J*, is negative if the interaction between spins is antiferromagnetic.

The magnetic ordering of antiferromagnets is not as simple as that of a ferromagnet due to the multiple combinations of dominating antiferromagnetic couplings of spins. Here, the case of the face centered cubic (f.c.c) cell shall be discussed since this structure is crucial to the main topic of this thesis with respect to geometric frustration.

The determination of general antiferromagnetic structures is normally explained with the molecular field theory. This theory is useful to understand possible antiferromagnetic structures if the interaction of spins gets complicated. In this theory, the concept of sub-lattices is adopted. The parent lattice is divided into equal sub-lattices based on the interactions of spins. In the theory, the magnetic field on a sublattice corresponds to the total magnetic field of its surrounding sublattices acting on this sublattice. When a parent lattice is divided into n equal sub-lattices, the molecular field of *i* th sub-lattice is expressed as follows using the molecular field coefficient a_{ij} and the magnetization of jth sub-lattice M_j, [6, 7],

$$H_i = \sum_j^n a_{ij} M_j + H \qquad (1.15)$$

$$\text{where } a_{ij} = \frac{n(2z_{ij}J_{ij})}{Ng^2{\mu_B}^2},\ a_{ii}=0,\ M_i = \frac{N}{n} g\mu_B S_i$$

In the above equation, a_{ij} is a molecular field coefficient, z is the number of the nearest neighbors, J is the exchange interaction between ith and jth sub-lattices and M_i is the magnetic moment of the ith sub-lattices. For convenience, M_i is expressed as follows with a high temperature approximation,

$$M_i = \frac{C}{nT} H_i = \frac{C}{nT}\left(H + \sum_{j=1}^n a_{ij} M_j\right) \qquad (1.16)$$

Using the total magnetization M= $\sum_{i=1}^{n} M_i$ and $a_{ij}=a_{ji}$, the magnetization and the susceptibility are expressed as,

$$\chi = \frac{C}{T(1-\frac{C}{nT}\sum_{j=1}^{n} a_{ij})} \qquad (1.17)$$

then the Weiss constant is expressed as,

$$\theta = \frac{C}{n}\sum_{j=1}^{n} a_{ij} = \frac{2S(S+1)}{3k}\sum_{j=1}^{n} z_{ij}J_{ij} \qquad (1.18)$$

For the f.c.c cell, a doubled cell, which contains eight equal sub-lattice (n=8) and the considerable interactions, the nearest neighbour and the next-nearest neighbour therefore *i*=2 (J_1 and J_2 only) are included. The critical temperature/Neel temperature is solved with a set of linear homogeneous equations derived from the equation above with the Brillouin function, $a_{ij} = a_{0j} = a_j$ and a condition of H=0. (The details of mathematical treatment is omitted here to avoid complexities.) According to the work by Adachi [6], the solution of the set of homogeneous equations gives the following solutions using the coefficient, a_i (i=1, 2)

$$T_c = \frac{C}{8}(a_1 + a_2), T_{N_1} = \frac{C}{8}(-\frac{a_1}{3} + a_2) \cdots \text{triple root,}$$

$$T_{N_2} = \frac{C}{8}(-a_2) \cdots \text{quadruple root, } T_{N_3} = \frac{C}{8}(-\frac{a_1}{3} + \frac{a_2}{3}) \qquad (1.19)$$

The critical temperature and each Neel temperatures are corresponded to a ferromagnetic structure (F), first type antiferromagnetic structure (AF1), second type (AF2) and third type (AF3) illustrated in Figure 1.1.

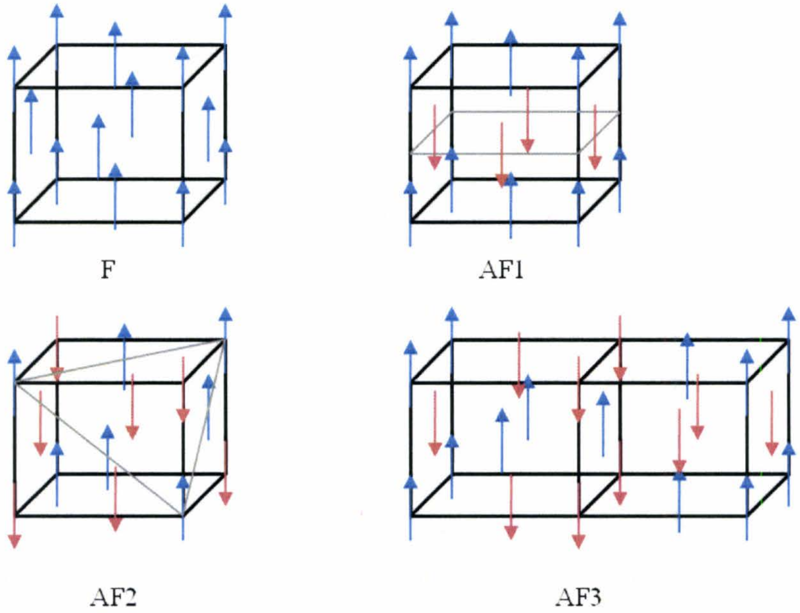
F AF1 AF2 AF3

Figure 1.1 Ferromagnetic structure and three types of antiferromagnetic structure derived from the molecular field theory. AF1: antiferromagnetic ordering is achieved inter-plane along [001] plane, in-plane relationship is ferromagnetic. AF2: antiferromagnetic coupling is between planes along [111], in-plane relationship is ferromagnetic. AF3: The periodicity of antiferromagnetic coupling requires two unit cells.

According to the resultant solutions and considering the transformation from one to the other structure, the relations of each structure in a_1-a_2 coordinates are displayed in Figure

1.2. (Note that a_1 and a_2 for a ferromagnetic structure are positive.) Consequently, for the f.c.c cell, the stability of each antiferromagnetic sub-lattice is retained when $1 \geq \theta/T_N \geq -5$ is achieved according to this theoretical work.

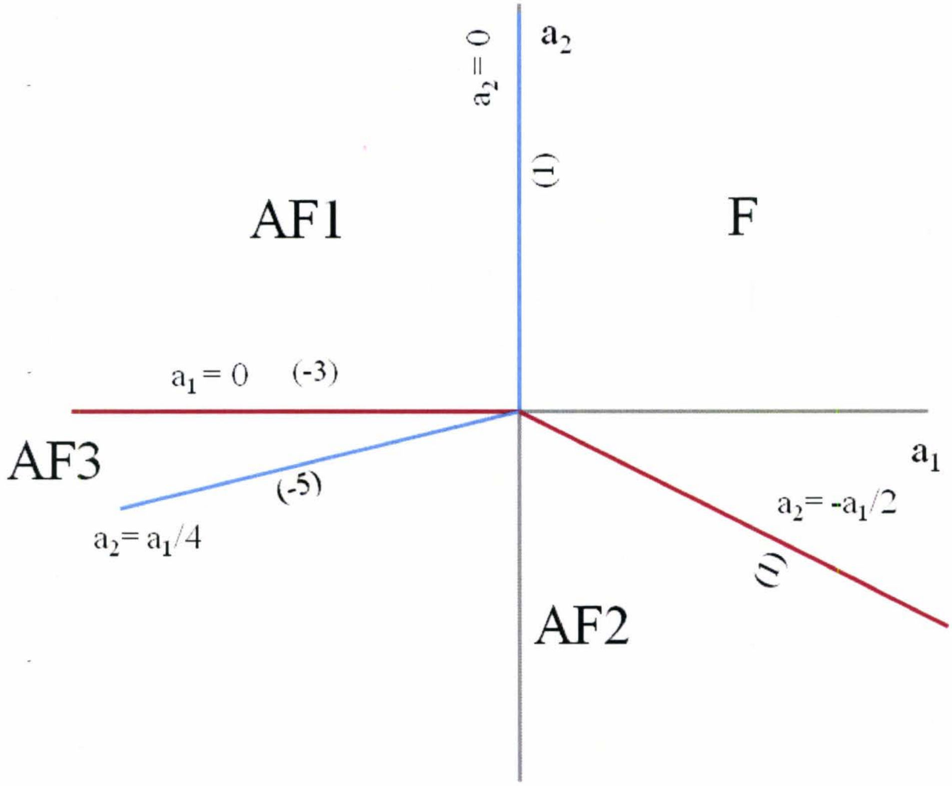

Figure 1.2 The map of the stable antiferromagnetic structures and their relationships for the f.c.c.cell. The colour lines show the borders between each antiferromagnetic structure. The numbers in parenthesis shows the value of the Weiss constant divided by the Neel temperature at each borders.

Geometrically frustrated antiferromagnets

Geometric magnetic frustration normally occurs when competing magnetic spins are highly concentrated in a solid and the frustration arises from their spatial arrangement/geometry, which involves triangular plaquettes. In that geometry, antiferromagnetic coupling of three spins is not satisfied simultaneously as illustrated in Figure 1.3. Clearly, when the directions of two spins are determined as antiferromagnetic, the third spin cannot satisfy simultaneous antiferromagnetic coupling [8] and is thus, frustrated.

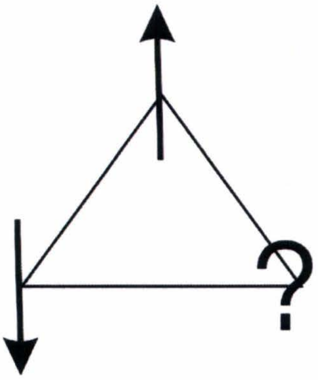

Figure 1.3 Antiferromagnetic spin coupling on an equilateral triangle

Thus, geometrically frustrated compounds have equilateral triangular or tetrahedral motifs in their crystal structures. Major sub-lattices are displayed in Figure 1.4 depending on the dimension of frustrated sub-lattices. Two-dimensional lattices are based on edge and corner sharing triangles (Kagome) while three dimensional lattice involves edge (f.c.c.) and corner sharing (Pyrochlore) tetrahedra.

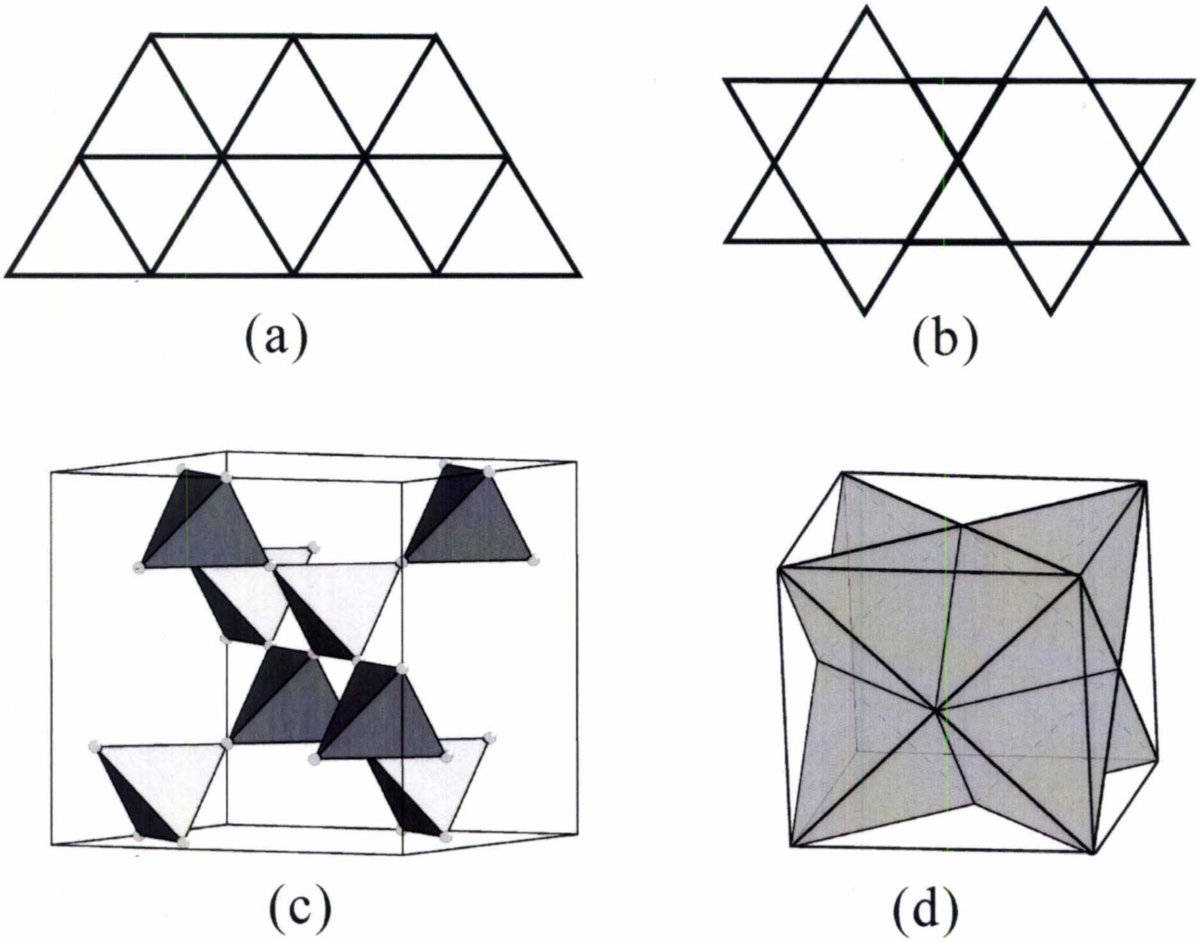

Figure 1.4 Examples of frustrated sub lattices; (a) equilateral triangles (b) Kagome pattern (c) Pyrochlore (corner sharing tetrahedra) (d) face centered cubic (f.c.c.) lattice (rock-salt, edge sharing tetrahedra)

Usually one can expect that this frustration leads to exotic magnetic ground states such as spin glass, spin ice and spin liquid. The illustration of these states is shown in Figure 1.5. The spin glass state is one where all spins are frozen with random orientation. In the spin ice state, which was found in $Dy_2Ti_2O_7$ and $Ho_2Ti_2O_7$[4], the conformation of spins in a solid is mimicking the orientation of water molecules in ice, where two spins point out and other two point in, elaborated on the analogy to H_2O, with two covalent bonds and two hydrogen bonds. Lastly, in the spin liquid state, all the spins are thought to form singlets (dimerized) of resonating valence bonds within possible configuration and a schematic picture is shown in the figure 1.5 (c). The left picture of Figure 1.5(c) is a formation of singlets at a moment. These parings of singlets travel similarly to the resonance of covalent bonds in a benzene ring, to form new singlets in another possible configuration at next moment. In total, the spins in liquid state appear as a superposition of singlets configuration. This time-dependent behaviour will be retained thus the spins remain dynamic in the spin liquid [8].

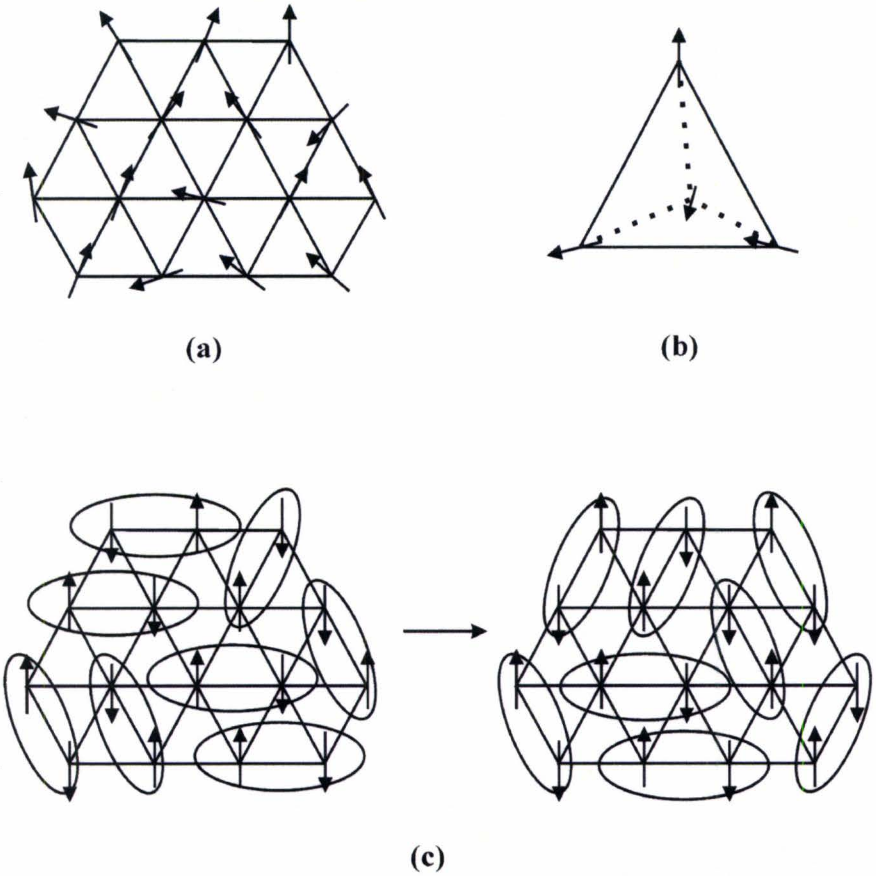

Figure 1.5 Illustration of exotic magnetic ground states, (a) spin glass (b) spin ice (c) spin liquid

The degree of the frustration of a geometrically frustrated compound is experimentally evaluated by the frustration index, *f*, which is the absolute value of the Weiss constant divided by its the transition temperature [8]. A compound will be recognized as highly frustrated when their $f > 10$ [8]. Additionally, since frustrated materials behave to avoid ordering and growth of correlation length beyond nearest neighbours, one will see linearity of Curie-Weiss law in χ^{-1} vs. T plot down to very low temperature [8]. The threshold for compounds with f.c.c symmetry, can be extracted from the molecular field theory, introduced in previous section [6, 7]. In that section, a theoretically derived frustration index of a general antiferromagnet is $f < 5$. Therefore, a geometrically frustrated antiferromagnet will be recognized when its frustration index is greater than 5.

The efforts to understand the developments of the exotic magnetic ground states of f.c.c. lattices from the theoretical point of view should be addressed here. In comparison with other frustrated lattices such as pyrochlore or kagome, the f.c.c. lattice has received relatively modest attention from theorists. Oguchi et al have shown that a f.c.c. S=1/2 Heisenberg system(3D)system with only the nearest neighbor interactions would not show any antiferromagnetic long range order (AF LRO) while within the XY(2D) model there is the possibility of a finite AF LRO.[9] Henley has also considered the f.c.c. lattice in the context of dilution by non-magnetic ions which is shown to induce an ordered state due to thermal fluctuations or a spin glassy behavior according upon further dilution.[10]

The most relevant study is that by Kuz'min, for the f.c.c. lattice with S=1/2 and only the nearest neighbor interactions using spin wave theory. It was concluded that the ground state of the system will be a gapped spin singlet or spin liquid [11]. Inclusion of a ferromagnetic interaction next nearest neighbors stabilizes an antiferromagnetic long range ordering in the system [11].

Face centered cubic double perovskites

The basic perovskite structure ABO_3, where A is a significantly larger cation than B, can be transformed to double perovskite, $A_2BB\ O_6$, by substituting a half of B site cation with other suitable cations. As with perovskite, double perovskite have a framework of corner linked BO_6 ($B\ O_6$) octahedra with A ion residing in an interstitial site. The arrangement of B-site ions in the double perovskites is divided into three types, random, layered or rock salt as shown in Figure 1.6 depending on the combination of B and B ions (A ion is omitted for clarity) [12].

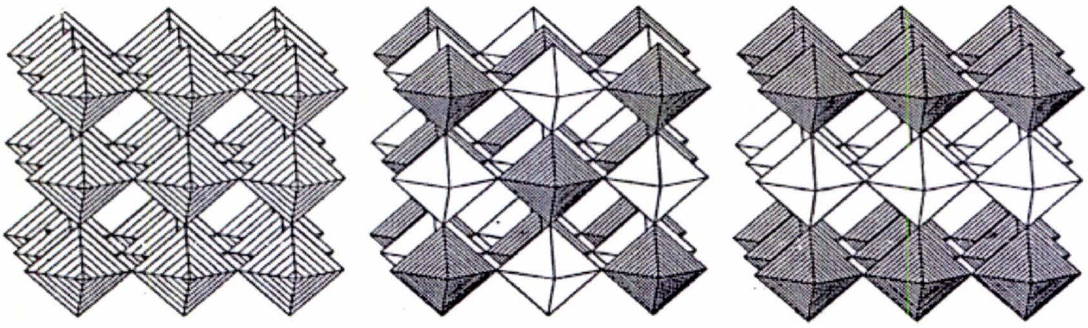

(a) (b) (c)

Figure 1.6 B site arrangement of double perovskite (a) random (b) layered (c) rock-salt (f.c.c.) A ions are omitted for clarity.

(Reprinted from Progress in solid state chemistry, Vol 22, M. T. Anderson et al, "B-cation Arrangements in Double Perovskites", p204., Copyright (1993), with permission from Elsevier[12])

According to a statistical study [12], rock salt (B-site ordered, f.c.c.) will be achieved when the charge difference between B and B ions is greater than two accompanied with a significant difference in their ionic radii as one can see in Figure 1.7. The rock salt type double perovskite represents the B-site ordered f.c.c. double perovskite.

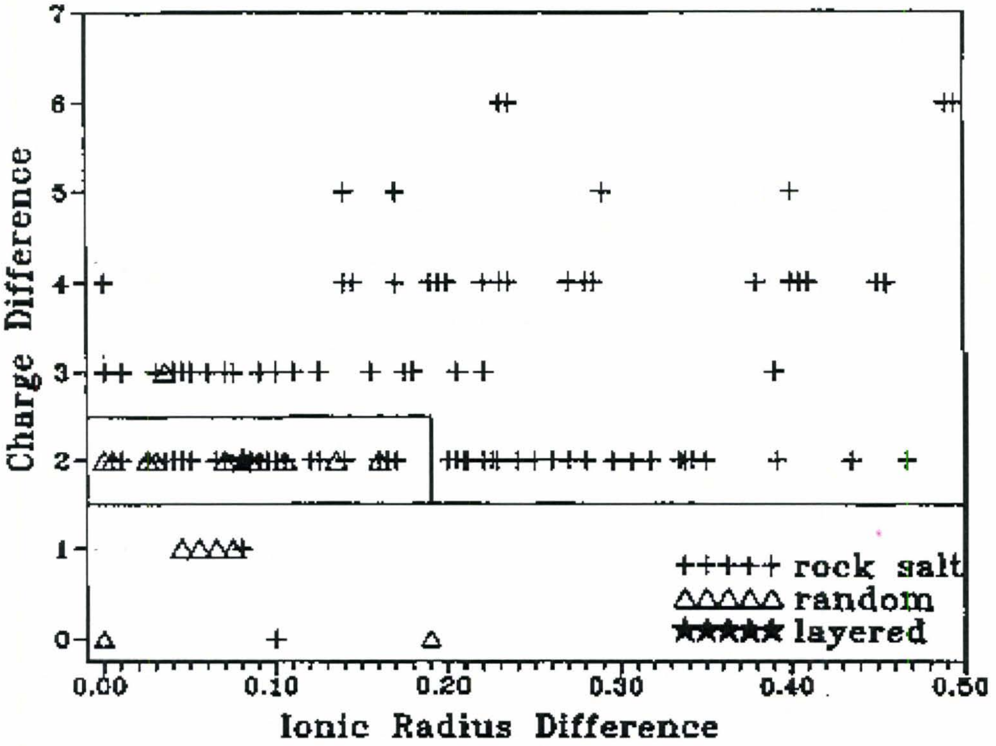

Figure 1.7 The diagram between charge difference and ionic radius difference in B site. The B site ordering will be safely achieved when the charge difference is greater than two and ionic radius difference is significant. (Reprinted from Progress in solid state chemistry, Vol 22, M. T. Anderson *et al*, "B-cation Arrangements in Double Perovskites", p217., Copyright (1993), with permission from Elsevier[12])

The crystal symmetry of a f.c.c. double perovskite varies depending on the combination of A, B and B ions. One can evaluate the selected combination with a tolerance factor, t, in Figure 1.8 and the equation 1.21 in order to estimate a deviation from an ideal cubic double perovskite structure. Usually, the more t deviates from 1, the more the structure of a f.c.c double perovskite distorts.

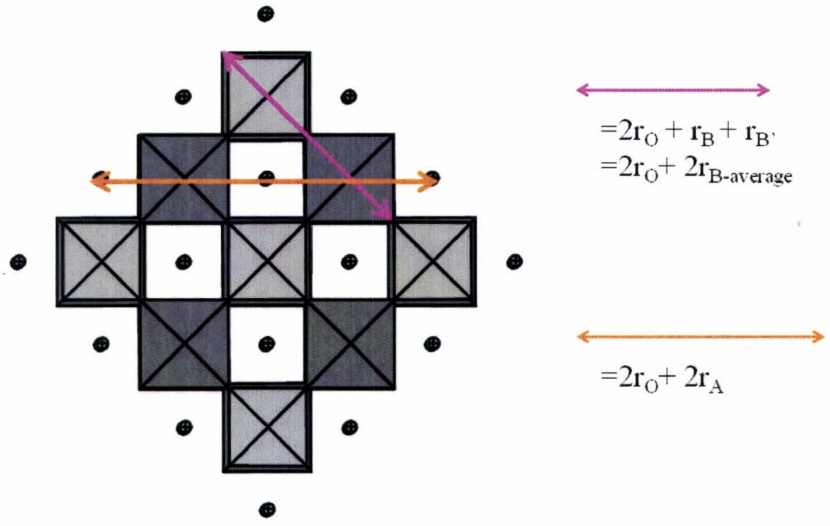

Figure 1.8 The geometry of and . The illustration is the projection to ac plane for convenience. The pink line represents the unit cell length, which is , and the orange line represents the diagonal path of unit cell on ac plane.

$$t = \text{———} \qquad (1.20)$$

where is the average radii of B and B ions, r_A, r_O represent A and oxygen ions

The structure variety of f.c.c. double perovskites $A_2BB'O_6$ will be found from cubic (S.G. $Fm\bar{3}m$) to tetragonal (P4/mnc, I4/m) and monoclinic structure ($P2_1/n$) according to the study based on group theory by Howard, Kennedy and Woodward as shown in Figure 1.9 [13]. The distortion is mainly initiated by tilting of BO_6 ($B'O_6$) octahedra, in-phase or/and out of phase tilting about to crystal axes. In-phase tilting is the rotation of each BO_6 octahedra in the same direction and one will see alternating direction of tilting of BO_6 octahedra in 'out of phase' tilting [13]. These tiltings are relatively slight resulting in a small elongation in cell constants for the tetragonal case and a deviation of β from 90 degree about a few tens degree in addition to slight elongation/compression of cell constants for monoclinic compounds as shown in Figure 1.10.

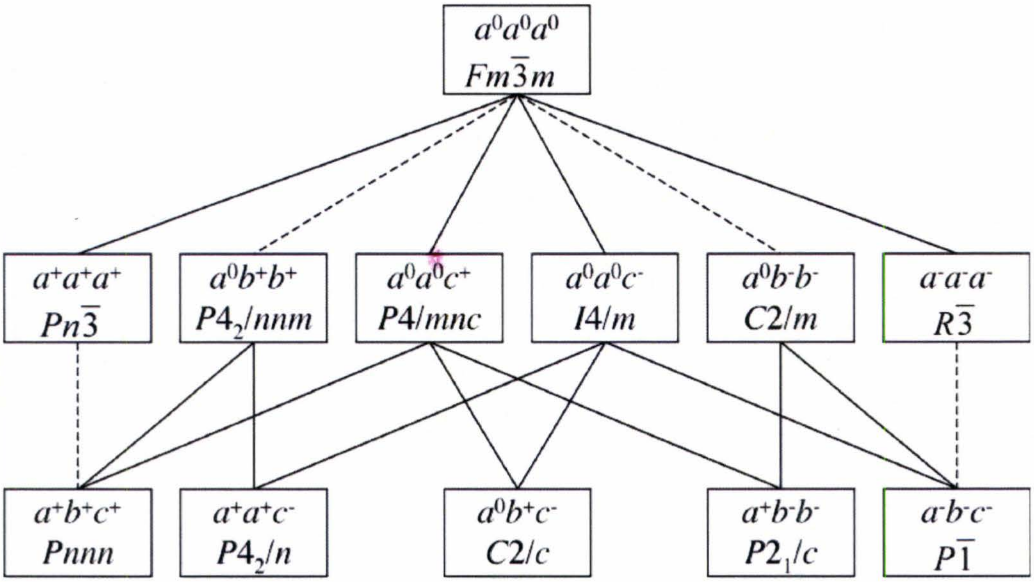

Figure 1.9 The pathway of structure distortion of B-site ordered double perovskites from cubic Fm3m to monoclinic $P2_1/c$ and tilting direction of octahedra in all derivatives (Reproduced with permission of the International Union of Crystallography [13])

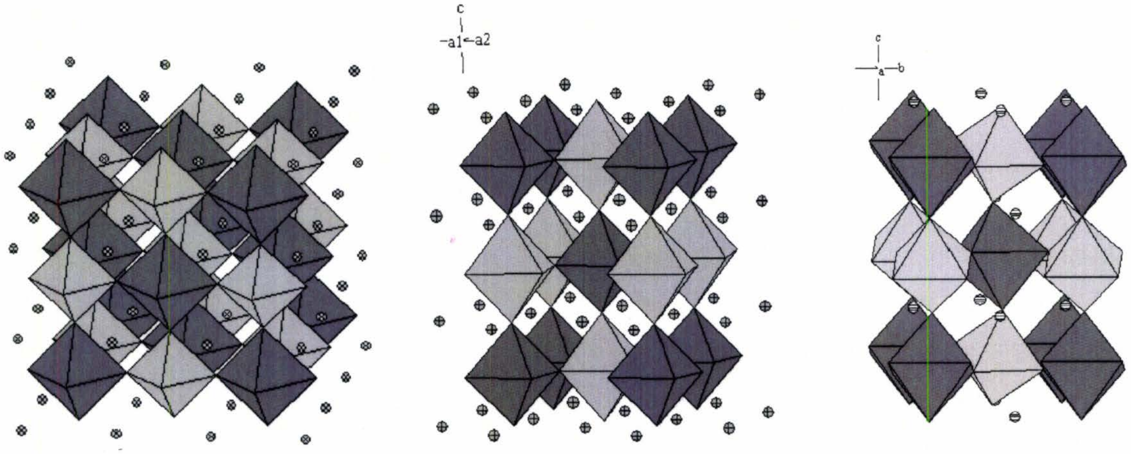

Figure 1.10 (left) The cubic structure of a f.c.c. double perovskite (Fm3m), (middle) the tetragonal structure (I4/m), with out of phase tilting to the c axis (right) the monoclinic structure ($P2_1/n$) , with in-phase tilting to the a axis and out of phase tilting to the b and c axes. All circles represent the A ion, dark grey octahedra is the B O_6, and light grey octahedra for BO_6

Additionally, as crystal structure distorts, the point symmetry of magnetic ion octahedron lowers its symmetry from m3m (in cubic), 4/m (in tetragonal) to -1 (in monoclinic). This distortion lifts the degeneracy of the t_{2g} orbitals of the magnetic ions hence the orbital ordering is expected to occur. The change in the energy of three t_{2g} levels will be still slight however, the order of orbital ordering would be different depending on the deformation of B O_6 octahedra as shown in Figure 1.11.

Moreover, the electronic configuration of a magnetic ion B can be also in some cases (i.e. d^1 and d^2electronic configurations) subject to a potential Jahn-Teller distortion.

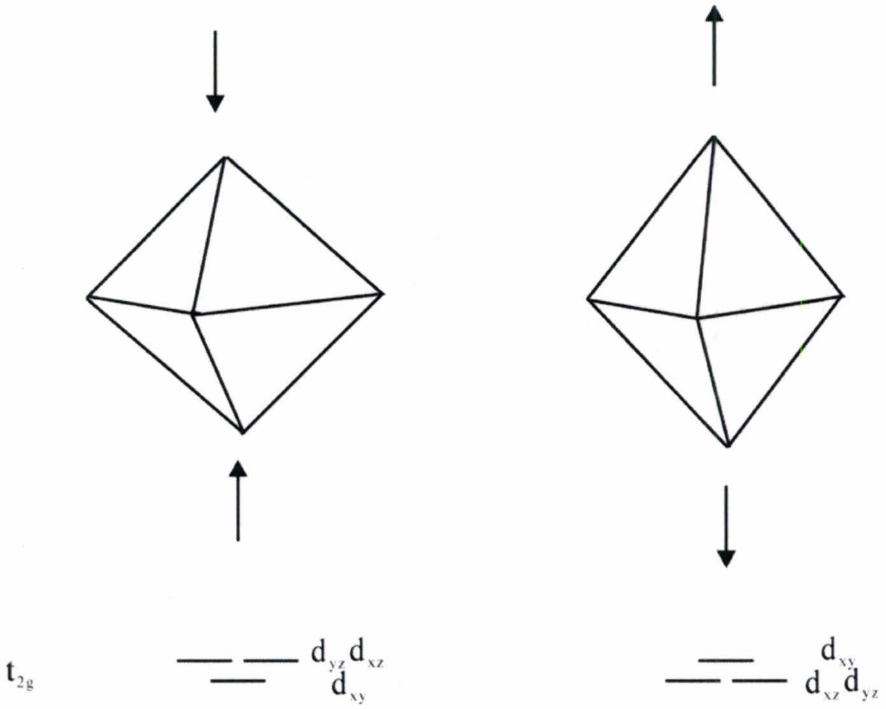

Figure 1.11 Distortion of local symmetry of octahedra and t_{2g} orbital ordering; compression (left) and elongation (right)

As mentioned in a previous section, f.c.c. double perovskites possess a frustrated geometry hence one can expect to see various magnetic ground states in this series. Selected f.c.c. double perovskites are shown in Table 1-I. It is likely that non-ordering states tend to be observed by lowering the spin quantum number. For compounds with higher spin quantum number, S=5/2 and S=3/2, an antiferromagnetic ordering is achieved while the compounds with lower spin quantum numbers, S=1 and S=1/2, it is not easy to achieve ordering and they rather become glassy or a disordered state, except for a few of cases (Ba_2LiOsO_6 and Ba_2NaOsO_6). This trend may originate in quantum fluctuation of spins. The number of possible spin states for the spin quantum number S is 2S+1, therefore the higher spin quantum number is, the more possible states of spins available and quantum fluctuation does not always change the direction of spins, which would play a role for falling into an ordered state. On the other hand, for lower spin quantum numbers, especially S=1/2, there are only two available states, up (↑) or down (↓), and a quantum fluctuation always changes the direction of spins. Therefore, a compound with a higher spin quantum number would achieve an antiferromagnetic state easier than the compounds with lower spin quantum number.

Moreover, the crystal structure of a compound, in other words, the local symmetry of B-site magnetic ions would play another role on the determination of the magnetic ground state of a compound since in cubic symmetry three t_{2g} orbital are degenerate (orbital disorder) while the t_{2g} orbital are split in non-cubic symmetry (orbital ordering). In this thesis, a cubic series and a monoclinic series of f.c.c. double perovskites, Ba_2YMO_6 and La_2LiMO_6 (M=Mo, Re and Ru), are employed to perform a systematic study of the dependence of spin quantum number and local symmetry (crystal structure) on the determination of the magnetic ground states of f.c.c. double perovskites.

Table 1-1 Selected B site ordered double perovskites and their ground state (AFLRO-antiferromagnetic long range order, FLRO-ferromagnetic long range order, S.G. –spin glass, ? – not determined)

S	Space Group	Compound	θ_C(K)	$T_{c,f}$(K)	*f*	B' site symmetry	Ground State	ref
5/2	Fm3m	Ba_2MnWO_6	-64	9	7	m3m	AFLRO	14
5/2	$P2_1/n$	Sr_2MnWO_6	-30	10	3	-1	AFLRO	15
3/2	Fm3m	Ba_2YRuO_6	-571	36	16	m3m	AFLRO	16
3/2	$P2_1/n$	La_2LiRuO_6	-170	30	6	-1	AFLRO	17
1	Fm3m	Ba_2YReO_6	-480	40	12	m3m	S.G.	18
1	Fm3m	Ba_2CaOsO_6	-157	51	3	m3m	AFLRO?	19
1	I4/m	Sr_2NiWO_6	-175	54	3	4/m	AFLRO	20
1/2	Fm3m	Ba_2LiOsO_6	-40	8	5	m3m	AFLRO	21
1/2	Fm3m	Ba_2NaOsO_6	-10	6.8	1.5	m3m	FLRO	21
1/2	Fm3m	Ba_2YMoO_6	-91	2<	>45	m3m	?	22
1/2	Fm3m-I4/m	Ba_2CaReO_6	?	14	?	4/m	?	19
1/2	I4/m	Sr_2MgReO_6	-426	45	9	4/m	S.G	23
1/2	$P2_1/n$	Sr_2CaReO_6	-443	14	32	-1	S.G.	23

Magnetic interactions in f.c.c. double perovskite

In earlier section, a macroscopic view of magnetic ground states, the crystal structures and their local symmetry of f.c.c. double perovskites were provided with an assumption that a compound has an antiferromagnetic interaction. In this section, the microscopic view of the magnetic interaction will be presented to show the origin of antiferromagnetic interactions in f.c.c. double perovskites.

The magnetic ground states of f.c.c. double perovskites originate their magnetic behaviours in their exchange interactions between spins as expressed in the equation 1.18. There are several magnetic interactions, which are usually applied to explain magnetic interactions, such as the magnetic dipole-dipole interaction, direct exchange, super-exchange, which is often employed for ionic solids, the RKKY interaction for metals and double exchange interactions for mixed valence compounds [24].

Normally, super exchange interaction is considered as major interaction in insulating oxides. In f.c.c. oxides, each magnetic ion is surrounded by six non-magnetic oxygen ions, which locate between magnetic ions and meditate this interaction. A simple example of the mechanism of this interaction is illustrated below (Figure 1.12).

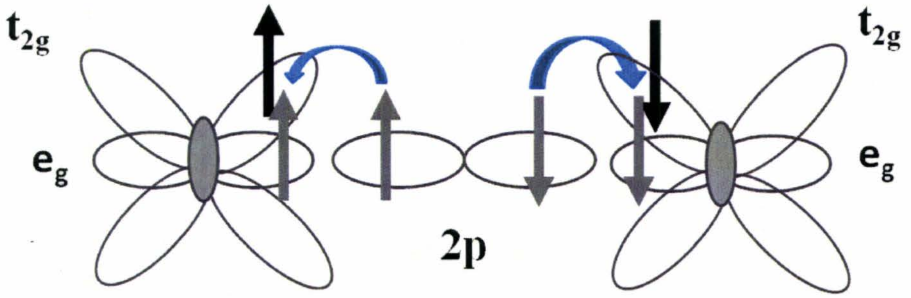

Figure 1.12 Superexchange interaction between two transition metal ions (B) and an oxygen ion

Here, the magnetic ions, B′, and the oxygen bond, B′-O- B′, has an angle of 180 degree. Due to partial covalency of the bond, partial electron can transfers from O2*p* orbital and 'up' spin is transferred according to the Hund's rule. Then, 'down' spin should be transferred to the other magnetic ion according to the Hund's rule as well. Thus, antiferromagnetic coupling is achieved between the two magnetic ions [1]. In a real f.c.c. compound, the interaction pathway involves a non-magnetic B cation as B -O-B-O- B . Therefore, the interaction between B and B mediated with the intermediate two oxygen ions and non-magnetic B ions will be expressed as super-super exchange interaction, which is extended version of super-exchange interaction described above.

References

[1] P.A. Cox, "*The electronic structure and chemistry of solids*" Oxford University Press, New York, 1987

[2] K. Mizushima, P.C. Jones, P.J. Wiseman, J.B. Goodenough, Materials Research Bulletin 15, 783–789 (1980)

[3] J. S. Gardner et al, PRL 82(5) 1012 (1999);J. S. Gardner et al, Physical Review B, vol. 68, 180401(2003); J. S. Gardner et al, Phys. Rev. B,64, 224416 (2001)

[4] J. S. Gardner, M. J. P. Gingras and J. E. Greedan, Rev. Mod. Phys, 82, 53 (2010); S. T. Blramwell et al, Science 294, 1495 (2001)

[5] F.E. Mabbs and D.J.Mashin, Magnetism and Transition Metal Complexes, Chapman and Hall ltd, London 1973

[6] Kengo Adachi, Magnetism of Compounds localized spin system, shokabo Tokyo(2001)

[7] J. Samuel Smart, "*Effective Field Theories of Magnetism*", W.B. Saunders company, Philadelphia & London, 1966

[8] A. P. Ramirez, Annu. Rev. Mater. Sci. 24, 453 (1994); J. E. Greedan, J. Mater. Chem., 11, 37 (2001); P. Fazekas and P. W. Anderson, Philosophical Magazine, 30, 423 (1974)

[9] T. Oguchi et al, J. Phys. Soc. Japan, 54, 4494 (1985), T. Oguchi et al, J. Phys. Soc. Japan, 55, 323 (1986)

[10] C. L. Henley, J. Applied Phys. 61(8) 3962 (1987)

[11] E. V. Kuz'min, J. Exp. Theo. Phys., 96(1), 129 (2003)

[12] M. T. Anderson et al, Prog. Solid St. Chem., 22, 197 (1993)

[13] C. J. Howard and H. T. Stokes, Acta Crystallographica A61, 93 (2005), C. J. Hooward, B. J. Kennedy and P. M. Woodward, Acra Crystallographica B 59, 463 (2003)

[14] A. K. Azad et al, Material Research Bulletin, 36(12), 2215 (2001)

[15] A. K. Azad et al, J. Mag. Mag. Mater., 237(2), 124 (2001)

[16] P. D. Battle, J. Solid State Chem., 78,108 (1989)

[17] P.D. Battle, J. Solid State Chem., 175, 20 (2003)

[18] Yoshinori Sasaki et al, j. Mater. Chem., 12, 2361(2002)

[19] Kazuhiro Yamanaka et al, J. solid State Chem., 179, 605 (2006)

[20] Daisuke Iwanaga et al, Material Research Bulletin 35 (3) 449 (2000)

[21] Katharine E. Stizer et al, Solid State Sciences, 4, 311 (2002)

[22] E.J. Cussen et al, Chemistry of Material, 18, 2855 (2006)

[23] C.R. Wiebe et al, Physical Review B 68, 134410 (2003); C. R. Wiebe et al, Physical Review B 65, 144413 (2002)

[24] Stephan Blundell, "*Magnetism in Condensed Matter*", Oxford University Press Inc., New York, 2001

Chapter Two

Experimental

Diffraction techniques

When a compound with periodicity of its atomic arrangement is exposed to a radiation such as X-ray, electron and neutron beams, the information of the atomic arrangement of the compound is obtained as a diffraction pattern. The diffraction pattern of a compound has characteristic peak positions and intensities which uniquely identify the compound. The fundamental law governing diffraction conditions is called Bragg's law. The illustration of the Bragg's law is shown in Figure 2.1. The atomic arrangement of a compound consists of a set of planes, which is drawn as lines separated by a distance d in Figure 2.1. An incident beam is diffracted by each plane of atoms of a compound.

According to the characteristics of the incident and the diffracted beams (X-ray, electron or neutron) as waves, the condition for constructive interference, is given by the equation below,

$$n\lambda = 2d\sin\theta \qquad (2.1)$$

,where λ is the wavelength of the incident radiation, d is the inter-plane distance

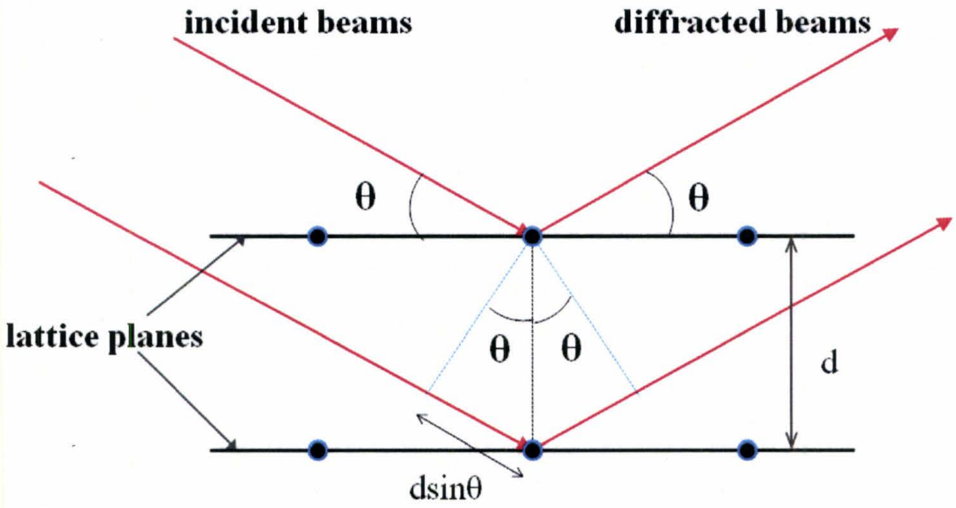

Figure 2.1 The geometry of a plane in a lattice and constructive interference of an incident radiation wave. The distance between lattice planes is d. The difference of pathways is proportional to 2*dsinθ, which is the principle of Bragg's law

The phenomenon of diffraction can also be explained using a concept of a reciprocal space and Ewald's sphere. The relationship between a reciprocal space and direct space is given by the equation 2.2 [1],

$$\boldsymbol{a}^* = \frac{\boldsymbol{b}\times\boldsymbol{c}}{\boldsymbol{a}\cdot[\boldsymbol{b}\times\boldsymbol{c}]} \quad \boldsymbol{b}^* = \frac{\boldsymbol{c}\times\boldsymbol{a}}{\boldsymbol{b}\cdot[\boldsymbol{c}\times\boldsymbol{a}]} \quad \boldsymbol{c}^* = \frac{\boldsymbol{a}\times\boldsymbol{b}}{\boldsymbol{c}\cdot[\boldsymbol{a}\times\boldsymbol{b}]} \qquad (2.2)$$

,where the direct space unit cell vectors (a, b, c) and the corresponding reciprocal space vectors (a*, b*, c*) are defined. It follows that $\boldsymbol{a}\cdot\boldsymbol{a}^* = \boldsymbol{b}\cdot\boldsymbol{b}^* = \boldsymbol{c}\cdot\boldsymbol{c}^* = 1$

The visualization of Ewald's sphere is shown in Figure. **k** and **k′** are the wave vectors of the incident beam and the diffracted beam. The reciprocal propagation vector, $\mathbf{G}_{hkl}$, is given by using Miller indices, (h, k, l,) [1],

$$\mathbf{G}_{hkl} = h\mathbf{a}^* + k\mathbf{b}^* + l\mathbf{c}^* \qquad (2.3)$$

, where $|G_{hkl}| = 1/d_{hkl}$, $\mathbf{G}_{hkl}$ is normal to a (h,k,l) plane in the direct space

Diffraction is an elastic process thus no energy change occurred during the process and $|\mathbf{k}| = |\mathbf{k}'| = 1/\lambda$ and the Ewald's sphere is presented as a circle with the radius of $1/\lambda$. When Ewald sphere is placed as the front of **k** locates at the origin of the reciprocal space as shown in Figure 2.2, the surface of Ewald sphere intersects with some lattice points in the reciprocal space. Then, a diffraction peak is observed corresponding to the representation of the lattice point and its 2θ [2].

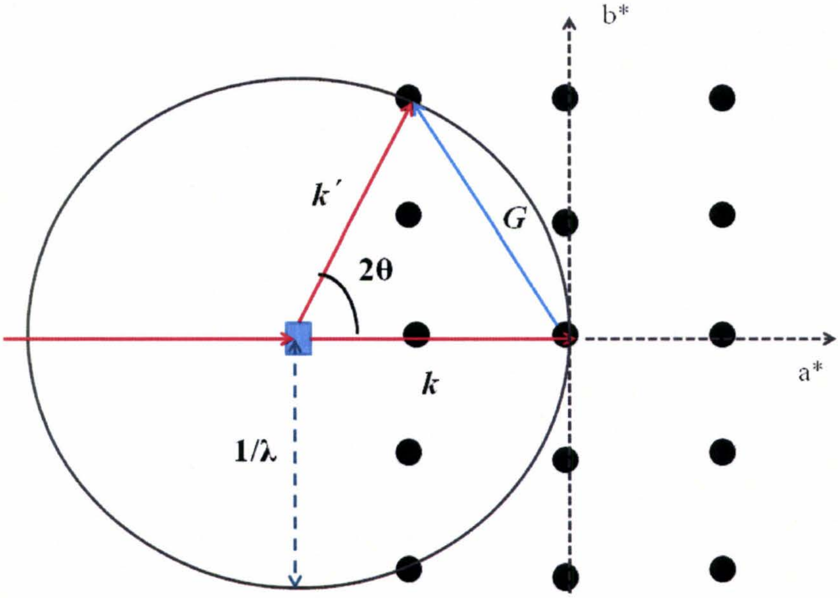

Figure 2.2 The visualization of Ewald's sphere and the reciprocal lattice. The intersection of the lattice point and **k**′ is [-1, 2]. The diffraction peak of d_{-12} is observed at corresponding 2θ in the diffraction pattern

The intensities of the peaks in a diffraction pattern are explained depending on the incident beams. X-ray and neutron were used as a light source in this thesis therefore these two cases are introduced here.

(1) X-ray diffraction

X-ray is an electromagnetic wave and it interacts with electron densities of an atom. The intensities of the peaks of a pattern are highly dependent on the scattering power of the electrons of an atom. The atomic scattering factor is defined by [1] where an atomic position vector ***r***,

$$f_x(\boldsymbol{G}) = \int \rho_e(\boldsymbol{r}) \exp\big(-2\pi i(\boldsymbol{G} \cdot \boldsymbol{r})\big) d\boldsymbol{r} \qquad (2.4)$$

When the electron density is thought as symmetrical, f_x becomes a function of $|\mathbf{G}| = 2\sin\theta/\lambda$ as follows [1]

$$f_x\left(\frac{sin\theta}{\lambda}\right) = \int_0^\infty u(r) \frac{\sin\left(\frac{4\pi r sin\theta}{\lambda}\right)}{\frac{4\pi r sin\theta}{\lambda}}\, dr \qquad (2.5)$$

where $u(r)dr = 4\pi^2 \rho(r) dr$ for spherical symmetry of electron density of an atom

The scattering factor at $\sin\theta/\lambda=0$ is given by [1],

$$f_x = \mathrm{Z}\ (\text{atomic number}) \qquad (2.6)$$

Therefore the atomic scattering factor of X-ray is atomic dependent (heavier atoms simply produce higher intensity).

Since all atoms of a compound are in vibration at high temperature, atomic position is influenced by that thermal vibration. The scattering factor, f_x, in this point of view is expressed by [3],

$$f_x = f_o exp^{-B(sin^2\theta)/\lambda^2} \qquad (2.7)$$

B in this equation is called the temperature factor (atomic displacement factor). This factor accounts for the loss of scattering power of electrons due to the vibration of the electron clouds. B is given by the following equation [3],

$$B = 8\pi\bar{u}^2 \quad (2.8)$$

,where $\bar{u}^2$ is an atomic displacement in Å^2

F_{hkl} is the structure factor, which is the all sum of atomic scattering factors in a compound, modified by a phase factor expressed as an exponential function in terms of the atomic positions of jth atom (x_j,y_j,z_j) and miller indices (h, k, l) [3],

$$F_{hkl} = \sum_j f_{x,j} e^{2\pi i(hx_j+ky_j+l_{z_j})} \quad (2.9)$$

The intensity of a peak is defined by the square of the structure factor, which is given by [1, 2, 3].

$$I \propto F_{hkl}^2 \quad (2.10)$$

Therefore, the intensity of peaks in a diffraction pattern rapidly decreases as diffraction angle 2θ increases. [There is also the Lorentz & polarization factor which contributes to this decrease]

(2) Neutron diffraction

Thermal neutrons produced in a nuclear reactor have characteristic properties useful for diffraction as the wavelength is that of interatomic distances. Neutrons are neutral particles and are not scattered by the electron cloud around an atom, but instead interact with other nucleons in the atomic nucleus. Additionally, neutrons have spin quantum number S=1/2 and, therefore, neutrons can interact with the magnetic field generated by the electron cloud of an atom. These double features enable us to obtain not only crystal structure of a compound but also the magnetic structure of a compound.

The velocity spectrum of thermal neutron produced from a reactor generally follows Maxwell distribution, whose relationship with neutron flux is given by [4],

$$\phi(v) \propto v^3 \exp\left(-\frac{\frac{1}{2}mv^2}{k_BT}\right) \qquad (2.11)$$

,where $\phi(v)dv$ is the number of neutron through unit area per second between the velocity v and v+dv, k_B is the Boltzmann constant and T is the temperature

Conventionally, a thermal neutron with its energy E is expressed as [4],

$$E = k_BT \qquad (2.12)$$

, and the de Broglie wave length of a thermal neutron is given by [4],

$$\lambda = \frac{h}{mv} \qquad (2.13)$$

Therefore the following relationship is obtained.

$$E = k_BT = \frac{1}{2}mv^2 = \frac{h^2}{2m\lambda^2} \qquad (2.14)$$

By substituting the following constants in the equation above; the mass of neutron (m_n=1.675x10^{-27}kg), Planck's constant (h=6.626x10^{-34} Js), Boltzmann constant (1.381x10^{-23} JK^{-1}), we get the following relation [4],

$$\lambda\,(\text{Å}) = 30.81/\sqrt{T} \qquad (2.15)$$

When an incident neutron beam is scattered, the probability of scattered neutrons in a particular angle per unit area is referred as cross-section. The cross section is defined as follows and the visualization of the solid angle is shown in Figure 2.3 [4],

$$\frac{d^2\sigma}{d\Omega dE} = \text{number of neutrons scattered per second into a solid angle } d\Omega$$

in the direction of θ,φ, in the energy level between E an E+dE (2.16)

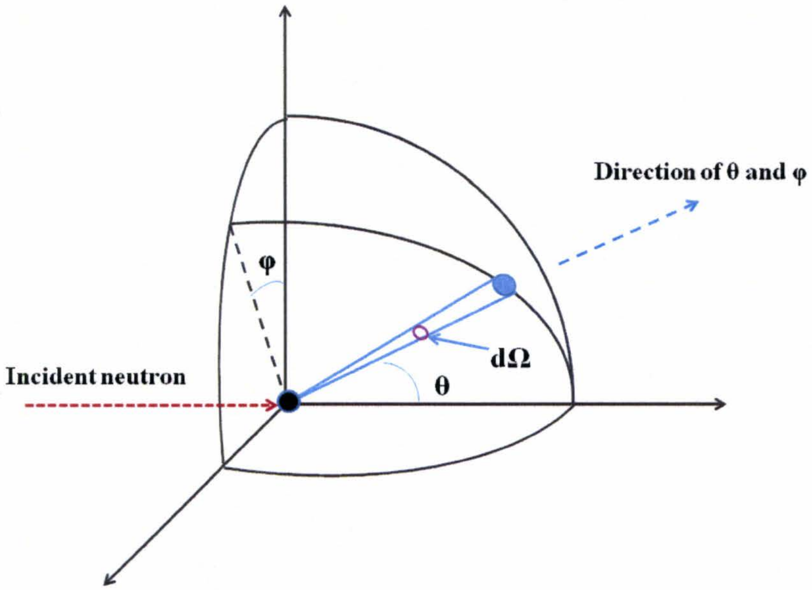

Figure 2.3 The geometry of incident neutron beam, solid angle dΩ in the direction of θ and φ

When the energy of thermal neutrons is not of consideration, the equation above is modified into,

— Number of neutrons scattered into a solid angle dΩ in the direction of θ,ϕ ,devided by Φ dΩ (2.17)

Then total scattering cross section is given by [4],

Total number of neutrons scattered per second / Φ (2.18)

The equation $d\sigma/d\Omega$, is defined using the scattering length, which is corresponded to the atomic scattering length of x-ray, as follows [4],

$$\frac{d\sigma}{d\Omega} = b^2, \qquad \sigma_{total} = 4\pi b^2 \qquad (2.19)$$

Note that scattering length of neutron is independent on scattering angle based on the equation (2.19). Moreover, it is also independent on an atomic number on the contrary to the atomic scattering factor of X-ray as shown in Figure 2.4. Therefore, a neutron diffraction measurement is suitable if a compound contains a light element such as C, N, and O.

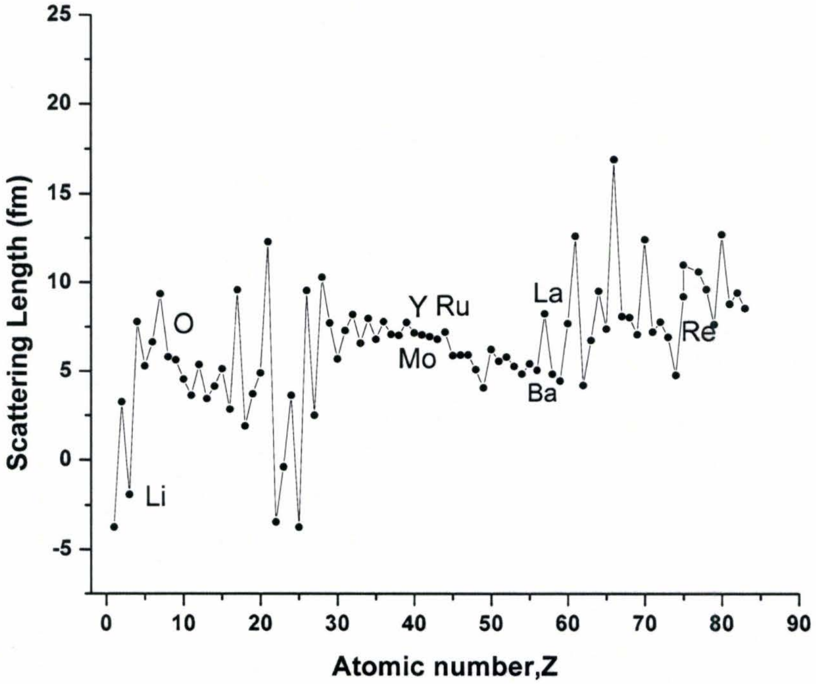

Figure 2.4 Neutron Scattering length (b) of atoms (atomic number 1-83)

Since the scattering of neutron is regarded as spherical thanks to that the nucleus is a point scatterer, the wave function of a scattered neutron is given by [1],

$$\Psi(r) = \frac{b}{r}\exp(2\pi i \frac{r}{\lambda}) \qquad (2.20)$$

where r is the distance from a nucleus and b is the scattering length of a given atom. The advantage of neutron diffraction is that b is roughly independent of atomic number or scattering angle θ, which is different from the X-ray case. Therefore, neutron diffraction is useful to determine the atomic position for light elements. The magnetic scattering of neutron is also defined as same as its nuclear analogue as follows [1],

$$\Psi_{\mathrm{m}} = \frac{\mathrm{b_m}}{\mathrm{r}}\exp(\,2\pi\mathrm{i}\frac{\mathrm{r}}{\lambda}) \qquad (2.21)$$

The magnetic scattering length b_m is defined by [1],

$$b_m = \frac{e^2}{mc^2}\gamma S_0 f_m \qquad (2.22)$$

,where γ is the magnetic moment of neutron, S_0 is spin quantum number, f_m is magnetic scattering factor.

For magnetic compounds, nuclear scattering and magnetic scattering coexist, and then the total cross section of a magnetic compound is modified as [1],

$$b_{total}^2 = b^2 + b_m^2 \ (for\ unpolarized\ neutrons) \qquad (2.23)$$

Since magnetic neutron scattering is based on the interaction of the magnetic moment of neutrons with the field created by electron cloud of an atom, the magnetic scattering factor is expressed similarly to atomic scattering factor [1] and the magnetic scattering factor has angle dependence [1].

$$f_m(\boldsymbol{G}) = \int \rho_m(\boldsymbol{r}) \exp\bigl(-2\pi i(\boldsymbol{G} \cdot \boldsymbol{r})\bigr) d\boldsymbol{r} \qquad (2.24)$$

where $\rho_m(\mathbf{r}) = \rho_m^+(\mathbf{r}) - \rho_m^-(\mathbf{r})$ which is the density of the magnetically polarized electron cloud of an atom, + represents up spin and – represent down spin

Magnetic structure factor of neutron is different from atomic scattering factor of X-ray since the amplitude of magnetic scattering is influenced by the direction of magnetization of a compound. In order to explain the geometry of the magnetic scattering of neutron, a magnetic interaction vector, **q**, is introduced. The magnetic interaction vector **q** is defined as follows [1] and the geometry of three vectors below is shown in Figure2.5,

$$\boldsymbol{q} = \boldsymbol{e}(\boldsymbol{e} \cdot \boldsymbol{m}) - \boldsymbol{m} \qquad (2.25)$$

,where **e** is a unit scattering vector normal to (h, k, l) plane, **m** is a unit vector of the direction of magnetic moment, $|\mathbf{e}|=|\mathbf{m}|=1$

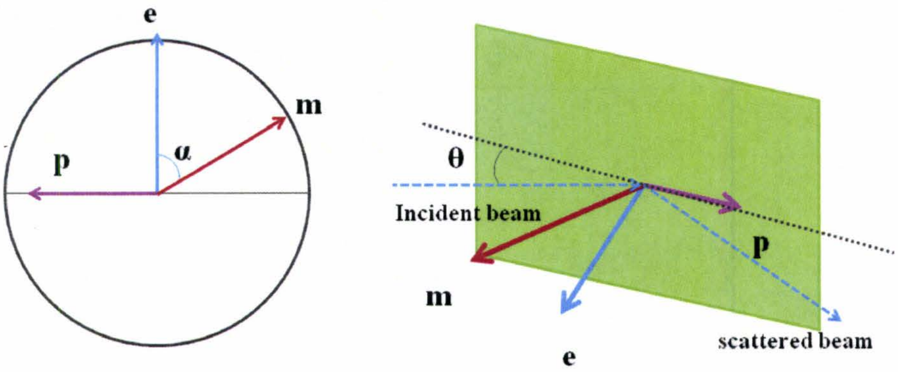

Figure 2.5 The geometry of the vectors of unit scattering vector **e**, magnetic scattering vector **m**, magnetic interaction vector **q**

When the angle between e and m is α, q is converted into [1],

(2.26)

The magnetic structure factor is given by [1] using Miller indices (h, k, l) and an atomic position vector r (x_j, y_j, z_j),

(2.27)

The intensity of magnetic scattering is proportional to F_m^{2}, and then the intensities of magnetic peaks are proportional to $q^2b_m^2$, which is also expressed using spin quantum number *S*,

$$I_{mag} \propto F_m^2 \propto q^2 b_m^2 \propto S^2 \qquad (2.28)$$

(3) Refinement of powder diffraction patterns

The obtained powder patterns are refined using the software GSAS or FULLPROF. Both programs utilize the Rietveld method to refine a crystal structure. The advantage of this method is that overlapped peaks, which are common for diffraction patterns of powder samples, are not required to be in deconvolution for the refinement of the pattern. The Rietveld method requires a good approximate model for a pattern to be refined and many parameters to input such as cell parameters, atomic positions, peak shape parameters, and so on. The peak shape parameters is known to have following relations, which is originally introduced by Caglioti et al[5] to incorporate instrumental influence on peak shape (broadening)

$$H^2 = Utan^2\theta + Vtan\theta + W \qquad (2.29)$$

H is the full width at half maximum as a function of θ. U, V, W are free valuables in this equation [2].

The assessment of the refinements is evaluated using a few R factors listed to minimize those numbers, which basically minimize the nonlinear least square of the difference between observed pattern and its calculated pattern.

Figures of Merit, which are used to evaluate the quality of a refinement, are as follows,

$$R_p = \frac{\sum_{i=1}^{n}\left|Y_i^{obs} - Y_i^{calc}\right|}{\sum_{i=1}^{n} Y_i^{obs}} \times 100\% \qquad (2.30)$$

$$R_{wp} = \left[\frac{\sum_{i=1}^{n} w_i (Y_i^{obs} - Y_i^{calc})^2}{\sum_{i=1}^{n} w_i (Y_i^{obs})^2}\right]^{1/2} \times 100\% \qquad (2.31)$$

$$R_B = \frac{\sum_{j=1}^{m}\left|I_j^{obs} - I_j^{calc}\right|}{\sum_{j}^{m} I_j^{obs}} \times 100\% \qquad (2.32)$$

$$R_{exp} = \left[\frac{n-p}{\sum_{i=1}^{n} w_i (Y_i^{obs})^2}\right] \times 100\% \qquad (2.33)$$

$$\chi^2 = \frac{\sum_{i=1}^{n} w_i (Y_i^{obs} - Y_i^{calc})^2}{n-p} = \left[\frac{R_{wp}}{R_{exp}}\right]^2 \qquad (2.34)$$

,where n is the total number of points measured in the diffraction pattern, Y^{obs} and Y^{calc} are the intensity of observed or calculated of the i^th data point, w_i is the weight of

i^{th} data point, m is the number of the independent Bragg peaks, I^{obs}_j and I^{calc}_j are the integrated intensity of observed or calculated at j^{th} Bragg peak, p is the number of free parameters in least squares refinement.

DC magnetic susceptibility

All the dc susceptibility data against temperature/applied fields were collected using a SQUID (Superconduncting QUantum Interference Device) in the MPMS (Magnetic Property Measurement System) by Quantum Design. For sample preparation, approximately 50mg of sample powder is encapsulated in a small gelatin capsule and placed in a straw. The straw is attached with the installation rod to load in the sample chamber in the MPMS. The temperature dependence of magnetic susceptibility was collected in a range of 2K – 300K, and field dependence was collected in a range of -5T to 5T if necessary.

A SQUID is a device, which is weakly superconducting (Josephson junction), and used to measure a change of magnetic flux. When a magnetic flux change induces a current in a SQUID, superconductivity of the device is destroyed at Josephson junction which generates a voltage. By measuring this voltage, the magnetic flux is calculated and then the magnitude of a magnetic moment is usually calculated [6].

There are two types of SQUID, dc-SQUID and rf-SQUID, depending on the power supply of its operation. A dc-SQUID is operated by direct current power supply while rf-SQUID is operated by radio frequency power supply. A dc-SQUID has better sensitivity however it is also sensitive to noise. A rf-SQUID is less sensitive with better tolerance to noise [6]. The MPMS used in the experiments for this thesis is a rf-SQUID.

In a MPMS, a SQUID probes the magnetic moment of a sample produced as the magnetic induction through the second-order coil, which is shown in the Figure 2.6.

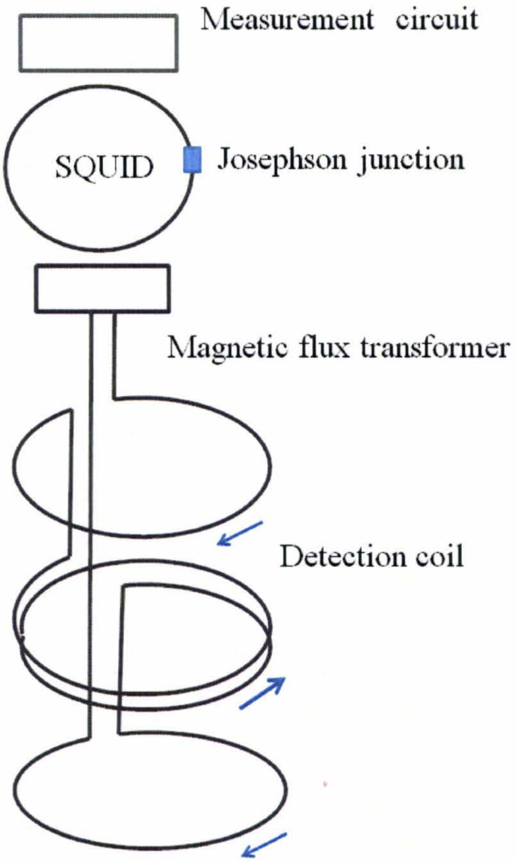

Figure 2.6 The geometry of detection coil, SQUID and magnetic flux transformer in a MPMS (magnetic property measurement system) A sample is inserted into the center of the second-order coil.

As the sample moves through the detection coil, a magnetic flux change is induced in detection coil. The change in magnetic flux inductively is coupled to the SQUID sensor and the output voltage of SQUID is proportional to the change in magnetic flux hence magnetic moment of a sample can be detected. The configuration of second-order detection coil contributes to reduce the noise of a measurement and minimize background drifts [7].

There are two mode to measure magnetic susceptibilities, dc mode and rso mode (reciprocating sample option). The rso mode has higher sensitivity than dc mode therefore the rso mode was used to collect the data.

In an actual measurement, a obtained magnetic moment in emu is converted to the magnetic susceptibility of the compound, χ, using the equation below,

$$\chi\left(\frac{emu}{mol}\right) = \frac{\dfrac{long\ moment\ (emu)}{mass\ of\ sample\ (g)/molar\ mass\ of\ sample\left(\frac{g}{mol}\right)}}{a\ field\ applied\ (Oe)} \qquad (2.35)$$

Heat Capacity

The heat capacity of a compound generally is described as an applied heat divided by the temperature change. Then, the heat capacity is expressed by the equation,

$$C = Q/\Delta T \qquad (2.36)$$

This simple equation is based on the assumption that the experimental unit is well isolated from the environment which causes heat loss. The implementation of this idea is difficult, thus an alternative method was developed.

The calorimetric technique to obtain the heat capacity of a solid used in the Oxford Maglab apparatus is called the relaxation method. In this method, the sample base is suspended (hanged) in vacuum with a weak thermal contact with a heat bath. The chip temperature (sample temperature) is given by the equation below [8],

$$T = T_1 + \Delta T_0 (1 - e^{-\frac{t}{\tau}}) \qquad (2.37)$$

,where T_1 is the initial temperature, and $T_1+\Delta T_0$ is the temperature after equilibrium is reached. From the equation is above, the temperature change is [8],

$$\Delta T = \Delta T_0 \,(1 - e^{-\frac{t}{\tau}}) \qquad (2.38)$$

The time constant, τ, is given by [8],

$$\tau = R_{TH} C \qquad (2.39)$$

.where the thermal resistivity is $R_{TH} = \Delta T_0/\Delta P$, ΔP is a applied power[8]. The illustration of the temperature change and the power supply duration is shown in Figure 2.7.

The obtained curve is fitted with the equation (2.38) and resulting T_0, τ, and R_{TH} are inserted into the equation above to calculate the heat capacity C.

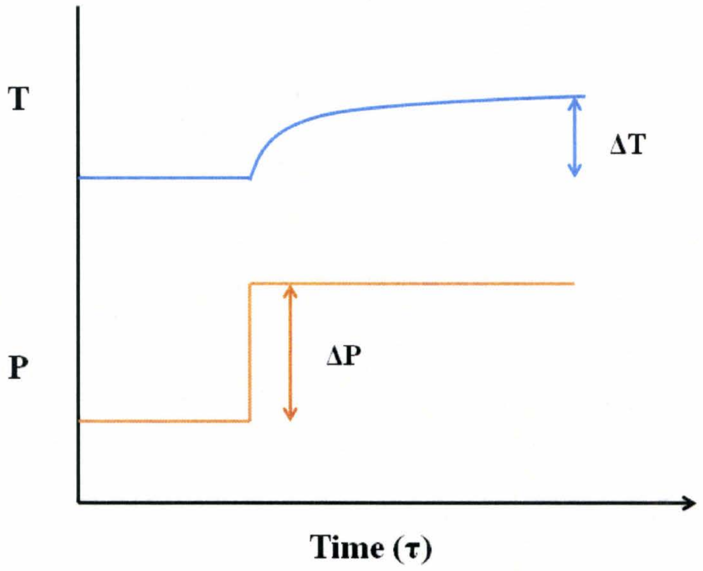

Figure 2.7 The illustration of the temperature change and the duration of power supply

The magnetic heat capacity, C_{mag}, of a magnetic compound is obtained from the subtraction of the heat capacity of a lattice from the total heat capacity if there is a distinct magnetic transition observed. Therefore non-magnetic analogue of the magnetic compound is synthesized to obtain the heat capacity of the lattice component of a magnetic compound. The obtained magnetic heat capacity is treated with the equation below [9],

$$S = \int \frac{C_{mag}}{T} \qquad (2.40)$$

to compare the entropy, *S*, consumed in a magnetic transition with the theoretical values, which is given by [9],

$$S = R \ln(2S + 1) \qquad (2.41)$$

,where R is gas constant, *S* is the spin quantum number of the magnetic ion.

Muon spin relaxation (μSR)

The muon is a probe to investigate spin dynamics of a magnetic compound similarly to NMR (nuclear magnetic resonance), in which a nucleus in a sample is a probe for any investigation. Muons are charged particles and possess spin quantum number ½. The weight of a muon is one-ninth of a proton and the magnetic moment of a muon is 3.18 times larger than a proton [10]. Muons are also recognized as "light protons" due to similarity in properties mentioned above.

Muon production is explained in particle physics as pion decay. Pions are produced from collisions of high energy protons with Be (beryllium) or C (carbon) in a meson factory. Then, the produced pions decay into muon and neutrino as shown in the equation 2.42. Thanks to the violation of parity, 100% spin polarized muons are produced in the process.

$$\pi^+(pion) \rightarrow \mu^+(muon) + \nu(neutrino) \qquad (2.42)$$

The geometry of a muon spin relaxation (μSR) measurement for ZF (zero field) and LF (longitudinal field) μSR is shown in Figure 2.8.

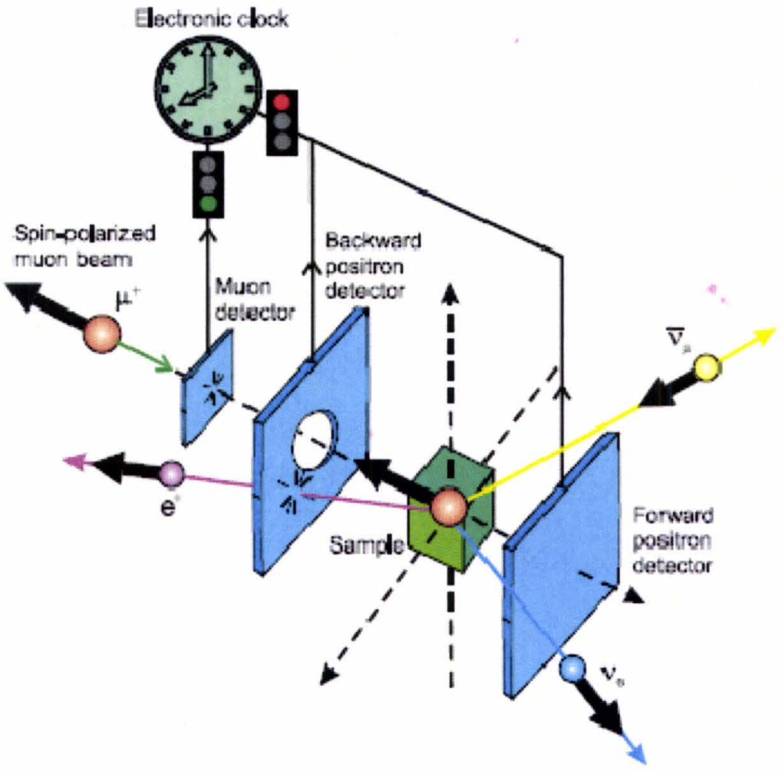

Figure 2.8 The geometry of muon spin relaxation experiment (ZF-μSR) (Permission obtained from Dr. Sonier, μSR Brochure)

The produced muons are implanted into sample and they decay into positron (e^+) and 2 neutrinos (υ_u) in micro seconds. The positrons, whose emitted direction is related to the direction of muon polarization, are detected by the back and forward detectors. The relaxation function given by the following equation, provides the information about spin dynamics in the magnetic compound [11].

$$G(t) = \frac{EF(t) - EB(t)}{EF(t) + EB\,(t)} \qquad (2.43)$$

,where $G_z(0) = 1$, EF and EB are the histograms on the forward counter and back counter, respectively, which are given by [11],

$$EF(t) = N_0 \exp\left(-\frac{t}{\tau_\mu}\right)[1 + AG_z(t)]\ ,\ EB(t) = N_0 \exp\left(-\frac{t}{\tau_\mu}\right)[1 - AG_z(t)] \qquad (2.44)$$

,where τ_μ is the average life of muons (2.2 μs), A is the initial asymmetry, which is generally ≈0.2

There are a few characteristic shapes of relaxation functions in zero field μSR (ZF-μSR), which will assist you, based on the spin dynamics. The schematic images of a well defined internal field in a compound, which generally is observed in ferromagnets and antiferromagnets, a Gaussian distribution of random fields, characteristic of a spin glass and rapidly fluctuating fields, typical of a paramagnet, are shown in Figure 2.9. In addition to the ZF-μSR, it is necessary to test static behavior of spins in the longitudinal field μSR (LF-μSR). The obtained relaxation functions are fitted with theoretically derived equations to interpret the dynamics of spins.

For a spin glass, the obtained relaxations at various temperatures are generally fitted with the Kubo-Toyabe function, which is given by [10],

$$G_z(t) = \frac{1}{3} + \frac{2}{3}(1 - \Delta^2 t^2)\exp\left(-\frac{\Delta^2 t^2}{2}\right) \qquad (2.45)$$

For a paramagnetic state, the function used for fitting is [10],

$$G_z(t, \nu) = \exp\left(-\frac{2\Delta^2 t}{\upsilon}\right) \qquad (2.46)$$

,where Δ is the width of a internal field and υ is the fluctuation rate of spins.

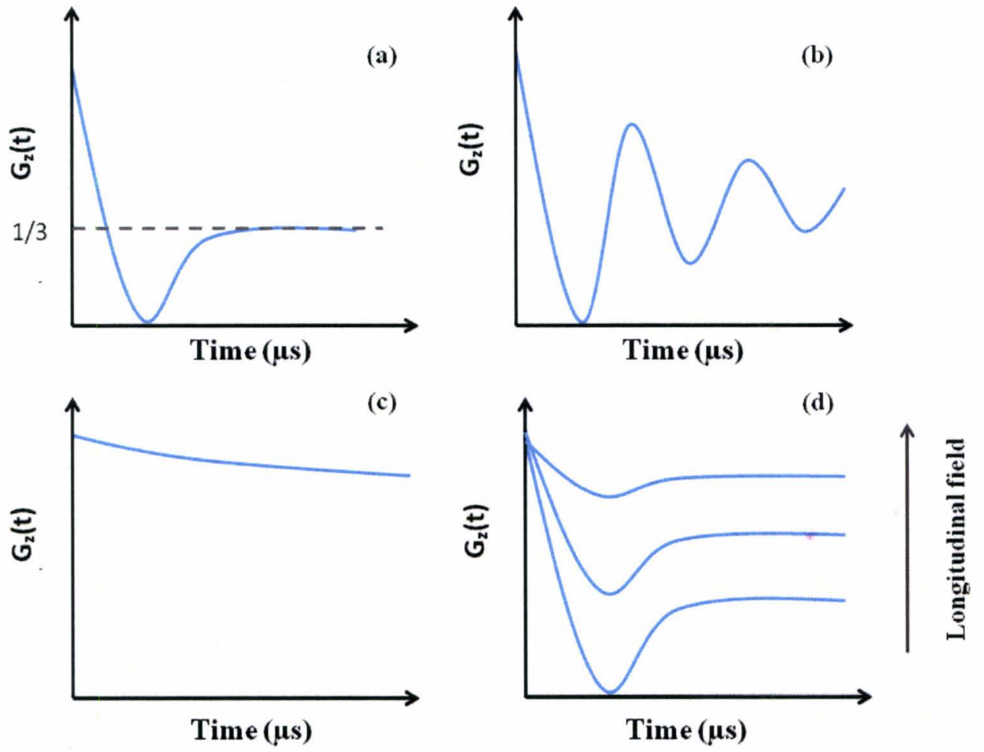

Figure 2.9 The schematic images of the relaxation functions (a) spin glass behavior: rapid relaxation (depolarization) of muons in early time and the presence of the bottom, and 1/3 recovery. This characteristic function is called the Kubo-Toyabe function. (b) a well defined field: a oscillation mode comes from the precession of muons around the local field. (c) Paramagnetic (dynamic, disordered) behavior; No relaxation or slight relaxation occurs (d) field dependence of relaxation functions, which is observable in a local static field. The higher field applies, the relaxation function shift toward up due to decoupling of muons from the local field [10,11]

^{89}Y Solid State NMR (Nuclear Magnetic Resonance)

NMR is a useful local probe to investigate not only chemical order/disorder but also magnetic order/disorder based on the information acquired as paramagnetic shift or Knight shift and a relaxation rate, $1/T_1$.

A shift in resonance peaks is observed due to the influence from the environment of the nuclear spins. An observed frequency in an experiment is expressed by [10],

$$\omega = \omega_0 + \Delta\omega = \gamma(H_0 + \Delta H) \qquad (2.47)$$

where ω_0 is the theoretical frequency for a resonance and ω is the observed frequency in the resonance, γ is a gyromagnetic ratio, H_0 is an applied field

The shift is given by $\Delta H/H_0$ based on the equation given above (2.47) and called a chemical shift, a paramagnetic shift or Knight shift in NMR.

The interaction between nuclear spins and electronic spins, which contributes to the shift, is called a hyperfine interaction. For magnetic oxides with d electron systems, the shift is defined by [10],

$$K_s = \frac{a_s \chi_s}{2\mu_B \gamma_n \hbar N} \qquad (2.48)$$

where a_s is the hyperfine constant for a given interaction, χ_s is the susceptibility of a compound, N is the number of ions, μ_B is Bohr magneton, γ_n is gyromagnetic ratio of a nucleus

The chemical order/disorder of B-site of Ba_2YMO_6 (M=Mo, Re and Ru) was probed by ^{89}Y MAS (magic angle spinning) NMR. MAS, as the name states, is a particular angle, 54.7 degrees relative to the axis of an applied field, about which the sample is rotated. Thanks to this setting, anisotropic contribution to the NMR signal are eliminated. The obtained spectra are assessed for the sign of peak position(s), the magnitude of shifts and the peak area ratio to extract the information of mixing rate if there are multiple peaks.

To interpret the sign of a peak position, the interpretation of the Li-NMR studies on lithium cathode materials by Pan et al and Lee et al [12] are employed. The sign of the peak is predicted to be dependent on the bond angle involved in spin density transfer from magnetic ion to the probing ions [12]. In their studies, the bond angle of Li-O-M (3d transition metal ion such as Mn, Cr and Co) is focused. When the bond angle is 180 degrees, the sign is predicted to be negative and negative shifts were observed in their materials [12]. If the bond angle is 90 degree, a positive shift is predicted and observed in their studies [12]. Moreover, the total magnitude of peak shift can be treated as the sum of contribution of the bonds involved [12]. The contribution from each bond is estimated by total magnitude of the shift divided by the coordination number of the probing ion. This interpretation has fitted reasonable with the results of some materials in their study, therefore the same interpretation was applied our studies. Additionally, the number of peaks in a spectrum provides the information about the number of different environments (sites) of the probing ions. For our study, there are crystallographically one Y site and one M (M=Mo, Re and Ru) site in Ba_2YMO_6 and there is the possibility of Y/M site mixing, in other words, a breakdown of B-site ordering (see Chap 1, figure 6&7). If there is only one peak in a spectrum, all the probing ions are thought in an identical environment thus there is no site mixing/substitution in the observed site. Consequently, there is no site mixing in the transition metal M ion site. If the presence of any site mixing exists, it can normally be recognized as the presence of additional peak(s) in a spectrum. According to the study by Grey et al [13] on Eu substituted yttrium titantate ($Y_2Ti_2O_7$: Eu), the presence of an extra peak was observed. This study also helps to estimate the site mixing rate by a comparison of the peak areas in a spectrum. In the study, the secondary peak, which is assigned for substitution of Y with 5 mol % Eu substitution, produces approximately 30% of total peak area (secondary: primary ≈ 30:70)[13]. Accounting for the coordination number of Y in the compound is six, the value of the peak area of an additional peak divided by the coordination number (30%/6=5%) has good match with the substitution ratio (5%).

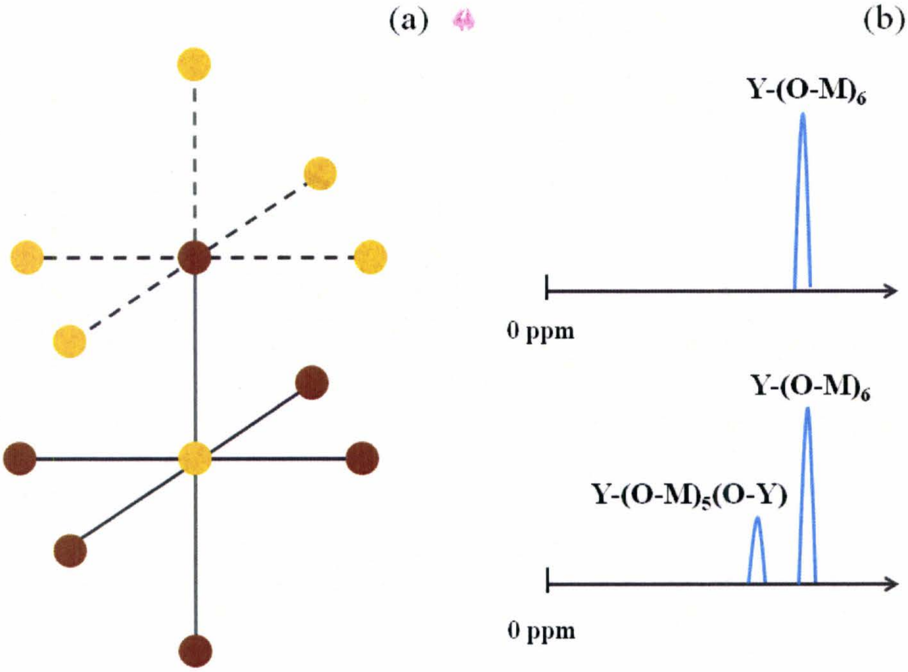

Figure 2.10 (a) the coordination geometry of Y ions in Ba_2YMO_6 (M=Mo, Re, and Ru) compounds, O ions are omitted for clarity. Yellow circles represent Y ions and brown circles are M ions (b) the illustration of spectra with no Y/M site mixing (top) and site mixing, one Y ion is altered with a M ion (bottom): note that the position of Y-(O-M)$_6$ locates at more negative ppm in this diagram.

This interpretation is also applied to explain our studies. For our cases, as described in Figure 2.10, a M ion is surrounded by six Y ions therefore abnormal behaviour of the M ion (i.e. substituted by a Y ion) influence on the six surrounding Y ions. The peak ratio produced by this irregular behaviour is divided by the coordination number of Y ions, 6, to estimate the percentage of Y/M mixing in the compounds. When the site mixing present as one Y site is substituted by M ions, which would cause a change in the spin density transferred, another peak appears in the spectrum in the positive direction [12] as illustrated in Figure 2.10.

The magnetic order of a compound is probed by a measurement of a relaxation rate ($1/T_1$) against temperature. T_1 is a relaxation time, which is the period that nuclear spins return to the original equilibrium after applied a field by exchanging the given energy to their lattice system (i.e. electronic spins) as shown in Figure 2.11.

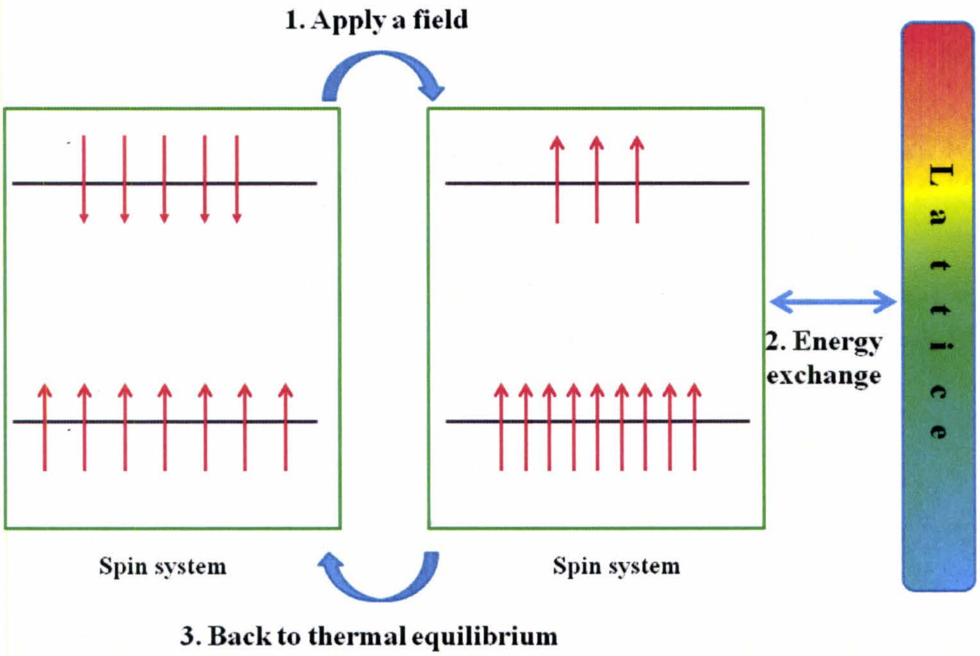

Figure 2.11 The process of T_1 relaxation. The time, which is required to return to thermal equilibrium (left) from the excited mode (right), is T_1. This process involves the energy exchange between spins and lattice to return to the original equilibrium.

The schematic image of a relaxation rate against temperature for an antiferromagnetic compound is shown in Figure 2.12. In high temperature region (a), where electronic spins fluctuate very rapidly beyond the NMR time window, the energy exchange between the nuclear spins and their lattice is not effective thus the relaxation rate is constant with the temperature. As lowering the temperature, the short range of antiferromagnetic correlation between spins develops, which is indicated as (b) region, a small drop in the relaxation rate will be observed. As approaching to the transition temperature, the relaxation rate rapidly increases. At the transition temperature of a compound, T_N, the energy exchange is thought quite rapid and T_1 becomes quite small. Thus the relaxation rate is very large, which appears as a divergence in the figure 2.12 (any signal cannot be obtained in the experiment) at this temperature as shown in figure 2.12 [14].

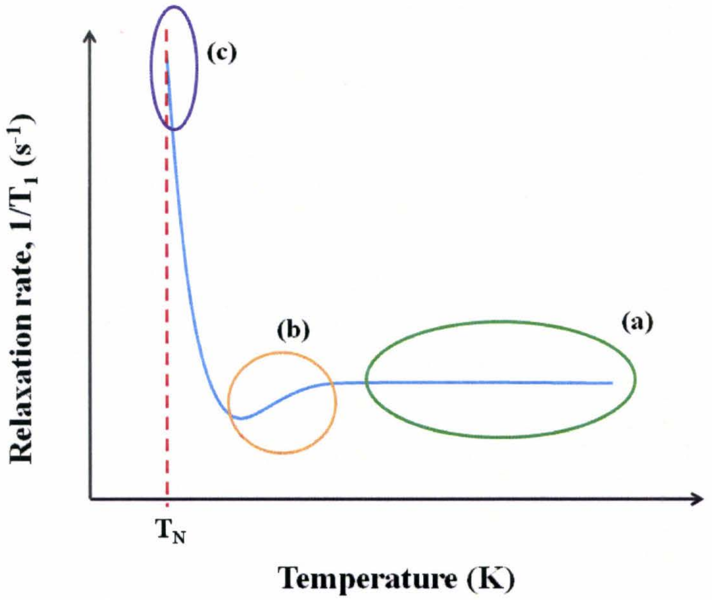

Figure 2.12 The illustration of the relaxation rate against temperature of an antiferromagnetic compound. (a) is paramagnetic region, (b) is the region with the growth of short range correlation between the electronic spins, (c) divergence at the transition temperature

According to the equation (2.48), NMR probes a local magnetic susceptibility. The magnetic susceptibility of an individual Y environment is a deconvolution of magnetic susceptibility given by a SQUID magnetometer. Reversely, the superposition of all susceptibility data taken by NMR should match with the one obtained by a SQUID magnetometer. For Ba_2YMO_6, if there are multiple Y environments, in other words, multiple behaviours of M ions, one can obtain individual magnetic susceptibilities to interpret individual spin behaviours if a suitable decomposition of the data is available.

References

[1] K. Adachi, "Magnetism of Compounds" (Localized Spin System) 3rd edition, Shokabo, Tokyo 2001

[2] V. Pecharsky and P. Zavalij, "Fundamentals of Powder Diffraction and Structural Characterization of Materials" Second edition, Springer, New York,2008

[3]Stout, G. H. Staut and L. H. Jensen, "X-ray Structure Determination" A Practical Guide, second edition, John Wiley & Sons, New York, 1989

[4] G. L. Squire, "Introduction to the Theory of Thermal Neutron Scattering" Dover Publication Inc., Mineola, New York, 1996 (originally published by Cambridge University Press in 1978)

[5] G. Caglioti, A. Paoletti and F. P. Ricci, Nuclear Instrument 3, 223 ,1958

[6] K. Kon and H. Yasuoka, "Jiki sokutei I" (Maruzen Jikkenn-butsurigaku kouza 6) Maruzen, Tokyo, 2000 (近　桂一郎、安岡　弘志、磁気測定 I　丸善　実験物理学講座 6)

[7] M. McElfresh, "Fundamentals of Magnetism and Mganetic Measurement"(Featuring Quantum Design's Mgantic Property Measurement System) MPMS application notes, San Diego Quantum Design Inc., http://www.qdusa.com/sitedocs/appNotes/mpms/FundPrimer.pdf

[8] Technical Reference note, "Heat Capacity (Relaxation) Probe" issus 1.1, Oxford Instrument, 2000

[9] E. S. R. Gopal, "Specific Heats at Low Temperatures", Plenum Press, New York, 1966

[10] S. J. Blundell, arXiv:cond-mat/0207699

[11] K. Kon and H. Yasuoka, "Jiki sokutei Ii" (Maruzen Jikkenn-butsurigaku kouza 7) Maruzen, Tokyo, 2000 (近　桂一郎、安岡　弘志、磁気測定 II　丸善　実験物理学講座 7)

[12] Y. J. Lee et al, J. Am. Chem. Soc., **120**, 12601, 1998, C. Pan et al, Chem. Mater., **14**, 2289, 2002

[13] C. P. Grey et al, J. Am. Chem. Soc.,**112**, 4670, 1990

[14] private discussion with Dr. Imai in physics at McMaster

Chapter Three

Magnetic properties of the S=3/2 geometrically frustrated double perovskites La_2LiRuO_6 and Ba_2YRuO_6

This chapter encompasses the manuscript "Magnetic properties of the S=3/2 geometrically frustrated double perovskites La_2LiRuO_6 and Ba_2YRuO_6" published in Physical Review B80, 134423 (2010). The candidate contributes all experimental parts except the NMR measurements. The candidate contributes the interpretation of all results and preparation of the manuscript.

With permission of the reproduction of the article; Tomoko Aharen, John E. Greedan, Fanlong Ning, Takashi Imai, Vladimir Michaelis, Scott Kroeker, Haidong Zhou, Chris R. Wiebe and Lachlan M.D. Cranswick, Physical Review B80, 134423 (2009), copyright 2010 by the American Physical Society.

Magnetic properties of S=3/2 geometrically frustrated double perovskites, La_2LiRuO_6 and Ba_2YRuO_6.

Tomoko Aharen[1], John. E. Greedan[1,2], Fanlong Ning[2,3], Takashi Imai[2,3,4], Vladimir Michaelis[5], Scott Kroeker[5], Haidong Zhou[6], Chris R. Wiebe [6,7] and Lachlan M.D. Cranswick[8]

[1]Department of Chemistry, McMaster University, Hamilton, Ontario, L8S 4M1, Canada,

[2]Brockhouse Institute for Materials Research, McMaster University, Hamilton, Ontario, L8S4M1, Canada, [3]Department of Physics and Astronomy, McMaster University, Hamilton, Ontario, L8S 4M1, Canada, [4]Canadian Institute for Advanced Research, Toronto, Ontario, M5G 1Z8, Canada, [5]Department of Chemistry, University of Manitoba, Winnipeg, MB, R3T 2N2, [6]Department of Physics, Florida State University, Tallahassee, 32310-4005, USA,

[7]National High Magnetic Field Laboratory, Florida State University, Tallahassee, 32310-4005, USA, [8]Canadian Neutron Beam Centre, National Research Council, Chalk River Laboratories, Chalk River, ON K0J 1J0, Canada

Abstract

Two B-site ordered double perovskites, Ba_2YRuO_6 and La_2LiRuO_6, have been re-investigated as part of a systematic study of geometric magnetic frustration in this class of oxide materials. Both involve Ru^{5+}($4d^3$, S = 3/2) as the magnetic ion residing on a face-centered cubic lattice – one of the canonical frustrated lattices. Results from d.c susceptibility, neutron diffraction, heat capacity, ^{7}Li and ^{89}Y NMR studies are presented. La_2LiRuO_6 ($P2_1/n$) shows long range antiferro-magnetic (AF) order below 24K from ^{7}Li NMR, heat capacity and magnetic susceptibility (Fisher's heat capacity) data which is well below the susceptibility maximum at 30K. Analysis of the entropy loss and the ^{7}Li data indicates the importance of short range spin correlations at higher temperatures, consistent with a frustrated system. Ba_2YRuO_6 retains Fm3m symmetry found at room temperature down to 2.8K with cell constants, a=8.33559(9)Å and a=8.3239(5)Å, respectively. However, ^{89}Y-MAS NMR detects a very low ~ 1% site mixing between Y and Ru ions. Magnetic susceptibility data are more complex than reported previously with two broad peaks around 37K and 47K. The transition temperature is 36K from heat capacity and variable temperature neutron diffraction data. The Weiss temperatures and frustration indices, $|\theta|/T_N$, for Ba_2YRuO_6 are -522K and 16, while much smaller values are observed for La_2LiRuO_6, -184K and 8, which can be attributed to the monoclinic structural distortion in the latter which weakens the superexchange interactions.

Introduction

Geometrically frustrated antiferromagnetic (AF) materials have attracted considerable interest over the past few years [1]. Such compounds often exhibit rather exotic magnetic ground states such as the spin glass, spin liquid or spin ice states instead of long range order as might be expected from the third Law of thermodynamics. Among such materials, the B-site ordered double perovskites, $A_2BB'O_6$, are a relatively less studied class. In this case a magnetic ion resides on the B' site, while B is nonmagnetic. Both the B and B' sites constitute interpenetrating face centered cubic sublattices, Figure 3.1, which, if the exchange constraint between nearest B' neighbors is antiferromagnetic, the basic criteria for geometric frustration are satisfied. The conditions for B- B' site ordering have been presented in the form of a phase diagram [2] and the space group family tree has been constructed[3]. For tolerance factors near unity, cubic symmetry is usually found which in this case is Fm3m. As the tolerance factor decreases the symmetry lowers and one finds cases of I4/m, $P2_1/n$ or P-1, for example.

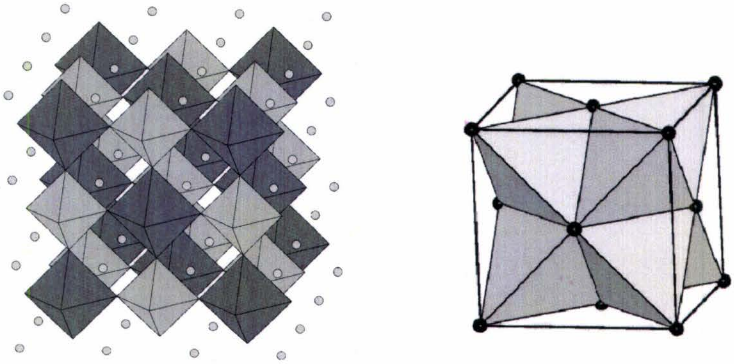

Figure 3.1.(Left) The crystal structure of B site ordered double perovskite,$A_2BB'O_6$. The grey spheres, light grey octahedra and dark grey octahedra represent A ions, BO_6 octahedra and $B'O_6$ octahedra, respectively. (Right) The geometrically frustrated face-centered-cubic lattice of edge sharing tetrahedra formed by both the B and B' sites.

A notable feature of B-site ordered double perovskites is the versatility of this structure type to chemical substitution. Indeed, much of the periodic table can be accommodated [2]. The large A-site ions are generally from Group 2 or 3 and the B and B' ions from the transition series 3d – 5d and 4f or small Group 1, 2 or 3 ions. Thus, this class of perovskites permits the systematic study of the effects of changes in, for example, the spin quantum number, S, and the space group and B' point group symmetry, which controls the "orbital ordering", on magnetic properties. For example in the Fm3m structure the site symmetry at B' is rigorously cubic, m3m, while for $P2_1/n$ this symmetry is reduced to -1. Thus, for electronic configurations of the type $t_{2g}{}^n$, the t_{2g} orbitals remain degenerate in m3m but this degeneracy will be lifted in -1. In this work the B site contains diamagnetic Y^{3+} and the B' site is occupied by Ru^{5+}, $4d^3(t_{2g}{}^3)$ and S = 3/2. Note that this ion is always an orbital singlet in a crystal field of octahedral symmetry, neglecting spin orbit coupling, and orbital ordering will not be an issue. In subsequent papers, studies of materials with controlled space group and local symmetry but with quantum spins, S =1 and S = ½ will be presented. There exists already evidence that quantum spin double perovskites behave rather differently than the S = 3/2 analogs. For example the S = ½ compounds Sr_2CaReO_6 ($P2_1/n$) [4] and Sr_2MgReO_6 (I4/m) [5] do not show long range AF order but instead, spin glass ground states.

A number of materials with Fm3m symmetry have been studied in the early 1990's such as the series Ba_2BRuO_6 where B = Y and Lu [6]. These phases were reported to be well-ordered Fm3m double perovskites which showed AF order (f.c.c. Type I) at ~

35K for the B = Lu compound, the Y case was not reported. As well, large, negative Weiss temperatures in the range of –630K were found suggesting a high degree of frustration by the frustration index criterion, $f \sim |\theta|/T_N \sim 18$ [7].

A Ru^{5+} based double perovskite with lower symmetry ($P2_1/n$), La_2LiRuO_6, has been studied more recently [8]. Again, this compound showed long range AF order (f.c.c. TypeI) at 4K and a susceptibility maximum at 30K. ^{7}Li MAS NMR indicated only one sharp peak which along with the refinement of neutron diffraction data indicated a well-ordered double perovskite. The exact value of T_N was not reported but assuming a value of ~ 30K and given θ_C = -167K, La_2LiRuO_6 is significantly less frustrated, f ~ 6, than Ba_2YRuO_6, f ~ 18, as already mentioned.

In this work, La_2LiRuO_6 and Ba_2YRuO_6 have been re-investigated within the context of geometric magnetic frustration. For the former, ^{7}Li NMR studies along with heat capacity and magnetic susceptibility data provide an accurate measure of T_N which is significantly lower than reported previously. For the latter, ^{89}Y MAS NMR indicate some degree of Y/Ru site disorder which is not easily detected from the neutron data. As well, the magnetic susceptibility is more complex than reported previously, showing signs of significant short range correlations above the critical temperature which is confirmed by neutron diffraction. Heat capacity measurements determine an accurate value for T_N, which was not reported in earlier studies. The study of these two materials provides a context for subsequent papers which will describe the results of lowering the spin quantum number to 1 and ½ in a set of exactly iso-structural materials.

Experimental Procedures.

La_2LiRuO_6 and Ba_2YRuO_6 were prepared using conventional solid state reactions. For La_2LiRuO_6 [7], a stoichiometric mixture of La_2O_3 (Aldrich, 99.9%) (pre-fired at 900°C to remove surface contaminants), RuO_2 (Alfa Aesar, 99.95%), and 10% excess of Li_2CO_3 (J.T. Baker Chemical Co., 99.1%) was ground, pelletized, heated to 600 °C and kept at that temperature overnight. This was followed by gradual heating up to 700 °C for one day and a final firing at 900 °C for about 2 days to complete the reaction. For Ba_2YRuO_6 [6], a stoichiometric mixture of the starting reagents, $BaCO_3$ (T. Baker Chemical Co.), Y_2O_3 (Alfa Aesar, 99.9%) (pre-heated) and RuO_2 (Alfa Aesar, 99.95%), was ground, pelletized and heated to 1350 °C for a total of 5 days with intermittent re-grinding. In addition to that, non magnetic analogues for both samples, La_2LiIrO_6 and Ba_2YTaO_6, were prepared. For La_2LiIrO_6, a mixture of La_2O_3 (pre-heated), Li_2CO_3 (10% excess) and Ir powder (CERAC, 99.9%) was heated in O_2 flow and kept at 1123K for 96 hours. For Ba_2YTaO_6, a stoichiometric mixture of $BaCO_3$, Y_2O_3 and Ta_2O_5 (Alfa Aesar 99.99% and SPEX) was heated in air at 1350 for about 3 days in total with intermediate regrinding. The purity of the samples was tested by X-ray diffraction using a Guinier-Hägg camera with Cu $K\alpha_1$ radiation.

Magnetic susceptibility was measured for both samples within the temperature range 2K (or 5K) to 300K using a Quantum Design magnetic properties measurement system superconducting quantum interference device magnetometer at McMaster

University. Zero-Field Cooling (ZFC) and Field Cooling (FC) data were obtained with an applied field of 500 Oe.

Heat capacity measurements were carried out for La_2LiRuO_6 and Ba_2YRuO_6 using an Oxford Maglab over the temperature ranges of 8K-49.9K, 5K-56.5K, respectively. Also, the heat capacity for La_2LiRuO_6 and its lattice match compound were measured at Florida State University using a Quantum Design physical properties measurement system in the temperature range of 2K - 70K. To extract magnetic heat capacity, the non-magnetic analogues of both samples, La_2LiIrO_6 and Ba_2YTaO_6 were prepared and the heat capacities of both samples were subtracted as lattice contribution on total heat capacities.

Neutron diffraction data were obtained for Ba_2YRuO_6 on the C2 diffractometer at the Canadian Neutron Beam Centre operated by the National Research Council of Canada at the Chalk River laboratories of Atomic Energy of Canada. The data were collected at 2.8, 20, 30, 33, 35, 40, and 298K with neutron wave lengths of 2.7319Å and/or 1.3305Å depending on measurement temperature. The crystal structure and magnetic structures were refined using GSAS[9] and FULLPROF [10].

For La_2LiRuO_6, the ^7Li NMR spin-lattice relaxation rate, $1/T_1$, as a function of temperature was measured at McMaster University over the temperature range 23.3K to 290K.

For Ba_2YRuO_6, ^{89}Y MAS NMR (magic-angle-spinning solid state nuclear magnetic resonance) was carried out in the department of Chemistry at the University of Manitoba. The spectrum was acquired using a Bloch pulse on a Varian Inova^{Unity}

600 (14.1T) spectrometer operating at a Larmour frequency, ν_L of 29.36 MHz. The black powdered sample was packed in a ZrO_2 MAS rotor with a 22 μL fill volume and spun to 20 000 +/- 6 Hz. Acquisition was carried out at room temperature using a 30° tip angle (rf of 42 kHz) on a 3.2 mm DR (H/F-X) Chemagnetics MAS probe, 470 784 co-added transients were collected with a recycle delay of 0.5 s. All spectra were referenced with respect to 2M $Y(NO_3)_3$ at 0.0 ppm.

Results and Discussion

La_2LiRuO_6.

The obtained powder sample was tested by X-ray diffraction and confirmed to be single phase. The temperature dependence of the magnetic susceptibility was measured as shown in Figure 3.2. The data were fitted to a Curie-Weiss Law with inclusion of a small temperature independent term, $\chi = C/(T - \theta) + \chi(TIP)$, giving the parameters C = 1.93(5) emu-K/mol, θ = -185(5)K and $\chi(TIP) = 5.1(5) \times 10^{-4}$ emu/mol. The Curie constant is in reasonable agreement with the expected spin-only value for a S = 3/2 ion, 1.87 emu-K/mol, and θ is slightly larger than that reported in [8], -167K. The inset in Figure 3.2 shows the low temperature data indicating a maximum at 29K-30K, as reported previously, and a ZFC/FC divergence below ~ 70K. These data were analyzed further by plotting d $\chi T/dT$ vs T, i.e., the Fisher heat capacity [11], shown in Figure 3.3, in which the relatively sharp peak at ~ 24K indicates that this is the true T_N for this material.

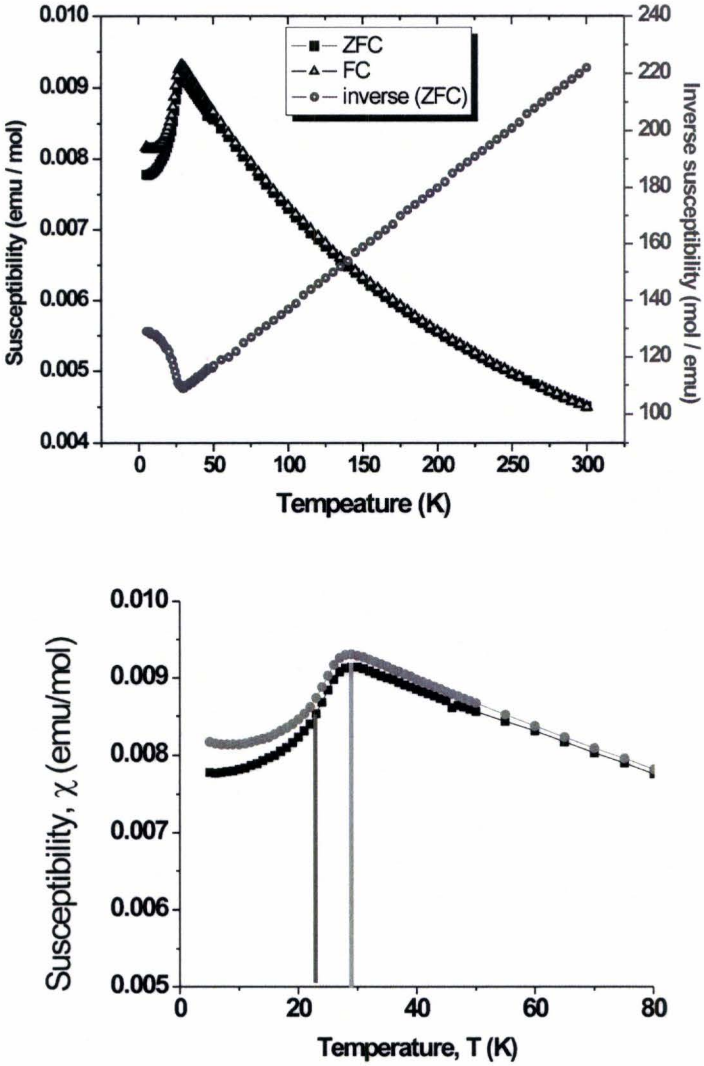

Figure 3.2. (top)The temperature dependence of the magnetic susceptibility and inverse magnetic susceptibility of La_2LiRuO_6. FC data were measured with an applied field of 500Oe. (bottom) the susceptibility near the temperature region around the transition. The right vertical line marks the susceptibility maximum and the left line locates the transition temperature from the heat capacity and NMR measurements.

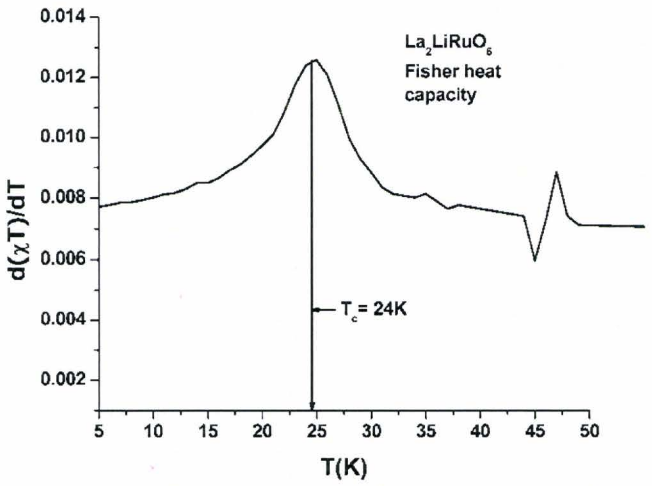

Figure 3.3. Fisher's heat capacity of La_2LiRuO_6.[11]

To verify this, the thermal heat capacity of La_2LiRuO_6 was measured from 2 to 70K. Note, Figure 3.4, the somewhat broad maximum around 23K-24K, whereas one might have expected a sharper λ-type anomaly. Shown also are data for the lattice match material, La_2LiIrO_6. In this compound the $Ir^{5+}(5d^4)$ ion is a single ion singlet state and has only a very weak temperature independent paramagnetic contribution.[12] Subtraction of the lattice match data, shown in the inset, sharpens the peak somewhat. The subtracted magnetic component of heat capacity indicates that about 53.7% of the theoretical total entropy, $S = R\ln(2S+1)$, where R is the gas constant and S is the spin quantum number, was lost during this transition. This suggests that short range correlations at higher temperatures are important which is consistent with a high level of frustration in this material.

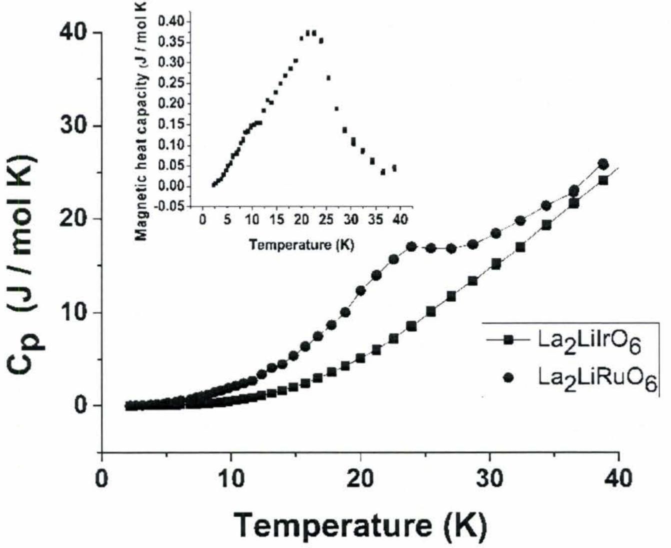

Figure 3.4. The heat capacity of La_2LiRuO_6 and the lattice match compound, La_2LiIrO_6. The magnetic heat capacity shows a somewhat broadened peak centered around 23K. The inset shows the magnetic heat capacity, C_{mag}/T versus T, from which the magnetic entropy of this compound was calculated. The entropy loss below 40K is 54% of the theoretical total. (See text)

Finally, further insight can be provided by study of the temperature dependence of the ^{7}Li nuclear spin lattice relaxation rate ($1/T_1$), Fig. 3.5 as the NMR experiment probes the local, low frequency spin dynamics. Note first that the data are roughly temperature independent above ~ 150K. This is indicative of paramagnetic (uncorrelated spins) behavior in the exchange narrowing limit as the electron spins fluctuate rapidly. Below about 70K, which is also roughly the temperature for which the ZFC/FC divergence in the bulk susceptibility becomes detectable, ($1/T_1$) begins to increase, indicating the onset of short range spin-spin correlations. The increase becomes very rapid below about 35K and shows a divergence around 24K (23.8K) as shown in Fig.3.5 due to the critical slowing down toward a long range ordered state. Thus, the ^{7}Li NMR data confirm T_N =23.8K for this material and provide further evidence for the importance of short range spin correlations at temperatures well above T_N, a feature expected for a frustrated spin system.

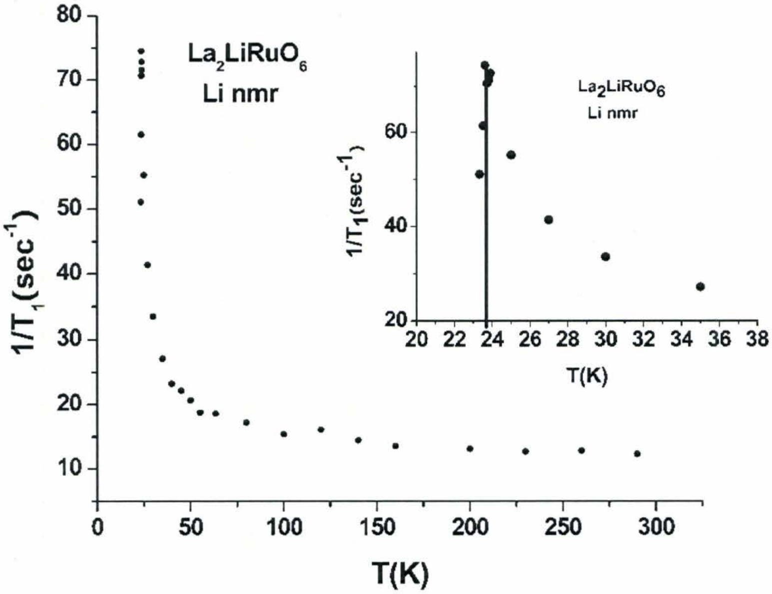

Figure 3.5. The ^{7}Li nuclear spin-lattice relaxation rate, $1/T_1$, as a function of temperature. The inset shows the divergence near the transition temperature, 24K.

Ba_2YRuO_6

Structural Details – Y/Ru order-disorder.

In the phase diagram of Anderson et al [2], this compound, with a B-site formal charge difference of two and size difference of Δr = 0.34 Å, [13] lies near the border for B-site order. It is of great interest to determine the degree of Y^{3+}/Ru^{5+} site order which has not been addressed previously. While the crystal structure of this material, refined from neutron powder diffraction data, had been reported earlier [6], a new study was carried out, along with MAS ^{89}Y NMR to address this question. The neutron scattering lengths for Y and Ru are relatively similar, 7.75 and 7.03 fm, respectively, about a 10% difference. The situation is similar for x-rays with about the same level of contrast, which is somewhat problematic for analysis of powder data for either case. However, in addition to the scattering power at the B and B' sites, the O^{2-} positional parameter,(x 0 0), is a critical measure of order/disorder. For the fully disordered model, which would be described in Pm3m rather than Fm3m with a unit cell edge of half the length, x = ¼ (retaining the Fm3m setting) and the B – O and B' – O bond lengths would be equal. Thus, the deviation from x = ¼ is a measure of site ordering. As neutrons are more sensitive to oxygen than x-rays, this is the diffraction method of choice.

Before proceeding to the results, it is important to review the general situation with B-site order in double perovskites. While the aforementioned phase diagram of Anderson et al gives a rough guide to the likelihood of B/B'-site order, more detailed studies exist, especially by Woodward et al who have focused on the B^{3+}/B'^{5+} case which is most relevant here. [14,15] To summarize some of their findings, for $\Delta r < 0.260$ Å, 100% B/B' -site order is never found, with one exception. The extent of B/B' site order is determined quantitatively by refinement of neutron powder diffraction data and it is remarked that in all cases of partial order, the hkl all-odd supercell reflections are measurably broader than the hkl all-even subcell reflections. For example, among the Fm3m phases studied, Ba_2YNbO_6 is judged to be 100% ordered,

$\Delta r = 0.260$ Å, while Ba_2ScNbO_6 and Ba_2ScTaO_6, with $\Delta r = 0.105$ Å, show only about 50% order. With smaller A-site ions and lower crystal symmetry, the degree of B/B'-site order appears to increase for the same combination of ions. For example Sr_2ScNbO_6 and Ca_2ScNbO_6, both $P2_1/n$ materials, show order levels of 69% and 96%, respectively. Ca_2YNbO_6 is classified as 100% ordered. Applying these findings to the specific case of Ba_2YRuO_6, where $\Delta r = 0.34$ Å, one would then expect ~100% B/B' - site order.

The results of the refinement of the neutron diffraction data at 299.6K on a fully ordered B/B' – site model are shown in Fig. 3.6 and Tables 3.1 and 3.2. The atomic positions and derived interatomic distances are in excellent agreement with those of ref. [6]. The observed atomic displacement parameters (ADP), U_{iso}, do not suggest that B/B' site disorder is significant. The anisotropic U_{ij} values for the O-site are very similar to those obtained for Ba_2YNbO_6, i.e. $U_{11} < U_{22} = U_{33}$, with a somewhat disc-like ellipsoid for the site.[14] Attempts to refine the occupation rates of the Y and Ru sites using the constraints applied in reference [14], did not yield reasonable values. Refinements imposing a few percent Y/Ru site mixing did yield reasonable results but for mixing greater than ~ 5 %, U_{iso} for the Ru site became negative. Finally, a comparison of the peak widths of the super cell and sub cell reflections, Table 3, does not constitute evidence for site disorder, either from the x-ray or neutron data. Taken together, the above observations suggest either negligible or at most, very slight, Y/Ru site mixing.

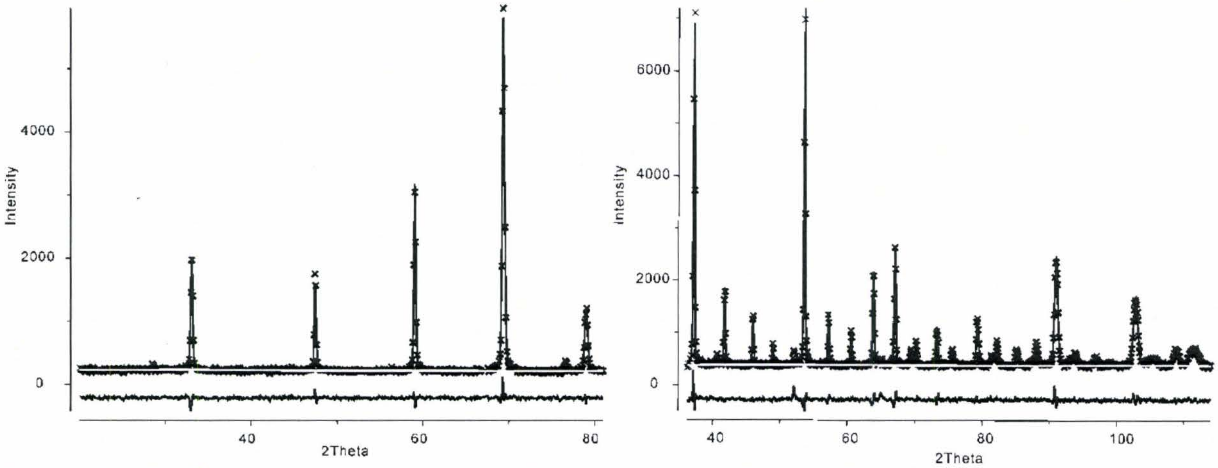

Figure 3.6. Refinement of the neutron diffraction data of Ba_2YRuO_6 using the GSAS software package [10] for two wavelengths, 2.37Å, left panel and 1.33Å, right panel, showing the experimental data (+) and the fit as a solid line. The vertical tic marks represent the Bragg peak positions and the bottom line is the difference between the calculated and experimental profiles.

Table 3.1 The atomic coordinates, isotropic displacement factors at 299.6K for Ba_2YRuO_6 (Space Group F m -3 m) R_{wp} = 0.0571, χ^2=1.6, cell constant a = 8.33559(9)Å. Anisotropic displacements refined for O: U_{11} = 0.0032(10), U_{22}=U_{33} = 0.0106(4) (Å^2)

atom	x	y	z	U_{iso} (Å^2)
Ba	0.25	0.25	0.25	0.0067(5)
Y	0.5	0.5	0.5	0.0082(18)
Ru	0	0	0	0.0049(19)
O	0.26513(24)	0	0	0.0103(4)

Table 3.2. Interatomic distances between oxygen and the B (B') site ions.

	distance (Å)	O-B-O angle (deg.)
Y - O	2.2175(20)	90, 180
Ru - O	1.9505(20)	90, 180

Table 3.3. Comparison of peak widths for super cell (all odd) and sub cell (all even) reflections for Ba_2YRuO_6, both powder neutron and x-ray data.

Neutron Data 3.8K

Reflection	Width (FWHM)(deg)	Ratio (super/sub)
(111)	0.24(6)	
		0.98(24)
(200)	0.244(3)	
(331)	0.33(1)	
		0.90(4)
(420)	0.365(4)	

X-ray Data 298K

(111)	0.087(4)	
		1.07(9)
(200)	0.081(3)	

Nonetheless, the ^{89}Y MAS NMR data of Figure 3.7 present evidence of a low level of site mixing. Here two distinct peaks are seen at chemical shifts of –5100 and -5860 ppm, with integrated areas in the ratio of roughly 7 and 93 ± 3 %, respectively. Assignment of these peaks and the interpretation of their relative intensities follows the related work of Grey et al. [16] where multiple ^{89}Y MAS NMR peaks observed in pyrochlore oxides $Y_{2-x}Ln_xTi_2O_7$ were interpreted in terms of the number of next-nearest neighbor cations. In $Y_{1.9}Eu_{.1}Ti_2O_7$ for example, peaks were assigned to Y – $(O\text{-}Y)_6$ and Y – $(O\text{-}Y)_5(O\text{-}Eu)$ with a ratio of intensities of ~ 3/1. While the Eu substitution level is only 5%, its influence is multiplied by the coordination number at the Y site, six, so the relative intensity of the two NMR peaks is in the ratio 3/1 rather than 20/1. Thus, in the spectrum of Ba_2YRuO_6 it is reasonable to assign the major peak at –5860 ppm to the environment Y – $(O\text{-}Ru)_6$, and the minor peak at –5100 ppm to Y – $(O\text{-}Ru)_5(O\text{-}Y)$. From the observed relative intensities we infer a Y/Ru mixing level of about 1%. This is certainly consistent with the neutron diffraction results for Ba_2YRuO_6 and illustrates in addition the power of the MAS method in detecting low levels of site mixing. It is worth noting that the ^{89}Y NMR peaks seen here are shifted significantly out of the known ^{89}Y chemical shielding range of 60-340 ppm for oxides, even exceeding that of the highly shielded cuprate Y_2BaCuO_5 at -1250 ppm, [17] and indicating that a significant amount of unpaired electron density is present at the Y nucleus. A detailed understanding of a shift of this magnitude requires further study.

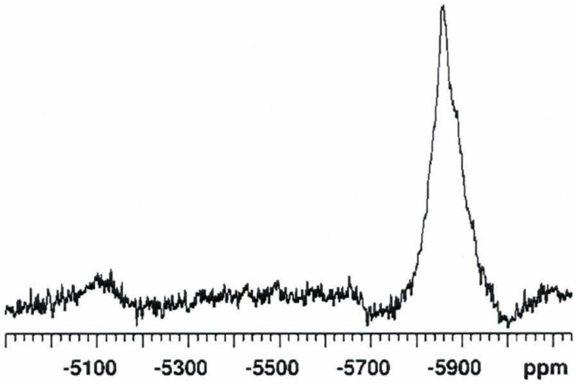

Figure 3.7. The ^{89}Y MAS NMR resonance peaks for Ba_2YRuO_6 at room temperature showing two distinct peaks at –5100 and –5880 ppm.

Magnetic Properties.

The magnetic susceptibility for this compound is shown in Fig. 3.8 and (inset) displays two broad peaks, around 37K and 47K. The ZFC/FC curves show a slight divergence around 115K. The inverse magnetic susceptibility was fitted with the Curie-Weiss law giving θ = -571(3) K and C = 2.69(1) mol/emu-K. The Curie constant is larger than the spin-only value of 1.88 mol/emu-K but agrees very well with that reported previously [6]. It is possible that a true Curie-Weiss regime does not exist for this compound below 300K. The weak upturn in the susceptibility at low temperatures is attributed to paramagnetic impurities. The data below 10K were fitted to a Curie-Weiss law with an added temperature independent term with the resulting parameters C = 0.001 mol/emu-K, θ = -1.3K and χ(TIP) = 4.0 x 10^{-3} emu/mol. This indicates that the paramagnetic impurity level is well below 1%.

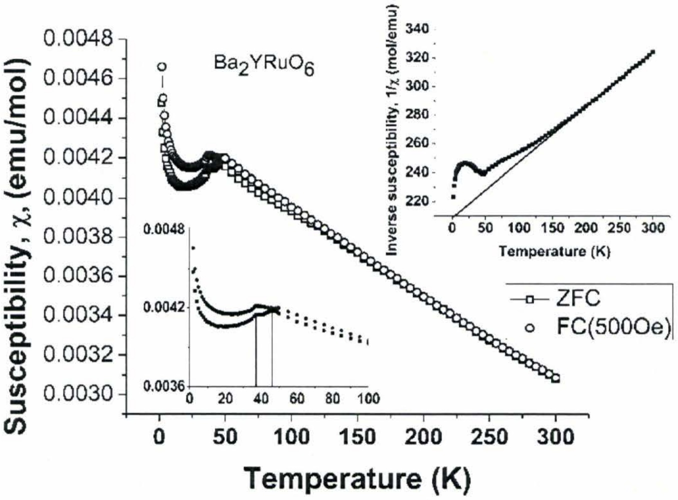

Figure 3.8. The temperature dependence of the magnetic susceptibility of Ba_2YRuO_6. The inset shows clearly the two maxima at 47K and 36K and the Curie-Weiss behavior

The observation of two susceptibility maxima was not reported previously and it is unclear which, if either, represents a transition to long range order. Thus, the heat capacity was measured, as shown in Fig.3.9. A sharp λ-type anomaly is evident at 36K, while no feature is observed at 47K. Therefore, the real transition temperature for Ba_2YRuO_6 is 36K. This gives a frustration index, f ~ 16 which is slightly smaller than the value of 18 reported earlier, but still indicative of a highly frustrated system. The broad susceptibility maximum at ~ 47K is thus attributed to short range spin correlations which are expected for a highly frustrated magnet above the critical temperature. The entropy loss below 44K was estimated for this material from the data shown in the inset of Fig. 3.9 to be 2.69 J/mol-K which is only 24% of the expected value for S = 3/2. This is further evidence for the importance of the postulated short range correlations above T_N.

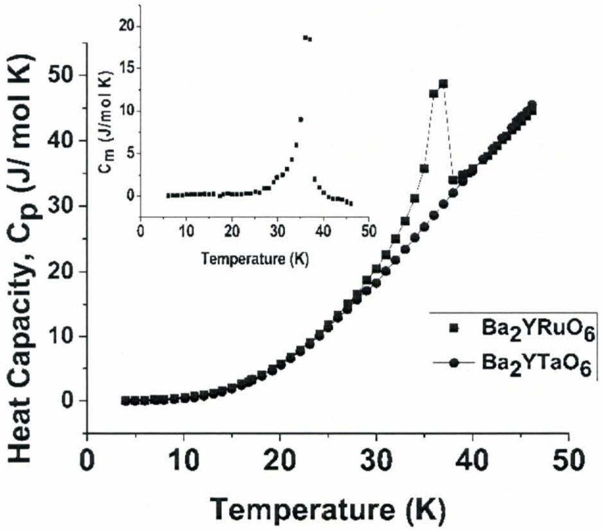

Figure 3.9. The heat capacity of Ba_2YRuO_6 and its lattice match analogue, Ba_2YTaO_6. Note the sharp lambda anomaly at 36K. The inset shows a plot of C_{mag}/T vs T from which the entropy removal (~ 24% of the theoretical value) was estimated.

To corroborate the heat capacity result and add more insight to the interpretation of the susceptibility data, neutron diffraction measurements were carried out at various temperatures above and below T_N. The Type I f.c.c. magnetic structure reported previously was confirmed with an ordered Ru^{5+} moment of 2.1(1)μ_B, much below the spin only value of 3 μ_B, but again in line with [6]. As well, the temperature dependence of the (100) magnetic reflection, Fig.3.10, is consistent with T_N = 36K. The critical exponent, β, derived from these data is 0.296(5) but the number of data points within the critical region is small and this value cannot be considered as highly accurate. Note also, inset, that magnetic scattering persists in the form of a broad, diffuse feature even at 39.8K, which is direct evidence for short range magnetic correlations. This peak was fitted to the standard Ornstein-Zernike Lorentzian of the form $I(Q) = A/((Q - Q_0)^2 + \kappa^2)$ where $Q = 4\pi\sin\theta/\lambda$ and κ is the inverse correlation length.[18] The derived values are $Q_0 = 0.750(4)$ Å^{-1} and $\kappa = 0.06(1)$ Å^{-1}, giving a correlation length, $\xi = 17(4)$ Å, which is approximately two unit cell lengths. The origin of this short range order likely results from the high level of geometric magnetic frustration. Note that the low, ~ 1%, level of site disorder is insufficient to destroy long range AF order which is clearly the ground state for this S = 3/2 material.

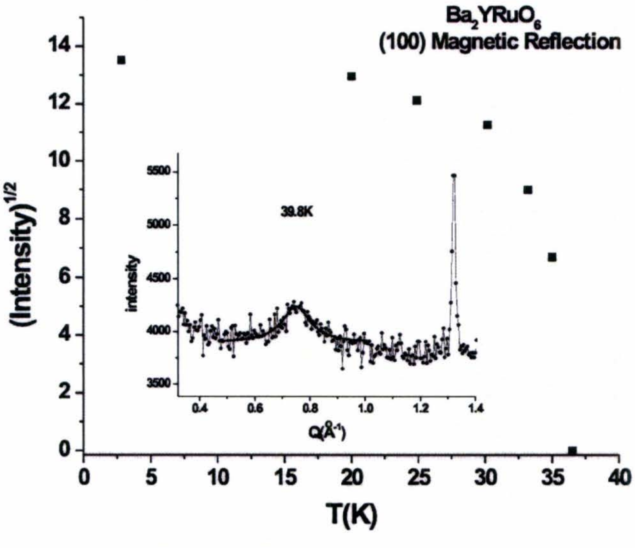

Figure 3.10. The intensity of the (100) magnetic reflection versus temperature below 37K. The data above 30K have been fitted to extract the critical exponent $\beta = 0.296(5)$. The inset shows the broad peak indicative of short range magnetic correlations at 39.8K. This feature at $Q = 0.750(4)$ Å^{-1} is fitted to the standard Ornstein-Zernike Lorenztian line shape [16] giving a correlation length, $\xi = 17(4)$ Å.

Summary and Conclusions.

Two B-site ordered double perovskites, La_2LiRuO_6 and Ba_2YRuO_6, with Ru^{5+} (S = 3/2) as the only magnetic ion, have been re-investigated from the perspective of the geometric magnetic frustration expected for the f.c.c. magnetic lattice. Both are indeed highly frustrated magnets with frustration indices, f ~ 9 and 16 for La_2LiRuO_6 and Ba_2YRuO_6, respectively. Heat capacity and ^{7}Li NMR data establish T_N = 23.8K in spite of the susceptibility maximum at ~ 30K for La_2LiRuO_6. The NMR results also show evidence for short range spin correlations well above T_N. Evidence for Y/Ru site disorder at the level of about than 1% is found from ^{89}Y MAS NMR for Ba_2YRuO_6. This latter phase shows a more complex bulk magnetic behavior than reported previously with two maxima at 47K and 36K. Heat capacity and neutron diffraction data establish T_N = 36K. Significant short range spin correlations are evident above T_N at 39.8K with a correlation length of ~ 17 Å which is about two cubic cell edge lengths. In spite of the high levels of frustration in both compounds and the presence of slight Y/Ru site disorder in one, the ground state is long range AF order for these S = 3/2 magnets. Subsequent studies will focus on isostructural S = 1 and S = ½ double perovskites to investigate the role of S among other factors on the determination of the ground state.

Acknowledgements

We would like to thank to Paul Dube for assistance in measuring susceptibilities and heat capacities at McMaster. J.E.G. and T.I thank NSERC for Discovery Grants. T.I.

also thanks the Canadian Foundation for Innovation and the Canadian Institute for Advanced Research. CRW thanks the NSF for funding through grant number DMR-08-04173. S.K. acknowledges CFI and NSERC for support. V.K.M. is grateful to NSERC.

References

[1] A. P. Ramirez, Annu. Rev. Mater. Sci. **24**, 453-80 (1994), J. E. Greedan, J. Mater. Chem. **11**, 37-53 (2001).

[2] Mark T. Anderson, Kevin B. Greenwood, Gregg A. Taylor, Kenneth R. Poppelmeier,

Prog. Solid St. Chem. **22**, 197 (1993).

[3] C. J. Howard and H. T. Stokes, Acta Cryst. **A61**, 93 (2005).

[4] C. R. Wiebe, J. E. Greedan, G. M. Luke, J. S. Gardner, Phys. Rev. B, **65**, 144413 (2002).

[5] C. R. Wiebe, J. E. Greedan, P. P. Kyriakou, G. M. Luke, J. S. Gardner, A. Fukaya, I.M. Gat-Malureanu, P. L. Russo, A. T. Savici, Y. J. Uemura, Phys. Rev. B **68**, 134410(2003).

[6] P. D. Battle, C. W. Jones, J. Solid State Chem., **78**, 108 (1989).

[7] P. Schiffer and A. P. Ramirez, Comments on Condensed Matter Physics **18**, 21 (1996).

[8] Peter D. Battle, Clare P. Grey, Maryvonne Hervieu, Christine Martin, Caroline A. Moore, Younkee Paik, J. Solid State Chem., **175**, 20 (2003).

[9] J. Rodriguez-Carvajal, Physica B **192**, 55 (1993)

[10] B.H. Toby, EXPGUI, a graphical user interface for GSAS, J. Appl. Cryst. **34**, 210

(2001), A. C. Larson and R. B. Von Dreele, General Structure Analysis System (GSAS), Los Alamos National Laboratory Report LAUR 86-748 (2004)

[11] Michel E. Fisher, Philos. Mag., **7**, 1731 (1962)

[12] K. Hayashi, G. Demazeau, M. Pouchard, P. Hagenmuller, Mat. Res. Bull., **15**, 461 (1980); J. Darriet, G. Demazeau, M. Pouchard, Mat. Res. Bull., **16**, 1013 (1981).

[13] R. D. Shannon, Acta. Cryst. **A32**, 751 (1976).

[14] P. Woodward, R-D. Hoffman, A. W. Sleight, J. Mater. Res., **9**, 2118 (1994).

[15] P. W. Barnes, M. E. Lufaso, P. M. Woodward, Acta. Cryst. **B62**, 384 (2006).

[16] C.P. Grey, M.E. Smith, A.K. Cheetham, C.M. Dobson and R. Dupree, J. Am. Chem. Soc. **112** 4670 (1990).

[17] K.J.D. MacKenzie and M.E. Smith, Multinuclear Solid-State NMR of Inorganic Materials, Pergamon, New York, 2002.

[18] Malcom F. Collins, *"Magnetic Critical Scattering"* Oxford University Press, NewYork, 1989

Chapter Four

Structure and magnetic properties of the S=1 geometrically frustrated double perovskites La_2LiReO_6 and Ba_2YReO_6

This chapter encompasses the manuscript," Structure and magnetic properties of the S=1 geometrically frustrated double perovskites La_2LiReO_6 and Ba_2YReO_6" published in Physical Review B81, 064436 (2010). The candidate contributes all experimental parts except the collection of neutron diffraction data and ^{89}Y MAS NMR measurement on Ba_2YReO_6. The candidate contributes the interpretation of all results and preparation of the manuscript.

With permission of the reproduction of the article; Tomoko Aharen, John E. Greedan, Craig A. Bridges, Adam A. Aczel, Jose Rodriguez, Greg MacDougall, Graeme M. Luke, Vladimir K. Michaelis, Scott Kroeker, Chris R. Wiebe, Haidong Zhou, and Lachlan M. D. Cranswick, Physical Review B81, 064436 (2010), copyright 2010 by the American Physical Society.

The structure and magnetic properties of S=1 geometrically frustrated double perovskite, La_2LiReO_6 and Ba_2YReO_6

Tomoko Aharen[1], John E. Greedan[12], Craig A. Bridges[1], Adam A. Aczel[3], Jose Rodriguez[3], Greg MacDougall[3], Graeme M. Luke[3], Vladimir. K. Michaelis[4], Scott Kroeker[4], Chris R. Wiebe[5], Haidong Zhou[5], Lachlan M. D. Cranswick[6]

[1]Department of Chemistry, McMaster University, Hamilton, Ontario, LA8S 4M1, Canada, [2]Brockhouse Institute for Materials Research, McMaster University, Hamilton, Ontario, L8S 4M1, Canada, [3]Department of Physics and Astronomy, McMaster University, Hamilton, Ontario, L8S 4M1,Canada, [4]Department of Chemistry, University of Manitoba, Winnipeg, R3T 2N2, Manitoba, Canada, [5]Department of Physics, Florida State University, Tallahassee, 32310-4005, Florida, USA and Department of Chemistry, University of Winnipeg, Winnipeg, MB, R3B 2E9 CANADA, [6]Canadian Neutron Beam Centre, National Research Council, Chalk River Laboratories, Chalk River, Ontario K0J 1J0, Canada.

Abstract

Two B-site ordered double perovskites, La_2LiReO_6 and Ba_2YReO_6, with $S = 1$ were investigated as geometrically frustrated antiferromagnets, using X-ray and neutron diffraction, SQUID magnetometry, heat capacity, muon spin relaxation and ^{89}Y MAS NMR. La_2LiReO_6 has a monoclinic structure ($P2_1/n$) with cell parameters at room temperature; a=5.58262(22)Å, b=5.67582(20)Å, c=7.88586(27)Å, β=90.240(4)°. A zero-field cooled/field cooled (ZFC/FC) divergence at 50K was observed in the susceptibility.

The ZFC susceptibility is zero below ~5K for polycrystalline samples, suggesting a cooperative singlet ground state but weak moments are induced by cooling in very small fields ~ 1mT. No evidence of long range ordering is evident in heat capacity, neutron diffraction or μSR (muon spin relaxation) data. The zero field (ZF) spin dynamics from μSR are anomalous and can be fitted to a stretched exponential rather than the Kubo-Toyabe form expected for random frozen spins but the muon spins are decoupled in longitudinal fields(LF), consistent with spin freezing of the fraction of spins relaxing within the muon time scale. The internal fields sensed by the muons are anomalously small, consistent with an electronic spin singlet state. Ba_2YReO_6 is found to be cubic (Fm3m) with cell parameter a=8.36278(2) Å at 300K with no change in symmetry at 3.8K, at variance with the Jahn-Teller theorem for a t_{2g}^2 configuration for Re^{5+}. ^{89}Y MAS NMR shows a single peak indicating that Y/Re site disorder is at most 0.5%. The susceptibility shows two broad peaks around 50K and 25K but no evidence for long range order from heat capacity, neutron diffraction or μSR. The ZF μSR result shows a two component ground state with both slow and fast relaxation and decoupling results in a 1kG LF, indicating spin freezing. These results are in sharp contrast to the long range AF order found in the S = 3/2 isostructural materials, La_2LiRuO_6 and Ba_2YRuO_6, indicating that the reduction to S =1 plays a major role in ground state determination.

Introduction

Geometrically frustrated antiferromagnetic materials have attracted considerable interest over the past few years, motivated by their tendency to form rather exotic magnetic ground states such as the spin glass, spin liquid or spin ice states instead of long range order in apparent defiance of the third law of thermodynamics.[1] Among the four "canonical" geometrically frustrated lattices: triangular planar, kagome, pyrochlore and face-centered cubic (fcc), the latter has received the least attention. In real materials the f.c.c magnetic lattice is conveniently realized in the B-site ordered double perovskites, $A_2BB'O_6$. Here a magnetic ion resides on the B' site, while B and A are nonmagnetic. Both the B and B' sites constitute interpenetrating face centered cubic sublattices, Figure 4.1, which, if the exchange constraint between nearest B' neighbors is antiferromagnetic, the basic criteria for geometric frustration are satisfied. The conditions for B- B' site ordering have been presented in the form of a phase diagram. [2]

A very important feature of B-site ordered double perovskites is the versatility of this structure type to chemical substitution. The large A-site ions are generally from Group 2 or 3 and the B and B' ions from the transition series 3d – 5d and 4f or small Group 1, 2 or 3 ions. The crystal symmetry can be tuned via the familiar tolerance factor, t, which for double perovskites can be written:

$$t = (r_A + r_O)/\ 2^{1/2}\ (r_{<B,B'>} + r_O)$$

where $r_{<B,B'>}$ is the average of the B and B' ionic radii, r_A is the radius of A and r_O that of the oxide ion . For t~1 one finds Fm3m crystal symmetry and cubic, m3m, point symmetry at the B-sites. As t decreases, the crystal symmetry descends and one commonly finds materials with I4/m(4/m), $P2_1/n(-1)$ and P-1(-1) space group and corresponding point group symmetries at the B' site indicated in parentheses.[3]

Thus, the B-site ordered double perovskites provide a unique opportunity for a systematic study of the roles of several factors, including the spin quantum number, S, and the local site symmetry on the nature of the magnetic ground state in the frustrated f.c.c. lattice. In a previous paper the S = 3/2 materials Ba_2YRuO_6 (Fm3m) and La_2LiRuO_6 ($P2_1/n$) were re-investigated in detail. While both show behavior typical of geometrically frustrated materials, long range AF order is found in both below 36K and 24K, respectively.[4] In this work the systematic study is extended to the S = 1 materials

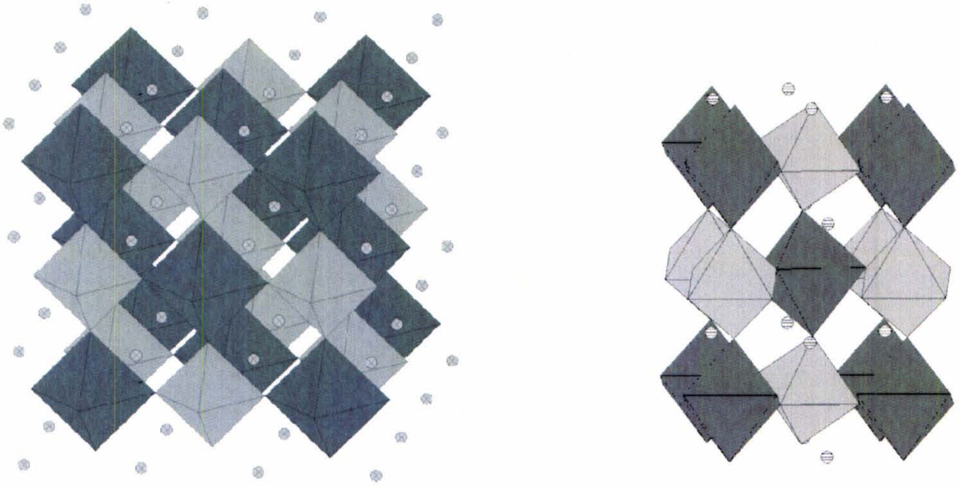

Figure 4.1. (Left)Cubic structure of B-site ordered double perovskite, $A_2BB'O_6$. Dark grey octahedra present $B'O_6$ octahedra and light grey octahedra present BO_6 octahedra. Small circles present A ions. (Right) monoclinic structure of B-site ordered double perovskite.

La_2LiReO_6 and Ba_2YReO_6. For the former, only a crystal structure has been reported while the latter has been investigated using x-ray diffraction, magnetic susceptibility and heat capacity.[5,6] For both materials the crystal structure is re-investigated using neutron diffraction, which resulted in new assignments of crystallographic symmetry, along with ^{89}Y MAS NMR to test Y/Re ordering in Ba_2YReO_6. In addition to SQUID magnetometry and heat capacity, the spin dynamics has been studied using muon spin relaxation. It is demonstrated that these S = 1 compounds do not show long range order down to 2K, unlike the S = 3/2 analogs but instead, anomalous spin freezing (Ba_2YReO_6) and the formation of a cooperative spin singlet state with a finite concentration of defects (La_2LiReO_6).

Experimental Procedures.

La_2LiReO_6 was prepared using a conventional solid state reaction. A mixture of La_2O_3 (Aldrich, 99.9%, pre-heated to remove moisture and surface contamination), 10% excess of Li_2CO_3(J.T. Baker Chemical Co., 99.1%), Re(Alfa Aesar, 99.997%) and ReO_3 (Rhenium Alloys Inc) was ground and heated in an Ar flow in two stages, first to 923K at 100°/h and held for 6 hours, then fired at 1173K for 10 hours. For Ba_2YReO_6, a stoichiometric mixture of starting reagents, $BaCO_3$ (J.T. Baker Chemical Co.), Y_2O_3 (Alfa Aesar, 99.9%, pre-heated), Re (Alfa Aesar, 99.997%) and ReO_3 (Rhenium Alloys Inc) was ground and heated in an Ar flow again in two stages, first at 1143K for 6 hours and then at 1573K for 24 hours. A second firing at 1573K for 24 hours was required for completion of the reaction. The obtained powders were black and the sample purity was tested by X-ray diffraction using a Gunier-Hägg camera with Cu $K\alpha_1$ radiation.

Magnetic susceptibility measurements were performed with applied fields of 10, 100 and 5000 Oe at McMaster University using a Quantum Design MPMS SQUID magnetometer. Zero-Field cooling (ZFC) and Field cooling (FC) data were collected in the temperature range of 2K to 300K. A hysteresis measurement for La_2LiReO_6 was performed at 5K with an applied field range between – 5.5T to 5.5T.

Heat capacity measurements were carried out at McMaster using an Oxford Maglab and at Florida State University/NHMFL using a Quantum Design PPMS system in the temperature range of 2K to 70K. Lattice match compounds, La_2LiIrO_6 and Ba_2YTaO_6 [7, 8] were prepared according to literature methods and measured to estimate the lattice heat capacity contribution for La_2LiReO_6 and Ba_2YReO_6.

Neutron diffraction measurements were performed on the C2 diffractometer at the Canadian Neutron Beam Centre operated by the National Research Council of Canada at the Chalk River laboratories of Atomic Energy of Canada. The data were collected at room temperature and 2.8K with neutron wave lengths of 2.7319Å and 1.3305Å for La_2LiReO_6 and at 4, 10, 20, 40 and 300K with neutron wave lengths of 2.36927 Å and 1.3286 Å for Ba_2YReO_6. The crystal structures of both compounds were refined using FULLPROF[9] or GSAS[10].

Local spin dynamics was investigated using zero field (ZF) and longitudinal field (LF) muon spin relaxation (μSR) at TRIUMF, Vancouver, Canada. The measurement temperatures were 2K and 10K with increments 10K to 60K in zero-field (ZF) μSR and

2K with applied fields of 100G and 500G in longitudinal-field (LF) μSR for La_2LiReO_6. For Ba_2YReO_6, the measurement temperatures were at 2, 5, 15, 25, 35, 40, 42.5, 50, 55 and 100K in ZF- μSR and 2K with an applied field of 1kG in LF- μSR. ^{89}Y magic-angle spinning (MAS) solid-state NMR was performed on Ba_2YReO_6 in the Department of Chemistry at the University of Manitoba. The spectrum was collected on a 3.2 mm double-resonance Varian-Chemagnetics MAS probe using a Bloch-decay pulse sequence on a Varian Inova^{UNITY} 600 (14.1 T) spectrometer operating at a Larmor frequency, ν_L of 29.36 MHz. The sample (black crushed powder) was packed into a 3.2 mm (o.d.) ZrO_2 rotor with a fill volume of 22 μL and spun at 22.000 ± 0.015 kHz. The spectrum is the result of 785 408 co-added transients, acquired with a 45° tip angle (ν_{rf} = 45 kHz) and a recycle delay of 400 ms. The sample temperature was maintained at 303 K, and the chemical shift was referenced with respect to external 2M $Y(NO_3)_3$ at 0.0 ppm [11].

Result and Discussion

La_2LiReO_6

Crystal structure

The obtained powder was confirmed to be single phase by X-ray diffraction. The crystal structure of this compound is shown in Figure 4.1. This compound was first reported to have an orthorhombic structure with cell parameters a=5.577(Å), b=5.663(Å) and c=7.876(Å) from X-ray powder diffraction [5]. On the contrary, two related compounds La_2LiRuO_6[4,12] and La_2LiMoO_6[13], have been reported as monoclinic, $P2_1/n$, from neutron powder or single crystal X-ray diffraction. From Shannon's ionic radii Re^{5+}

resides between Mo^{5+} and Ru^{5+} (Mo^{5+} = 0.61Å, Re^{5+} = 0.58Å and Ru^{5+} = 0.565Å [14]), therefore, it is highly likely that La_2LiReO_6 is monoclinic as well. Thus, the neutron diffraction data collected at 2.8K and 298K were refined in $P2_1/n$, and the results are shown in Figure 4.2 and Table 4.1 where the fit is seen to be excellent with a β angle significantly greater than 90.00(deg). Examination of the interatomic distances, Table 4.2, indicates that the nearest neighbor coordination environment of Re shows a weak pseudo-tetragonal compression at 298K which is enhanced somewhat at 2.8K.

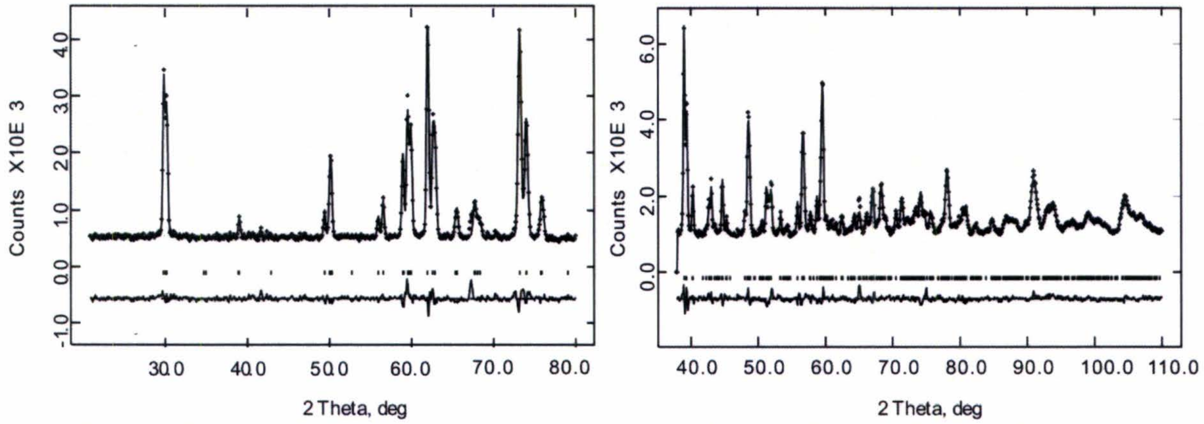

Figure 4.2. A Rietveld fit to the neutron diffraction data for La_2LiReO_6 for two wavelengths, λ = 2.37192Å (left) and λ = 1.33052Å (right) at 298K

Table 4.1.The refined cell parameters and atomic positions of La_2LiReO_6 from neutron powder data at 298K and 2.8K.

	298 K				2.8K			
	x	y	z	U_{iso}(Å^2)	x	y	z	U_{iso}(Å^2)
La	-0.0104(8)	0.0476(5)	0.2525(6)	0.0095(8)	-0.0117(9)	0.0493(7)	0.2559(6)	0.0033(12)
Li	0.5	0	0	0.017(5)	0.5	0	0	0.001(6)
Re	0.5	0	0.5	0.0059(9)	0.5	0	0.5	0.0034(14)
O1	0.1936(10)	0.2192(10)	-0.0446(8)	0.0105(18)	0.1926(12)	0.2187(11)	-0.0474(9)	0.0065(24)
O2	0.2828(10)	-0.3048(11)	-0.0414(9)	0.0143(17)	0.2869(12)	-0.3042(11)	-0.0405(10)	0.0058(21)
O3	0.0830(9)	-0.5192(8)	0.2395(7)	0.0107(13)	0.0823(11)	-0.5216(11)	0.2399(8)	0.0091(20)
a	5.58262(22)				5.58070(31)			
b	5.67582(20)				5.68591(28)			
c	7.88586(27)				7.8405(4)			
β	90.240(4)				90.464(5)			
χ^2	1.71				2.61			
R_p	0.0367				0.0443			
R_{wp}	0.0505				0.0635			

Table 4.2. Selected bond distances(Å) and angles(°)for La_2LiReO_6 at 298K and 2.8K.

bond length(Å)	2.8K	298K
Li - O1	2.149(6)	2.143(5)
Li - O2	2.122(6)	2.137(5)
Li - O3	2.097(6)	2.110(5)
Re - O1	1.964(6)	1.959(5)
Re - O2	1.978(6)	1.957(6)
Re - O3	1.937(6)	1.946(5)
bond angle(°)	**2.8K**	**298K**
Li - O1 -Re	151.1(4)	152.1(4)
Li - O2 -Re	152.7(4)	152.9(4)
Li - O3- Re	152.7(4)	152.82(29)

Magnetic properties

First, the inverse susceptibility, Fig. 4.3, was fitted to the Curie-Weiss law for the range 100K – 300K, yielding a Weiss temperature, θ = -204(2)K, and an effective magnetic moment of 1.97μ_B, which is smaller than the spin-only value (2.82 μ_B) for a S = 1 ion. The large, negative, θ indicates predominant antiferromagnetic exchange and the magnitude is somewhat larger than for the S = 3/2 analog, La_2LiRuO_6 (-185K)[4,12]. This indicates, given the smaller S value, even stronger overall AF exchange for the Re compound. The magnetic susceptibility at low temperatures is shown in Figure 4.4 at an applied field of 0.5T. Note the ZFC/FC divergence below ~ 50K. The ZFC curve shows a broad maximum at 33K but this shifts to higher temperatures for smaller fields (1 mT and 10 mT - data not shown). Note that the ZFC susceptibility at an applied field of 0.5T approaches zero at low temperatures. This is shown more clearly in the inset to Fig. 4.4 where the low temperature Curie-Weiss tail has been subtracted. Such behavior is remarkable for a polycrystalline sample and is consistent with a spin singlet ground state. The FC susceptibility shows that a very weak moment is induced below 50K by cooling in small fields, Figure 4.5, and that hysteresis is found at 5K with induced moments on the order of 10^{-2} μ_B per Re ion (inset). The observation of ZFC/FC divergences and hysteresis indicates that the singlet state is collective and not single ion in nature. The most consistent interpretation of the bulk susceptibility is that a collective spin singlet state is the ground state but that a low concentration of non-singlet defects can be induced by cooling in very low fields. The presence or absence of a spin gap in this material is unclear at this time. Further studies including inelastiv neutron scattering and Li NMR are planned to investigate this possibility.

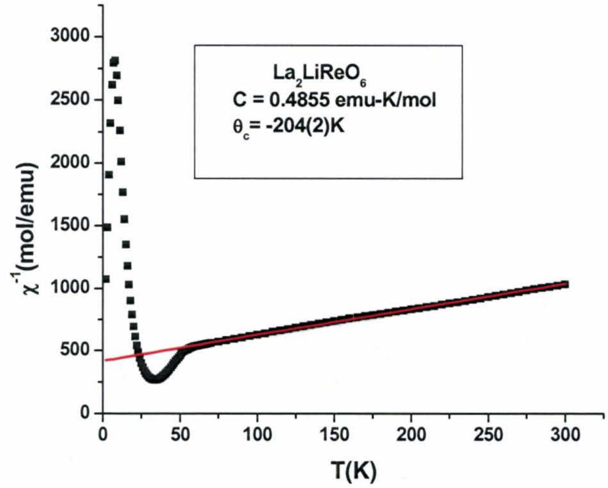

Figure 4.3. Inverse susceptibility for La_2LiReO_6 showing the Curie-Weiss fit.

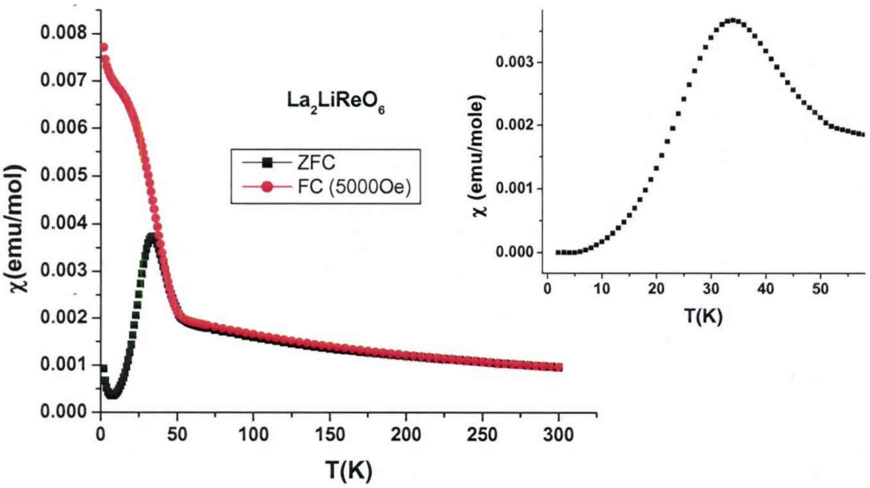

Figure 4.4. Temperature dependence of the susceptibility of La_2LiReO_6 at an applied field of 0.5T. The inset shows the result of subtracting the weak Curie tail and evidence for a magnetic singlet ground state.

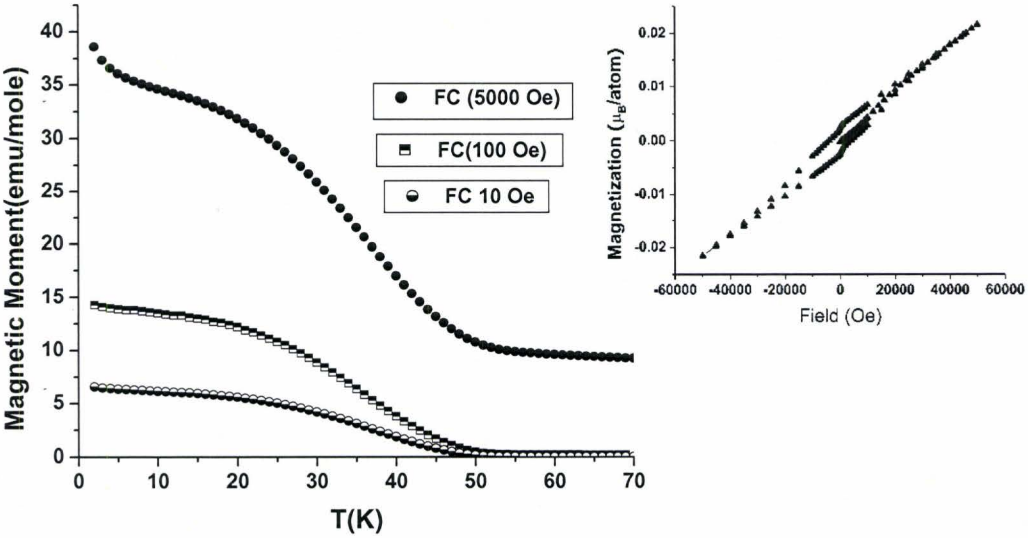

Figure 4.5. Temperature dependence of the FC susceptibility showing onset of a very weak moment below 50K for all applied fields. The inset shows hysteresis at 5K.

To search for evidence for or against long range magnetic order heat capacity data were collected over the range including the ZFC/FC divergence and below and no lambda anomaly is seen, Figure 4.6. Note that the data are superimposed on those for the lattice match material below about 10K which suggests no electronic contribution. The magnetic component shows a very broad maximum between 40-50K, consistent with the bulk susceptibility. Entropy removal within the temperature range studied is 3.5 J/mol-K^2 which is ~ 38% of the total entropy expected for a S = 1 system.

As well, a difference plot of the neutron diffraction data for 2.8K and 298K was examined for magnetic Bragg peaks with negative results, Figure 4.7. Such features were easily seen for the isostructural, S = 3/2 analog, La_2LiRuO_6.[12]. Given the difference in spin quantum number, one would expect corresponding magnetic Bragg peaks for the Re compound to be reduced in intensity by a factor of ~ 2. Assuming the same magnetic structure, such reflections should have been detected and they are clearly absent. Thus, both heat capacity and neutron diffraction data support the absence of long range magnetic order in La_2LiReO_6.

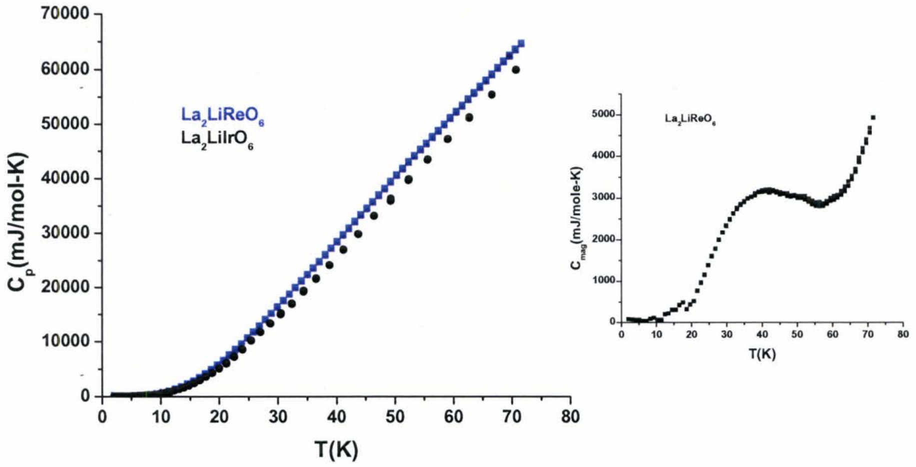

Figure 4.6. The heat capacity of La_2LiReO_6 and the lattice match sample, La_2LiIrO_6. The inset shows the magnetic component and a very broad maximum between 40-50K.

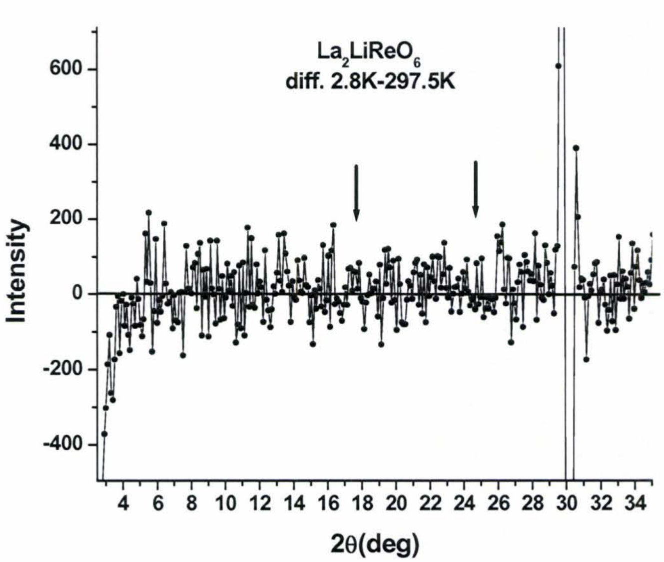

Figure 4.7. A low angle neutron diffraction difference plot 2.8K – 297.5K showing the absence of magnetic Bragg peaks. The arrows show the location of expected reflections for a Type I f.c.c. structure as found for La_2LiRuO_6.[4]

To investigate the local spin dynamics, muon spin relaxation (μSR) measurements were performed. The corrected data for zero field μSR (ZF- μSR) at 60K (paramagnetic), 40K (just below the ZFC/FC divergence), 20K and 1.7K are shown in Figure 4.8. Below 20K (inset) there are clearly two components, one rapidly relaxing in the region < 0.1 μs, and one slowly relaxing which extends to several μs. It proved impossible to fit the all of the data to a two component relaxation function including the fast component, so the data for the slow component only were fitted, shown as the solid line, with a stretched exponential, $A(t) = A_0 * \exp[-(\lambda t)^{\beta}]$, where A is an amplitude and λ is a relaxation rate. The temperature dependence of the extracted relaxation rate is shown in Figure 4.9a along with the behavior of the exponent, β. The rate is roughly constant until ~ 50K (the ZFC/FC divergence temperature) and then increases gradually, reaching a saturation value only below ~ 20K consistent with some level of spin freezing. The β-value remains constant at ~ 2 down to 50K, consistent with paramagnetic relaxation, then decreases sharply, indicating that electron spins are involved. In contrast to other Re based double perovskites with S= 1/2 such as Sr_2CaReO_6 or Sr_2MgReO_6[15,16], the relaxation data do not exhibit the classic Kubo-Toyabe line shape often found for frozen spin ground state materials in which essentially all of the spins freeze. Instead, the observed stretched exponential decay is typical of dilute spin systems, which is curious as the concentration of magnetic Re^{5+} ions is nominally high in this material. Application of a 500 Oe longitudinal (LF) field, Figure 4.9b, decouples the muons at 2K, indicating that the electron spins which couple to the muons are static at this temperature. The very slow relaxation of the muons in La_2LiReO_6 indicates coupling to very weak electronic fields which is consistent with the singlet ground state behavior seen in the bulk susceptibility, if it is postulated that most of the Re spins are involved in the singlet state, leaving only a remnant fraction to couple with the muon spins. It is worth noting that the weak local fields cannot be due to some type of symmetry cancellation in this system as the muon will be hydrogen bonded to the O atoms which are in sites of very low crystallographic symmetry.

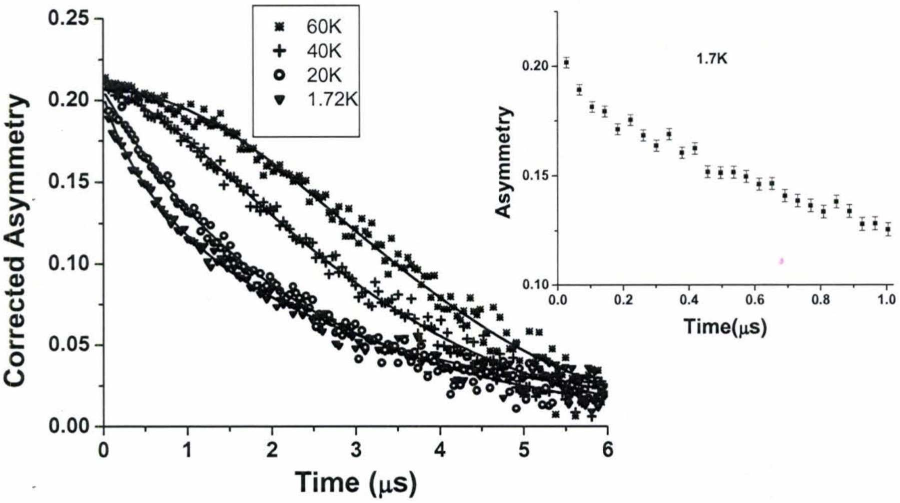

Fig. 4.8. Fit of the slowly relaxing component, t > 0.02 μsec to a stretched exponential. The inset shows the weak, rapidly relaxing component for t < 0.1 μsec which develops below 20K. Only the 1.7K data are shown.

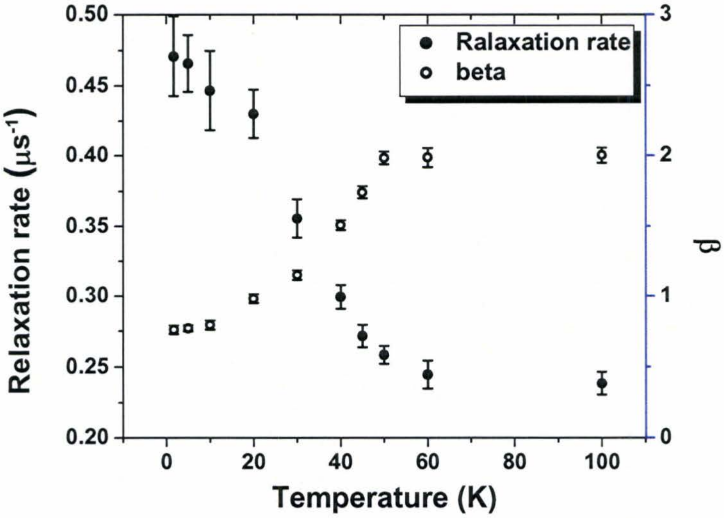

Figure 4.9a. Temperature dependence of the relaxation rate and the exponent, β, extracted From the fit to a stretched exponential function for the data of Figure 4.8.

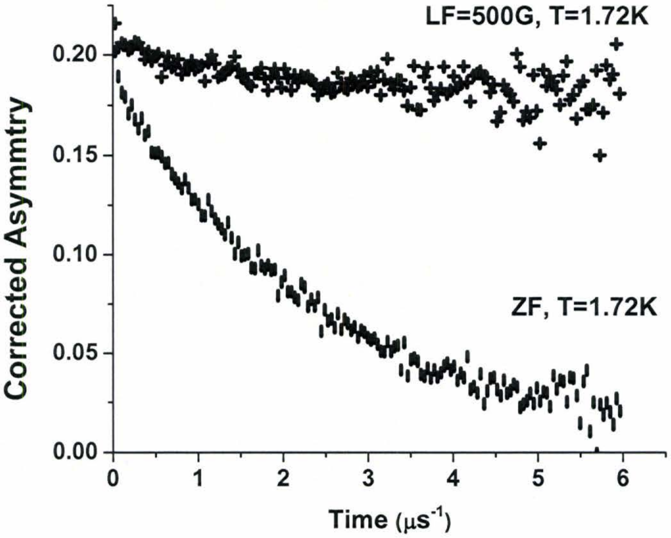

Figure 4.9b. Application of a 500 Oe longitudinal field LF (upper curve) for La_2LiReO_6 showing decoupling of both components at 1.7K.

Ba_2YReO_6

Crystal structure

This compound was previously studied by Sasaki *et al* and reported to be monoclinic, $P2_1/n$ by the refinement of a powder X-ray diffraction data collected at room temperature[6]. Examination of the results from this study revealed that the monoclinic cell constants were metrically cubic to within experimental error. Thus, the neutron diffraction data obtained here were refined in Fm3m. The results, given in Figure 4.10a and Table 4.3 and 4.4, show that the choice of Fm3m is correct. As seen in Figure 10b, there is no detectable distortion from cubic symmetry at 300K or 3.5K within the resolution of the neutron data which is $\Delta d/d \sim 2 \times 10^{-3}$ for the 2θ range covered in the figure. This result is of considerable interest as Re^{5+}, $5d^2$ has the t_{2g}^2 configuration in cubic symmetry and is thus subject to the Jahn-Teller theorem and some distortion would be expected.

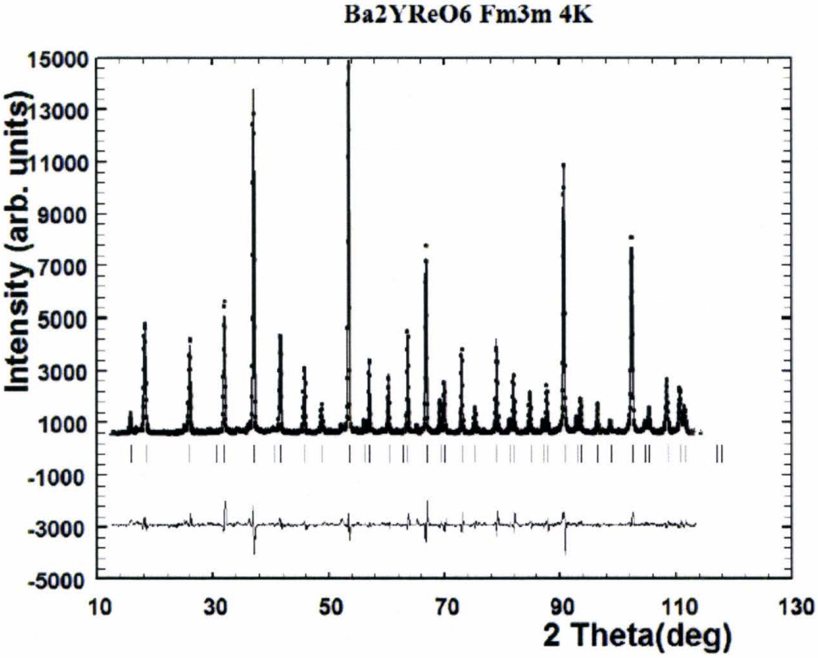

Figure 4.10a. Neutron diffraction pattern and the refinement for Ba_2YReO_6 at 3.5K.

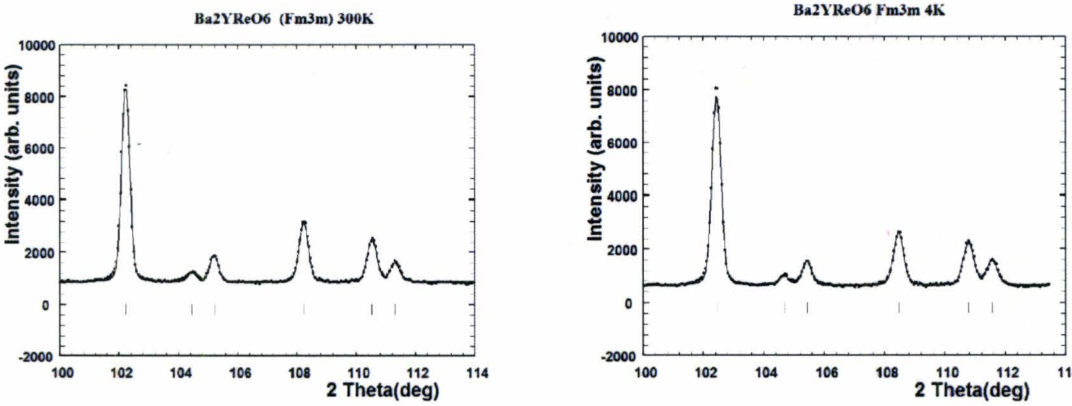

Figure 4.10b. High angle, high resolution ($\Delta d/d \sim 2 \times 10^{-3}$) neutron diffraction data for 3.5K (right) and 300K (left) showing no distortion from cubic symmetry.

Table 4.3. The refined cell parameters and atomic positions of Ba_2YReO_6 from neutron powder data.

	4K				300K			
	x	y	z	$B_{iso}(\AA^2)$	x	y	z	$B_{iso}(\AA^2)$
Ba	0.25	0.25	0.25	0.44(2)	0.25	0.25	0.25	0.91(2)
Y	0.5	0.5	0.5	0.68(4)	0.5	0.5	0.5	1.01(5)
Re	0	0	0	0.14(3)	0	0	0	0.23(3)
O	0.23396(1)	0	0	0.66(1)		0	0	1.09(2)
a	8.3395(2)				8.3627(2)			
χ^2	5.32				5.83			
R_p	5.42				5.05			
R_{wp}	7.31				6.91			

Table 4.4. Selected interatomic distances (Å) for Ba_2YReO_6 at 300K and 4K.

bond length(Å)	4K	300K
Y-O	2.2186(1)	2.2262(1)
Re-O	1.9512(1)	1.9552(13)

In addition to the crystal structure, Y/Re ordering is an issue to be addressed since the charge difference of 2 and the ionic radii difference between Y^{3+} and Re^{5+} ions places this material near the border of the phase diagram of Anderson *et al*[2] for B-site ordering in double perovskites. Thus, a ^{89}Y MAS NMR measurement was carried out to investigate the level of Y/Re ordering. Previously, the same technique disclosed a 1% site mixing between Y and Ru in isostructural Ba_2YRuO_6.[4] As shown in Figure 4.11, a single peak is observed at -2320 ppm with a peak width (FWHM = 2.55 kHz) comparable to that in Ba_2YRuO_6. [4] No additional signals could be detected over a 6000 ppm range. It may be noted that the peak position is midway between the "normal" ^{89}Y chemical shielding range and the ca. -5800 ppm positions observed for the S = 3/2 Ba_2YRuO_6, evidence that interaction with the unpaired electron spins dominates the nuclear shielding properties. From these results it can be concluded that there is no convincing evidence for Y/Re site disorder in Ba_2YReO_6. Using the arguments of references 4 and 17 an upper limit of Y/Re disorder is generously estimated to be 0.5%.

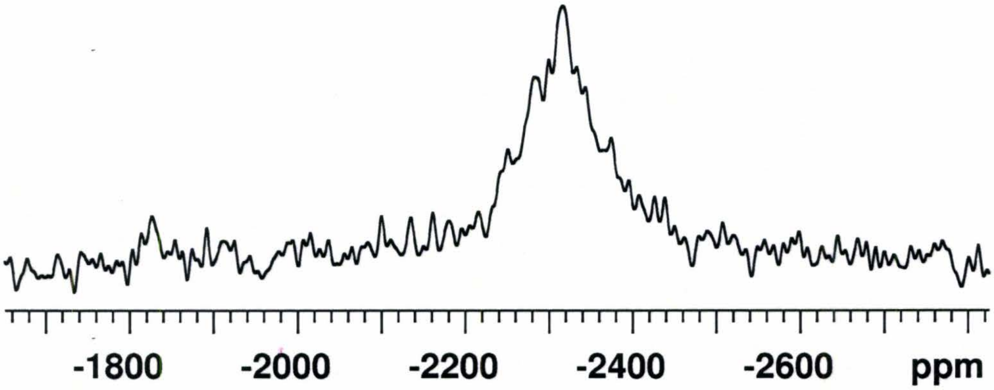

Figure 4.11. ^{89}Y MAS NMR of Ba_2YReO_6 acquired at 22 kHz. The center of gravity chemical shift is – 2315 +/- 15 ppm with a width of 90 ppm. The apparent peak at ~ -1820 ppm is an experimental artifact from the transmitter.

Magnetic Properties

The magnetic susceptibility for Ba_2YReO_6 is displayed in Figure 4.12. It shows two broad maxima at 50K and 25K, which is consistent with the data previously reported by Sasaki et al [6] although their results do not show the 25K anomaly so clearly. The ZFC/FC curves show a slight divergence around 125K. The inverse susceptibility was fitted with the Curie Weiss law yielding a Weiss temperature, θ = - 616(7) K and an effective magnetic moment, $\mu_{eff}=1.93\mu_B$. This reduced effective moment compared to its spin only value (2.83 μ_B) may be due to orbital contributions. The reported Weiss temperature (θ = -723K) of Sasaki et al is somewhat larger than that seen here which could result from a different choice of the temperature region for the fitting. The frustration index derived here is f ~15.

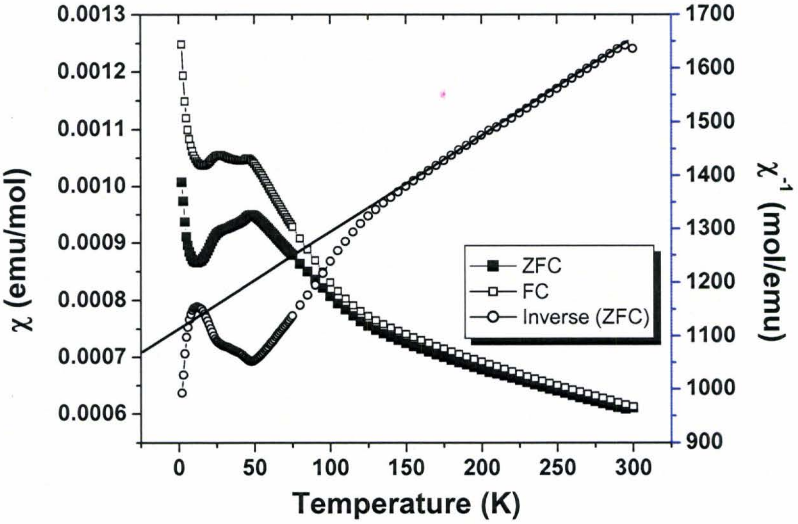

Figure 4.12. The magnetic susceptibility of Ba_2YReO_6. A Curie-Weiss fit of the inverse susceptibility data, solid line, yields the parameters C = 0.554(5) (emu/mole-K)and θ = -616(7)K.

Previous heat capacity data from Sasaki et al showed the absence of any lambda peak which would signal long range magnetic order. [6] The data of Figure 4.13 show the heat capacity of Ba_2YReO_6 compared with a lattice match material, Ba_2YTaO_6. In the inset is plotted the magnetic component, as C_{MAG}/T vs T. Two broad anomalies near 25K and 50K are evident as is the absence of a sharp lambda peak. Also shown is the Fisher heat capacity, $d(\chi T)/dT$ vs T, derived from the susceptibility data.[18] The total entropy removed below 60K is 5.79 J/mol-K^2, 63% of that expected for S = 1.

In order to clarify further the ground state of this compound, we have conducted neutron diffraction measurements and muon spin relaxation measurements. The difference neutron diffraction data, 4K - 300K, are shown in Figure 4.14. Magnetic Bragg peaks are absent, providing evidence against long range order.

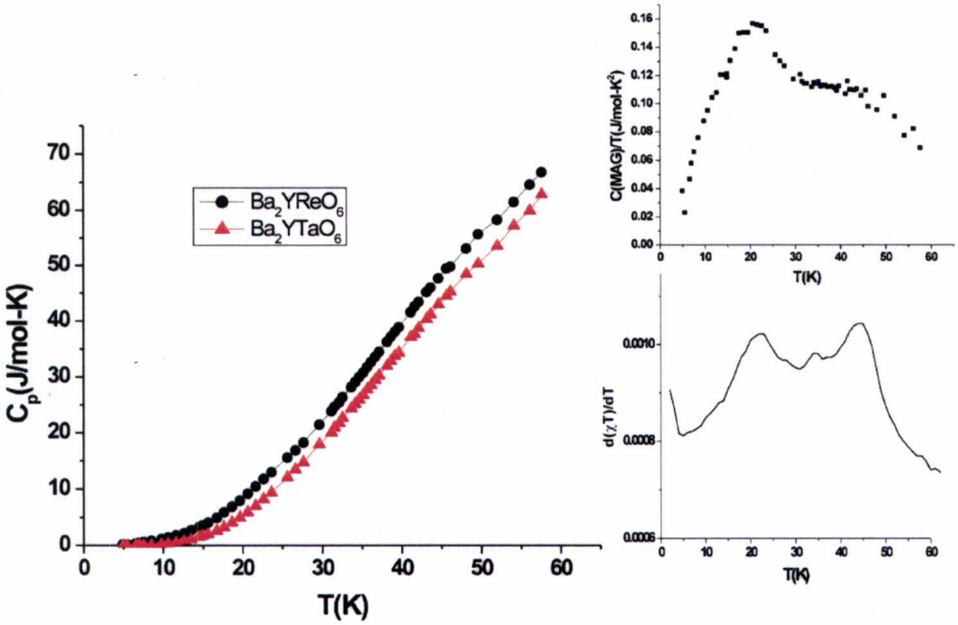

Figure 4.13. Heat capacity of Ba_2YReO_6 and Ba_2YTaO_6. The insets show: (Top) The magnetic component plotted as C(MAG)/T vs T. (Bottom) Fisher's heat capacity, $d(\chi T)/dT$ vs T. [18]

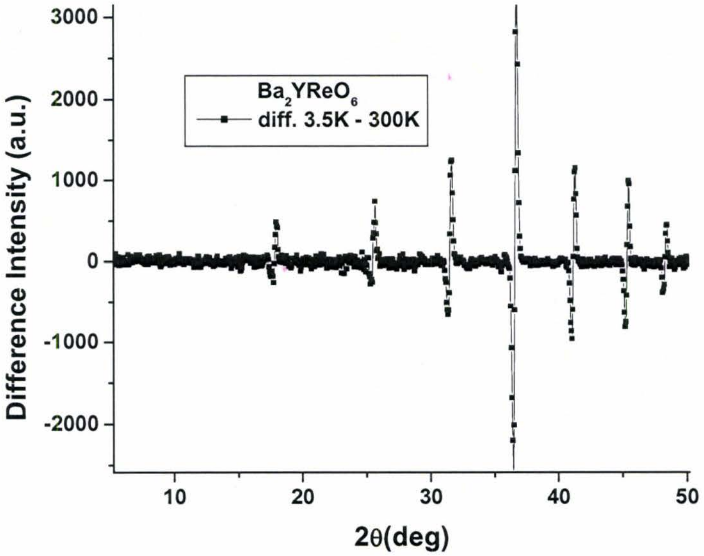

Figure 4.14. The difference neutron diffraction pattern, 3.5K - 300K for Ba_2YReO_6, showing the absence of detectable magnetic Bragg peaks.

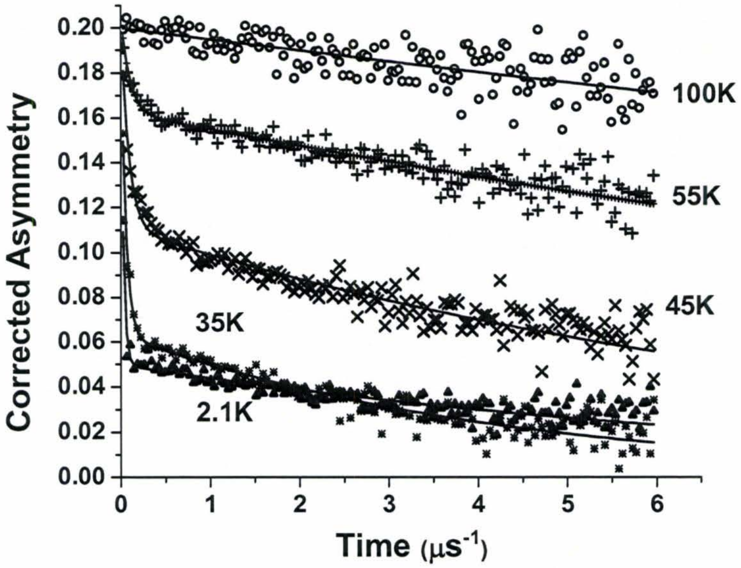

Figure 4.15. ZF μSR relaxation data at selected temperatures for Ba_2YReO_6.The fitted lines are to a sum of two exponential decay functions, see text.

The μSR relaxation data for Ba_2YReO_6 are shown in Figure 4.15. Data at 100K show paramagnetic behavior, but the line shape has clearly become non-Gaussian indicating that the relaxation is partially due to coupling to electron spins. As the temperature decreases, two components develop, a fast relaxing one at short t due to quasi-static internal fields and a slowly relaxing one extending to long t. Fitting over the entire t-range was done with the equation, $F(t) = A_{fast}*\exp(-\lambda_{fast}*t) + A_{slow}*\exp(-\lambda_{slow}*t)$ and the extracted amplitudes and frequencies for the two components are shown versus temperature in Figure 4.16. From the amplitudes in Figure 4.16a, the fast component builds gradually until ~ 40K and saturates below ~ 30K at ~ 3/4 of the total spins while the slow tail amplitude decreases gradually and also saturates below 30K at ~ 1/4 of the total spins. The observation of two spin components for this material is puzzling as there is only one crystallographic oxygen site, and thus, normally one muon site. More remarkably, the rates for the two components show very different temperature dependencies, Fig. 4.16b. The slow component peaks at ~ 35K, just below the higher temperature feature in the susceptibility and heat capacity data, which suggests that this is the spin freezing temperature. The fast component shows no peak but saturates below 20K, near the lower temperature feature in the bulk susceptibility and heat capacity.

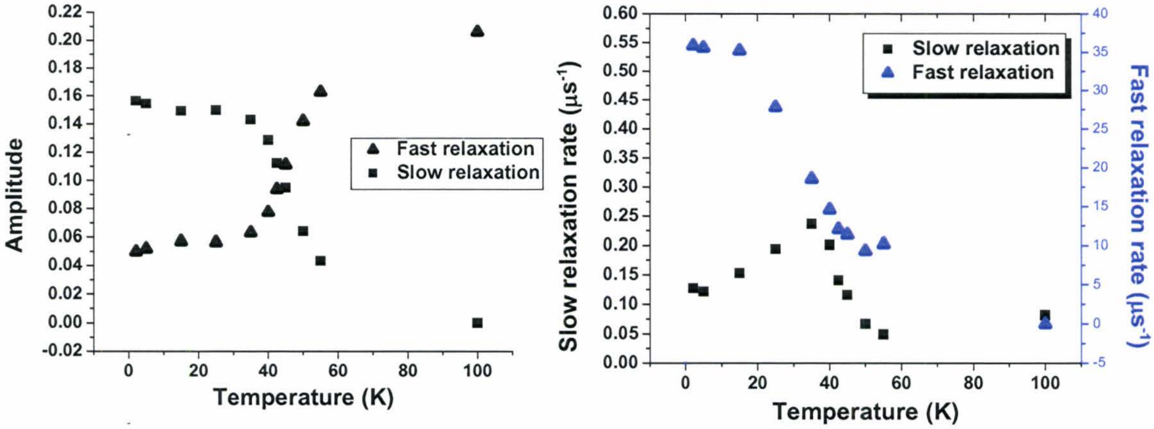

Figure 4.16. (a)(Left) The temperature dependence of the amplitudes of the fast and slow components in μSR for Ba_2YReO_6. (b) (Right) The temperature dependences of the relaxation rates of the slow and fast components.

According to the LF-μSR data collected at 2.1K, Figure 4.17, essentially all of the relaxation is decoupled with an applied field of 1kG, therefore, both components show spin freezing. Nonetheless, the ground state is clearly inhomogeneous compared to more conventional spin glasses which usually follow the Kubo-Toyabe model in ZF wherein the amplitude fractions of the fast and slow components are 2/3 and1/3, respectively, and are not generally strongly temperature dependent within the frozen spin regime. Thus, Ba_2YReO_6 shows a somewhat more conventional frozen spin ground state rather than the exotic singlet state found for La_2LiReO_6. Nonetheless, chemical disorder in this material is below the detection limits of either neutron diffraction or ^{89}Y MAS NMR. Thus, the origin of the spin frozen state is unclear at this time. It is important to recall that a detectable level of site disorder, ~ 1 – 2 %, was found in the S = 3/2 analog, Ba_2YRuO_6 which was insufficient to destroy long range AF order. [4]

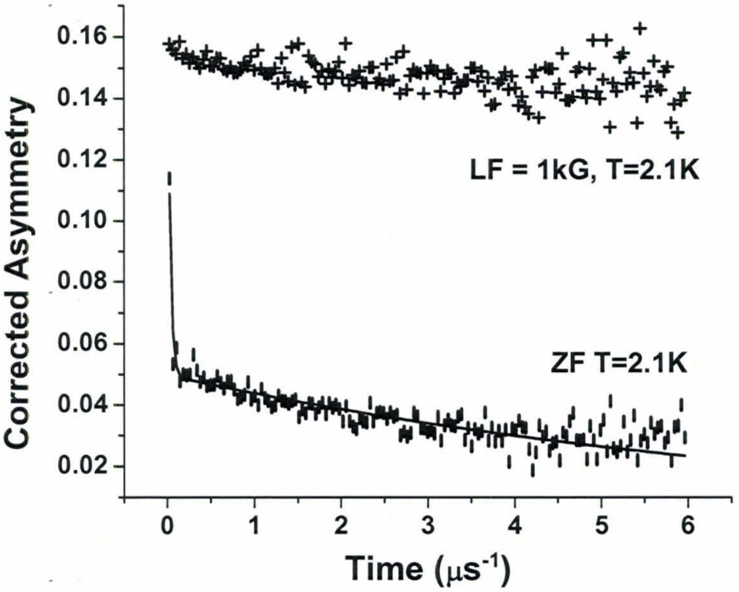

Figure 4.17. μSR relaxation for Ba_2YReO_6 in zero field and a LF of 1 kG at 2.1K, showing complete decoupling and only weak relaxation, an indication of essentially static spins.

Summary and Conclusions

The structure and magnetic properties of the B-site ordered double perovskites La_2LiReO_6 and Ba_2YReO_6, in which the S = 1 ion, Re^{5+}, resides on a f.c.c. lattice were investigated from the perspective of geometric magnetic frustration. The crystal structures are different from previous reports, monoclinic ($P2_1/n$) rather than orthorhombic for La_2LiReO_6, and cubic (Fm3m) rather than monoclinic for Ba_2YReO_6

but consistent with those of compositionally similar materials. The latter shows no detectable Y/Re disorder using the very sensitive probe of ^{89}Y MAS NMR. No long range order was found to 2K from SQUID magnetometry, heat capacity, neutron diffraction and μSR for either material. For La_2LiReO_6 bulk susceptibility, heat capacity and μSR data point toward a collective spin singlet ground state which must involve a finite defect concentration, as weak spontaneous moments are induced by cooling in small fields. Ba_2YReO_6 shows somewhat more conventional behavior leading to a frozen spin ground state but without an obvious source of positional disorder. It is clear that long range order is quenched for both cubic and monoclinic symmetries for these $S = 1$ double perovskites, in contrast to their $S = 3/2$ analogs, Ba_2YRuO_6 and La_2LiRuO_6, which show evidence for strong geometric frustration but which ultimately undergo AF long range order. [4] Of equal interest is the striking difference in behavior of the two $S = 1$, Re^{5+} double perovskites. The most obvious electronic difference between the two materials would appear to be the orbital degeneracy. The t_{2g}^2 configuration is retained in cubic Ba_2YReO_6 which implies an orbital liquid, while an orbital singlet state should exist for monoclinic La_2LiReO_6. The evidence for a collective spin singlet ground state for the latter is remarkable and unexpected for a $S = 1$ system. Clearly, much further work, both experiment and theory, is needed for a more complete understanding of these results.

Acknowledgements.

We thank Paul Dube for assistance with SQUID and heat capacity measurements.
J.E.G, G.M.L. V. K. M and S.K. thank NSERC. S.K. thanks the Canadian Foundation for Innovation and G.M.L. thanks the Canadian Institute for Advanced Research. For work done at Florida State University, C.R.W. thanks the NSF for funding through grant number DMR-08-04173. We appreciate the technical support of the TRIUMF Center for Materials and Molecular Science and the Canadian Neutron Beam Centre.

References

[1] A. P. Ramirez, Ann. Rev. Mater. Sci. **24**, 453-80 (1994) J. E. Greedan, J. Mater. Chem., **11,** 37-53 (2001).

[2] Mark T. Anderson, Kevin B. Greenwood, Gregg A. Taylor, Kenneth R. Poppelmeier, Prog. Solid St. Chem. **22,** 197-233 (1993).

[3] C. J. Howard, B. J. Kennedy and P. M. Woodwords, Acta Crystallogr., sect. B:Struc. Sci. 59**,** 463 (2003).

[4] T. Aharen, J.E. Greedan, F. Ning, T. Imai, V. K. Michaelis, S. Kroeker, H. Zhou, C.R. Wiebe and L.M.D. Cranswick, Phys. Rev. **B80,** 134423 (2009).

[5] K. Hayashi, H. Noguchi and M. Ishii, Mat. Res. Bull. **21,** 401 (1986).

[6] Y. Sasaki, Y. Doi and Y. Hinatsu, J. Mater. Chem. **12,** 2361 (2002).

[7] K. Hayashi, G. Demazeau, M. Pouchard, P. Hagenmuller, Mat. Res. Bull., **15** 461 (1980); J. Darriet, G. Demazeau, M. Pouchard, Mat. Res. Bull. **16,** 1013 (1981).

[8] P.J. Saines, J.R. Spencer, B.J. Kennedy and M. Avdeev, J. Solid State Chem. **180,** 2991 (2007).

[9] J. Rodriguez-Carvajal, "Recent Advances in Magnetic Structure Determination by Neutron Powder Diffraction", Physica **B 192**, 55-69 (1993)

[10] B.H. Toby, EXPGUI, a graphical user interface for GSAS, J. Appl. Cryst. **34**, 210 (2001), A. C. Larson and R. B. Von Dreele, General Structure Analysis System (GSAS), Los Alamos National Laboratory Report LAUR 86-748 (2004)

[11] K. J. D. MacKenzie and M. E. Smith, *Multinuclear Solid-State NMR of Inorganic Materials* □Pergamon, New York, 2002

[12] Peter D. Battle, Clare P. Grey, Maryvonne Hervieu, Christine Martin, Caroline A. Moore, Younkee Paik, J. Solid State Chem. **175,** 20-26 (2003).

[13] J. Tortelier and P. Gougeon, Acta. Cryst. **C52,** 500 (1996).

[14] R. D. Shannon, Acta. Cryst. **A32,** 751 (1976).

[15] C. R. Wiebe, J. E. Greedan, G. M. Luke, J. S. Gardner, Phys. Rev. **B 65**, 144413 (2002).

[16] C. R. Wiebe, J. E. Greedan, P. P. Kyriakou, G. M. Luke, J. S. Gardner, A. Fukaya, I.M. Gat-Malureanu, P. L. Russo, A. T. Savici, Y. J. Uemura, Phys. Rev. **B 68**, 134410 (2003).

[17] C.P. Grey, M.E. Smith, A.K. Cheetham, C.M. Dobson and R. Dupre, J. Am. Chem. Soc. **112**, 4670 (1990).

[18] M.E. Fisher, Philos. Mag. **7**, 1731 (1962).

Chapter Five

Magnetic properties of the geometrically frustrated S=1/2 antiferromagnets, La_2LiMoO_6 and Ba_2YMoO_6, with the B-site ordered double perovskite structure: Evidence for a collective spin-singlet ground state

This chapter encompasses the manuscript "Magnetic properties of the geometrically frustrated S=1/2 antiferromagnets, La_2LiMoO_6 and Ba_2YMoO_6, with the B-site ordered double perovskite structure: Evidence for a collective spin-singlet ground state" published in Physical Review B81, 224409 (2010). The candidate contributes all the experimental parts except NMR measurements on Ba_2YMoO_6. The candidate contributes interpretation of all results and preparation of the manuscript, except solid state NMR measurement part.

With permission of the reproduction of the article; Tomoko Aharen, John E. Greedan, Craig A. Bridges, Adam A. Aczel, Jose Rodriguez, Greg MacDougall, Graeme M. Luke,

Magnetic properties of the geometrically frustrated S = 1/2 antiferromagnets, La_2LiMoO_6 and Ba_2YMoO_6, with the B-site ordered double perovskite structure. Evidence for a Collective Spin Singlet Ground State.

Tomoko Aharen[1], John E. Greedan[1,2], Craig A. Bridges[1], Adam A. Aczel[3], Jose Rodriguez[3], Greg MacDougall[3], Graeme M. Luke[2,3,4], Takashi Imai[2,3,4], Vladimir. K. Michaelis[5], Scott Kroeker[5], Haidong Zhou[6], Chris Wiebe[6,7], Lachlan M.D. Cranswick[8]

[1]Department of Chemistry, McMaster University, Hamilton, Ontario, L8S 4M1, Canada, [2]Brockhouse Institute of Material Research, McMaster University, Hamilton, Ontario, L8S 4M1, Canada, [3]Department of Physics and Astronomy, McMaster University, Hamilton, Ontario, L8S 4M1,Canada, [4]Canadian Institute for Advanced Research, Toronto, Ontario M5G 1Z8, [5]Department of Chemistry, University of Manitoba, Winnipeg, R3T 2N2, Manitoba, Canada, [6]Department of Physics, Florida State University, Tallahassee, 32310-4005, Florida, USA, [7]Department of Chemistry, University of Winnipeg, Winnipeg, MB, R3B 2E9 CANADA, [8]Canadian Neutron Beam Centre, National Research Council, Chalk River Laboratories, Chalk River, Ontario K0J 1J0, Canada,.

Abstract

Two B-site ordered double perovskites, La_2LiMoO_6 and Ba_2YMoO_6, based on the S = ½ ion, Mo^{5+}, have been investigated in the context of geometric magnetic frustration. Powder neutron diffraction, heat capacity, susceptibility, muon spin relaxation(μSR), and ^{89}Y NMR- including MAS NMR- data have been collected. La_2LiMoO_6 crystallizes in $P2_1/n$ with a = 5.59392(19) Å, b = 5.69241(16) Å, c = 7.88029(22), β = 90.2601(30) deg at 299.7K, while Ba_2YMoO_6 is cubic, Fm3m, with a = 8.39199(65) Å at 297.8 K. Ba_2YMoO_6 shows no distortion from cubic symmetry even at 2.8K in apparent violation of the Jahn-Teller theorem for a t_{2g}^1 ion. ^{89}Y NMR MAS data indicate about a 3% level of Y/Mo site mixing. La_2LiMoO_6 deviates strongly from simple Curie-Weiss paramagnetic behavior below 150K and zero-field cooled/ field cooled (ZFC/FC) irreversibility occurs below 20K with a weak, broad susceptibility maximum near 5K in the ZFC data. A Curie-Weiss fit shows a reduced μ_{eff} = 1.42 μ_B, (spin only = 1.73 μ_B) and a Weiss temperature, θ_C, which depends strongly on the temperature range of the fit. Powder neutron diffraction, heat capacity and ^{7}Li NMR show no evidence for long range magnetic order to 2K. On the other hand oscillations develop below 20K in μSR indicating at least short range magnetic correlations . Susceptibility data for Ba_2YMoO_6 also deviate strongly from the C-W law below 150K with a nearly spin only μ_{eff} = 1.72 μ_B and θ_C = - 219(1)K. There is no discernable ZFC/FC irreversibility to 2K. Heat capacity, neutron powder diffraction and μSR data show no evidence for long range order to 2K but a very broad, weak maximum appears in the heat capacity. The ^{89}Y NMR paramagnetic Knight shift shows a remarkable local spin susceptibility behavior below about 70K with two components from roughly equal sample volumes, one indicating a singlet state and the other a strongly fluctuating paramagnetic state. Further evidence for a singlet state comes from the behavior of the relaxation rate, $1/T_1$. These results are discussed and compared with those from other isostructural S = ½ materials and those based on S = 3/2 and S = 1.

Introduction

Geometric magnetic frustration (GMF) generally originates if spins, constrained by an antiferromagnetic nearest neighbor exchange coupling, are situated on lattices with a topology of triangles or tetrahedra. Magnetic properties of GMF compounds have been studied intensively in recent years due to their exotic ground states, such as spin glasses, spin ices and spin liquids[1]. Since the theoretical proposal by Anderson of one possible model for the spin liquid for frustrated antiferromagnets with S=1/2, researchers have been inspired to seek experimental evidence for the existence of spin liquid states [2]. In this model the spins form a collective singlet ground state and the dynamics of singlets is normally retained down to low temperature. The pyrochlore compound $Tb_2Ti_2O_7$[3] and the so-called hyper-kagome compound[4], $Na_4Ir_3O_8$[5], have been proposed as spin-liquid compounds or candidates.

B-site ordered double perovskites with chemical formula $A_2BB'O_6$, where magnetic ions reside on the B'-site, present a face-centered cubic (fcc) symmetry, which is a three dimensional lattice based on edge sharing tetrahedral and is, thus, geometrically frustrated. In previous work, double perovskites with S = 3/2 and S = 1 spins and both cubic and monoclinic lattice symmetries have been studied in detail from the perspective of geometric frustration. [6,7]

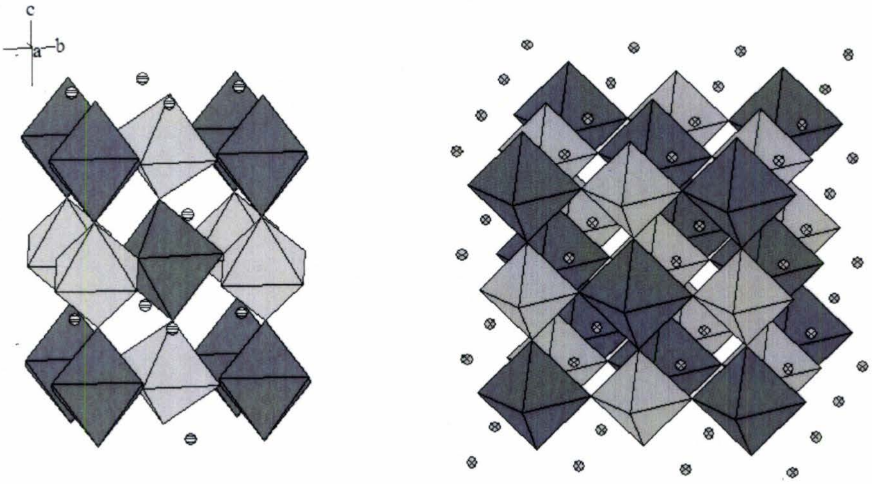

Figure 5.1. (left) Crystal structure of La_2LiMoO_6, $P2_1/n$. Dark grey octahedra represent MoO_6 and light grey octahedral, LiO_6. Dashed circles represent the La ions. (right) Crystal structure of Ba_2YMoO_6, Fm3m. Dark grey octahedra represent MoO_6 and light grey octahedra, YO_6. The small crossed spheres represent the Ba ions.

Unit cells for the two crystallographic symmetries are shown in Figure 5.1. For the S = 3/2 materials it was found that, while frustration was clearly important, both Ba_2YRuO_6 and La_2LiRuO_6 did eventually show long range antiferromagnetic order, even in the case of the former where a 1% level of Y/Ru site mixing was detected by ^{89}Y magic angle spinning (MAS) NMR. In the case of the S = 1 phases, long range order was clearly quenched for both symmetries. La_2LiReO_6 showed a very unusual singlet ground state, while Ba_2YReO_6, which retains cubic symmetry in apparent violation of the Jahn-Teller theorem, undergoes spin freezing. Paradoxically, Y/Re site mixing was undetectable via

^{89}Y MAS NMR. In this work, two S = ½ double perovskites, the cubic Ba_2YMoO_6 and monoclinic La_2LiMoO_6, have been studied in detail using a wide range of probes including powder neutron diffraction, neutron inelastic scattering, bulk magnetic susceptibility, heat capacity, muon spin relaxation and ^{89}Y NMR, both MAS and paramagnetic Knight shift measurements. Ba_2YMoO_6 had been reported previously to remain paramagnetic to 2K while no magnetic properties studies exist for La_2LiMoO_6.[8,9] The results are compared with other isostructural S = ½ B-site ordered double perovskites such as the monoclinic spin glass, Sr_2CaReO_6, the cubic ferromagnet, Ba_2NaOsO_6 and the cubic antiferromagnet, Ba_2LiOsO_6.[10, 11]

Experimental

Polycrystalline samples of La_2LiMoO_6 and Ba_2YMoO_6 were prepared using conventional solid state reaction. For La_2LiMoO_6, a stoichiometric mixture of pre-fired La_2O_3, Li_2MoO_4 and MoO_2 were ground and sealed in a Mo crucible, heated to 1100°C in an Ar atmosphere, and kept for 48 hours. For Ba_2YMoO_6, $BaCO_3$, pre-fired Y_2O_3 and MoO_3, were weighed out stoichiometrically and the mixture was fired at 950°C for 12hr., re-ground, then heated to 1300°C in 5% H_2/ Ar and held for 48h.

Phase purity was assessed using a focusing Guinier-Hägg camera and PanAlytical X-Pert X-ray diffraction apparatus.

Thermal gravimetric analysis (TGA) was carried out on Ba_2YMoO_6 by heating in air to determine the oxidation state of Mo. The weight gain was 1.45% compared to the expected 1.44% indicating the Mo^{5+} state to better than 1%.

d.c. magnetic susceptibility as a function of temperature was measured in 0.01-0.05T applied fields within the temperature range of 2K to 300K and isothermal magnetization data were collected for La_2LiMoO_6 in the field range from -5T to 5T at 5 and 20K using Quantum Design magnetic properties measurement system (MPMS) superconducting quantum interference device (SQUID) magnetometer at McMaster University.

The powder neutron diffraction measurements were carried out on the C2 diffractometer at the Canadian Neutron Beam Centre, NRC, Chalk River Laboratories. The measurements were performed at 3.3 and 299.7K with neutron wave lengths, λ =1.32873 and λ =2.36937 for La_2LiMoO_6, and λ= 1.33052 and 2.37192Å at 2.8 and 297.8K for Ba_2YMoO_6. Additionally, higher resolution diffraction data at 2.8K with λ=1.33052Å was collected for this compound. Refinements were done either with the GSAS or FULLPROF software packages.[12,13]

Heat capacity measurements were carried out using an Oxford MagLab calorimeter at McMaster University and an Quantum Design physical properties measurement system(PPMS) at Florida State University. The lattice match compounds La_2LiIrO_6 and Ba_2YNbO_6 were prepared using solid state reactions as well. The synthesis method for La_2LiIrO_6 is described in ref [14]. For Ba_2YNbO_6 a stoichiometric mixture of $BaCO_3$, pre-fired Y_2O_3 and Nb_2O_5 was heated at 1300°C for 36 h in air.

Muon spin relaxation (μSR) measurements were carried out on the M20 beamline at TRIUMF in Vancouver. The zero field μSR (ZF- μSR) data were collected at various temperatures between 1.66 and 25K for La_2LiMoO_6, and at 2, 5, 10 and 20K for

Ba_2YMoO_6. For La_2LiMoO_6, longitudinal field μSR (LF-μSR) was also collected at 1.66K for the field of 100, 400, 800, 1200 and 1600G.

^{89}Y MAS NMR was carried out at the University of Manitoba using a Varian $^{\mathrm{UNITY}}$*Inova* 600 (B_0 = 14.1 T) spectrometer operating at a Larmor frequency of 29.36 MHz. Ba_2YMoO_6 powder was packed in a ZrO_2 MAS rotor with a 22 μL fill volume and spun at 20000 ± 6 Hz in a 3.2 mm double-resonance Varian-Chemagnetics probe. Acquisition was carried out using a 20° tip angle (ν_{rf} = 42 kHz), 270 000 co-added transients, and a recycle delay of 0.8 s. Frequency shifts are referenced with respect to 2M $Y(NO_3)_3$ at 0.0 ppm.

^{89}Y NMR (nuclear spin I = 1/2, nuclear gyromagnetic ratio $^{89}\gamma_n/2\pi$ = 2.0859 MHz/Tesla), Knight shift measurements were carried out at McMaster University in a fixed magnetic field of B = 7.7 Tesla. The NMR lineshape was obtained by applying the standard Fourier transform (FFT) technique for the spin echo envelope at ~100 K or higher. However, gradual line broadening was observed and the linewidth exceeded the bandwidth of our rf excitations at lower temperature. Accordingly, it was needed to convolute multiple FFT envelopes to obtain the entire lineshape below ~100K down to ~63 K. Below ~63 K, due to the extremely broad lineshape, the lineshape was measured point-by-point by integrating the spin echo intensity. It was confirmed that the point-by-point measurements agree well with the convolution of the multiple FFT envelopes at 63 K. The ^{89}Y nuclear spin-lattice relaxation rate, $1/T_1$, was measured by applying saturation comb pulses prior to a regular spin-echo sequence, and varying the delay time between them. The single exponential fit of the recovery of nuclear magnetization was good, as expected for a nuclear spin $I = 1/2$ nucleus.

Results and Discussion.

La_2LiMoO_6

Crystal structure

The crystal structure of La_2LiMoO_6 was confirmed by both x-ray diffraction and neutron diffraction measurements to be monoclinic with space group $P2_1/n$, consistent with the previous X-ray single crystal diffraction result of Tortelier and Gougeon [9]. The unit cell constants refined from the data collected at 300K are a= 5.5939(2)Å, b=5.6924(2)Å, c=7.8803(2)Å and β=90.260(3)°. The overall refinement results are shown in Fig.5.2 and Table 5.1 where both datasets were refined simultaneously using GSAS.

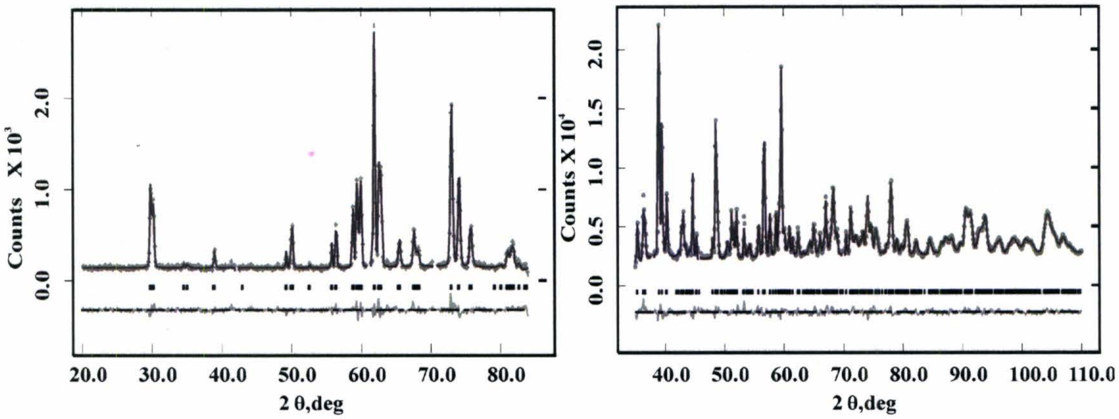

Figure 5.2. Rietveld refinement of neutron diffraction data collected with two wavelengths, 2.37Å (left) and 1.33 Å(right) at 297K for La_2LiMoO_6. The vertical tick marks locate the Bragg peak positions and the lower horizontal line represents the difference between the data,(crosses) and the model (solid line). A weak impurity peak near 70 deg was excluded for the 2.37Å pattern.

The model assumes full ordering of the B-site cations (Li and Mo). This is consistent with the empirical study of B site ion ordering in the double perovskites by Anderson *et al* [15] which shows that for a formal charge difference of 4, full B-site ordering is found, regardless of the difference in radii, Δr. For this compound even Δr is significant as the radii for Mo^{5+} (0.61Å) and Li^{+} (0.76Å) differ by almost 25%.[16] Moreover, the isostructural compound, La_2LiRuO_6, was shown to have no detectable Li/Ru disorder using ^{7}Li MAS NMR[17]. There is no indication from the B-site atomic displacement parameters that this is not correct. The crystal structure of this compound at 3.3K was also refined and the monoclinic structure, $P2_1/n$ was retained.

Note that in spite of the overall monoclinic symmetry, the nearest neighbor environments of both B-site ions are those of a nearly perfect octahedron with a weak tetragonal compression. Especially for the Mo – O polyhedron, the O – Mo – O angles are either 90 or 180 degrees to within a few tenths of a degree. The weak tetragonal compression will split the nominally t_{2g}^{1} configuration into a lower orbital singlet (d_{xy}) and a higher doublet (d_{xz},d_{yz}).

Table 1a. The results for a Rietveld refinement using GSAS[12] of neutron powder data for La_2LiMoO_6 (299.7K) in $P2_1/n$. a= 5.5939(2) Å, b = 5.6924(2) Å, c = 7.8803(2) Å, β = 90.260(3)°. $R_{wp} = 0.0519$, $\chi^2 = 2.47$.

atom	x	y	z	U_{iso}(Å^2)
La	-0.0098(6)	0.05034(35)	0.2516(4)	0.0106(5)
Li	0.5	0	0	0.029(5)
Mo	0.5	0	0.5	0.0119(10)
O1	0.1917(8)	0.2159(8)	-0.0460(6)	0.0137(12)
O2	0.2855(7)	-0.3077(8)	-0.0421(6)	0.0105(11)
O3	0.0836(7)	-0.5207(5)	0.2387(5)	0.0108(8)

Table 1b. Selected interatomic distances (Å) and angles (°) for La_2LiMoO_6 at 299.7K.

bond	dis. / angle
Mo-O1(x2)	1.975(4)
Mo-O1(x2)	1.966(4)
Mo-O3(x2)	1.940(4)
Li-O1(x2)	2.148(4)
Li-O2(x2)	2.148(4)
Li-O3(x2)	2.117(4)
O1-Mo-O1	180.0
O1-Mo-O2	89.02(23)
O1-Mo-O3	90.03(15)
O2-Mo-O2	179.96
O2-Mo-O3	89.72(18)
O3-Mo-O3	180.0
Li-O1-Mo	150.93(24)
Li-O2-Mo	151.86(25)
Li-O3-Mo	152.42(20)

Magnetic properties

The susceptibility of this compound is shown in Fig. 5.3. Note the deviation from the Curie-Weiss (C-W) law below ~ 150K. Data were fitted to the Curie-Weiss law, $\chi = C/(T-\theta)$ for the range T >150K, yielding, θ= -45(2)K and C = 0.253(1) (emu/mol-K) corresponding to $\mu_{eff} = 1.42\ \mu_B$, compared to the spin only value of 1.73 μ_B. A zero-field-cooled/field-cooled (ZFC/FC) divergence was observed at 20K and a broad peak around 5K. It should be noted that there was some sample to sample variability for this material, especially in terms of the derived θ value which varied from ~ -10K to -45K. Nonetheless, robust observations for all samples include the deviation from the C-W law below 150K, the ZFC/FC divergence at 20K and the broad maximum near 5K. Thus, an average frustration index, $f = |\theta|/T^*$, falls in the range ~ 1 - 2 taking the divergence temperature as T^*, in stark contrast to the isostructural S = 3/2 and S = 1 materials, La_2LiRuO_6 and La_1LiReO_6, where f ~7 for each.[6 , 7] Thus, from the bulk susceptibility there is no evidence for magnetic frustration, at least from the frustration index.

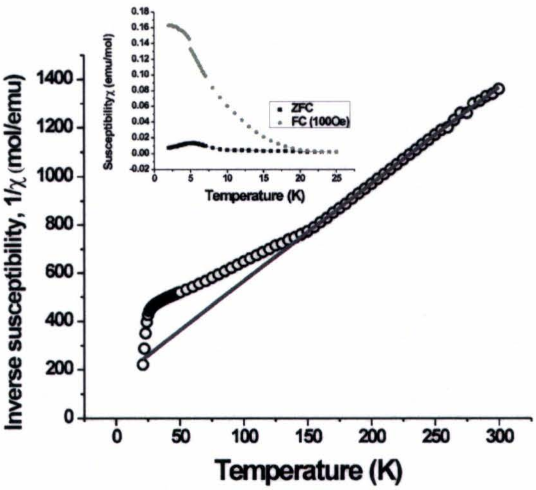

Figure 5.3. The inverse magnetic susceptibility of La_2LiMoO_6 showing Curie-Weiss behavior below 150K. (Inset) The susceptibility below 25K at an applied field of 100Oe. Note the zfc/fc divergence below ~ 20K and the broad maximum at 5K in the zfc data.

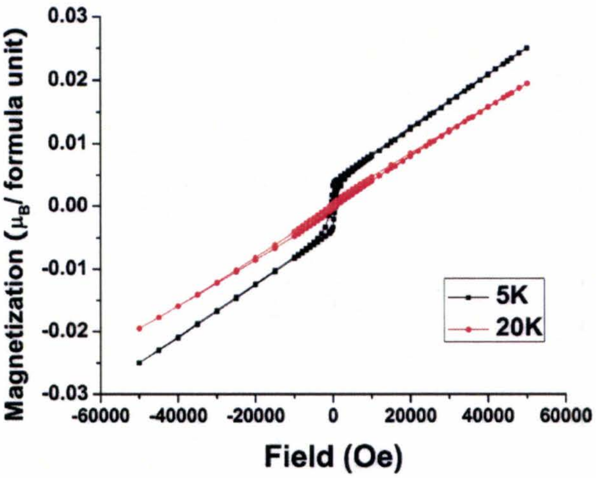

Figure 5.4. Hysteresis loops for La_2LiMoO_6 at 5K and 20K.

The field dependence of the susceptibility shown in Figure 5.4 discloses a weak hysteresis at 5K, which disappears at 20K, indicating the presence of a weak spontaneous moment below 20K.

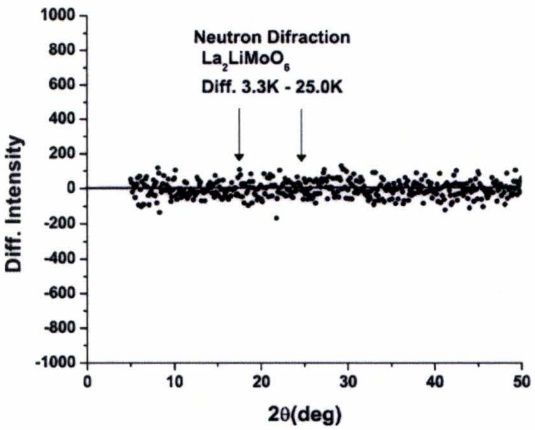

Figure 5. The difference neutron diffraction pattern for La_2LiMoO_6, 3.3K – 25.0K. The arrows show the positions expected for magnetic reflections assuming a Type 1 fcc magnetic structure as found for La_2LiRuO_6.[19]

Magnetic Neutron Diffraction.

There is no sign of long range order in the neutron powder diffraction data, Fig. 5.5, where the difference plot, 3.3K – 25K is shown. Of course, the intensities of magnetic Bragg peaks for $S = \frac{1}{2}$ spins is expected to be ~ ten times weaker than those from the $S = 3/2$ analog, La_2LiRuO_6, where such peaks were readily visible above background.[17]

Heat Capacity.

Heat capacity data, Fig. 5.6 shows only broad features at 20 and 5K, consistent with the bulk susceptibility and supportive of the absence of long range magnetic order. Unfortunately, the chosen lattice match material, La_2LiIrO_6 was not useful here as its heat capacity actually exceeded that for $LaLiMoO_6$ above 20K. The entropy removal from 7 – 2K, including the peak at 5K, is 0.25 J/mol-K^2 or 4.4% of that expected for S = 1/2.

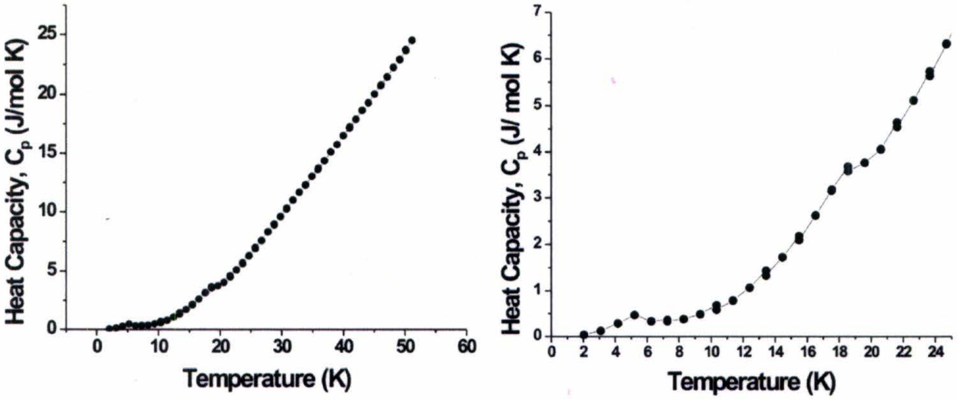

Figure 5.6. (Left)The heat capacity C_p as a function of temperature for La_2LiMoO_6. (Right) The region below 25K showing two broad peaks at ~ 18K and 5K.

Muon Spin Relaxation.

Muon spin relaxation (μSR) is a local probe of magnetism and is therefore complementary to the bulk techniques just described. Zero-field (ZF) μSR data are shown in Fig. 5.7(a). Although one observes only weak, paramagnetic relaxation at 25 K, well-defined oscillations are observed at 5 K. The latter indicates that each muon senses a static, unique field in the low temperature regime. A fast Fourier transform (FFT) of the data at 6 K detects three peak frequencies, and this is consistent with the presence of three magnetically-inequivalent oxygen sites in the crystal structure (see Table 5.1). As a result, the data was fit to the following function: $A_oP(t)= A_1\exp(-\omega_1 t)\cos(\omega_1 t+\theta) + A_2\exp(-\omega_2 t)\cos(\omega_2 t+\theta) + A_3\exp(-\omega_3 t)\cos(\omega_3 t+\theta) + A_{tail}\exp(-\lambda_{tail} t) + A_G G_{KT}$.

The three frequencies are given by ω_1, ω_2, and ω_3, respectively, and their temperature-dependences are plotted in Fig. 5.7(b). The onset of these frequencies is around 20 K, in line with the susceptibility and heat capacity data. The A_{tail} term accounts for the volume fraction of the sample that is ordered but with a local field parallel to the muon spin. Finally, the Gaussian Kubo-Toyabe term (temperature-independent relaxation rate was assumed in this analysis) accounts for the volume fraction of the sample that is not ordered. Note that the amplitude of this component quickly dropped to zero below ~ 20 K, and so 100% of the volume fraction was found to be ordered at low temperatures.

For the data collected below 5K, an additional frequency peak was observed in the FFTs at ~ 2 MHz shown in the inset to Fig. 5.7b. This is likely related to the broad 5K peak in the susceptibility and heat capacity and may signify a change in the local magnetic structure. As well, longitudinal field data (not shown) at 1.7K show that decoupling occurs for an applied field of 800 Oe, indicating a static spin ground state.

While the behavior seen for La_2LiMoO_6 could be taken as evidence for long range magnetic order, the evidence from heat capacity and neutron diffraction indicate otherwise. Of course it is not possible to measure a correlation length for the magnetic order sensed by a local probe such as μSR and it is thus not possible to distinguish between true long range order and order on a finite but significant length scale. A similar situation was encountered with $Li_2Mn_2O_4$ for which strong oscillations were detected by μSR, whereas, the length scale of the magnetic correlations is known to be finite but of the order 90 Å. [18]

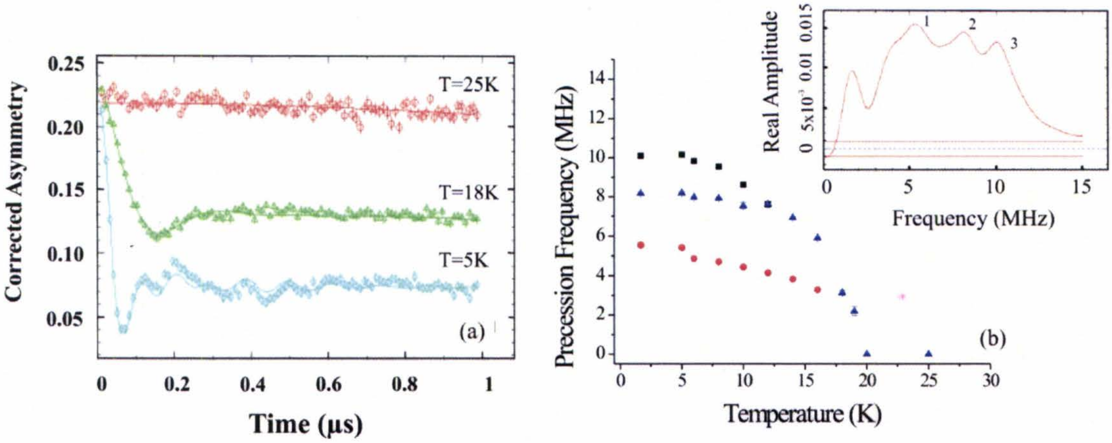

Figure 5.7. a. (Left) μSR results for La_2LiMoO_6. Corrected asymmetry at selected temperatures. b.(Right) Temperature dependence of the amplitudes of the three frequencies (1-3) obtained from a fast fourier transform (see text) of the data. The inset shows the result at 1.7K where a fourth, low amplitude frequency at ~ 2MHz is seen.This feature disappears above 5K. (Color online)

Ba_2YMoO_6

Crystal Structure

The neutron diffraction data collected at 2.7 and 298K with λ = 1.33 Å and 2.37 Å were refined and the results are shown in Fig. 5.8 and Table. 5.2. The results are in excellent agreement with those of Cussens et al. [8] According to the refinement, the compound retains cubic symmetry with space group Fm3m, and the lattice constant was determined to be 8.3827(7) Å at 2.7K.

Surprisingly, even at 2.7K, there is no clear distortion observed this compound although one could expect to see Jahn-Teller distortion arising from d^1 electronic configuration of Mo^{5+}. Additionally, no distortion was observed with higher resolution data, ($\Delta d/d \sim 2 \times 10^{-3}$) collected at 2.7K, Figure 5.8(bottom). While the symmetry consequences of a J-T distortion in this material are not clear, certainly a lowering of the m-3m site symmetry at the Mo site must occur. This will likely result in a lowering of the space group symmetry. Such an effect was not observed in our data but a very subtle distortion below the resolution of the data cannot of course be ruled out. It is important to note that room temperature x-ray diffraction data of much better resolution, $\Delta d/d \sim 1 \times 10^{-3}$, also did not show any distortion from Fm3m symmetry.

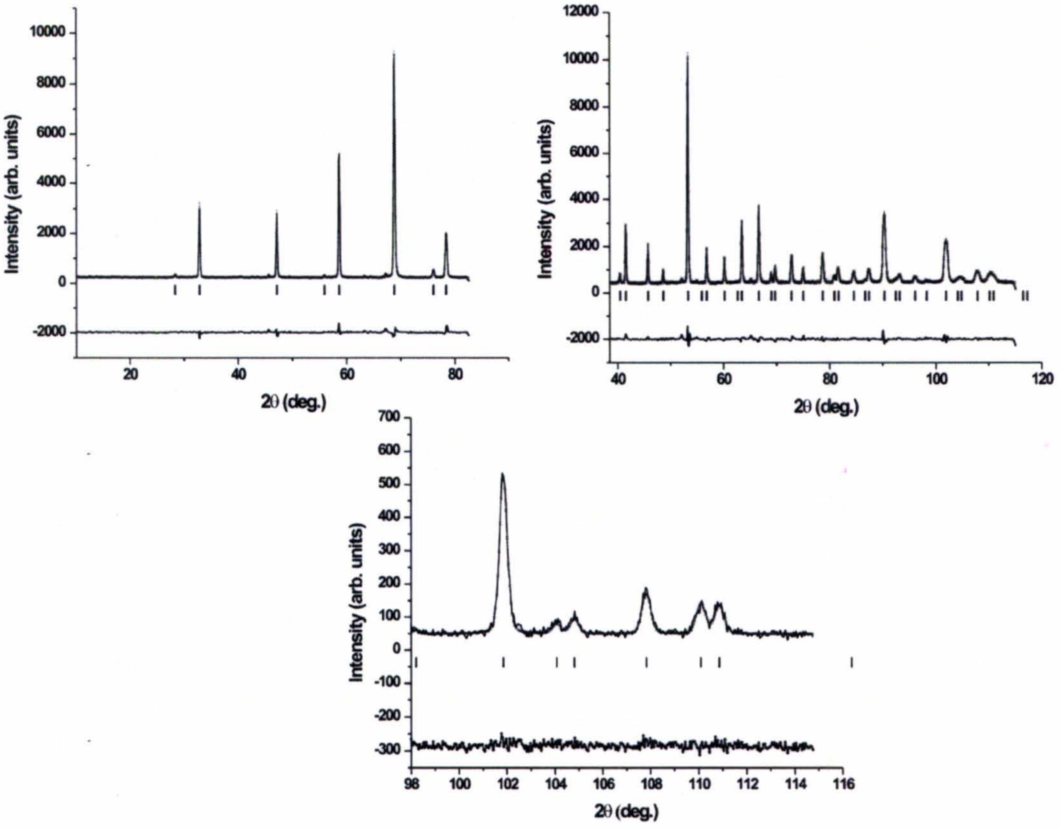

Figure 5.8. (Top) The refinement result of neutron diffraction pattern for two wavelengths, 2.37Å (left) and 1.33 Å(right), collected at 2.7K for Ba_2YMoO_6. (Bottom) Higher resolution($\Delta d/d \sim 2 \times 10^{-3}$), high angle data showing that cubic symmetry is retained. The vertical tick marks locate the Bragg peaks and the lower horizontal line is the difference between the data (circles) and the fit (solid line).

Table 5.2a. The results for a Rietveld refinement using FULLPROF[13] of neutron powder data for Ba_2YMoO_6 in Fm3m at 297.8K and 2.7K. a = 8.3920(6) Å (297.8K), a = 8.3784(6) Å (2.7K). Agreement indices at 297.8K: $R_{wp} = 0.063[0.076]$, $\chi^2 = 2.51[2.08]$, $R_B = 0.031[0.021]$ and at 2.7K: $R_{wp} = 0.067[0.054]$, $\chi^2 = 3.00[9.45]$, $R_B = 0.035[0.011]$. Numbers in [ ] are those from refinement of the λ=2.37Å data and the others from λ=1.33Å data.

297.8K	x	y	z	$U_{iso}(Å^2)$	U_{11}	U_{22}	U_{33}
Ba	0.25	0.25	0.25	0.0072	0.0020(2)	0.0020(2)	0.0020(2)
Y	0.5	0.5	0.5	0.0043	0.0012(4)	0.0012(4)	0.0012(4)
Mo	0	0	0	0.0044	0.0012(4)	0.0012(4)	0.0012(4)
O	0.2347(2)	0	0	0.0123	0.0017(4)	0.0043(3)	0.0043(3)

2.7K	x	y	z	$U_{iso}(Å^2)$	U_{11}	U_{22}	U_{33}
Ba	0.25	0.25	0.25	0.0015	0.0005(3)	0.0005(3)	0.0005(3)
Y	0.5	0.5	0.5	0.0023	0.0006(4)	0.0006(4)	0.0006(4)
Mo	0	0	0	0.0008	0.0002(1)	0.0002(1)	0.0002(1)
O	0.2341(2)	0	0	0.0069	0.0005(4)	0.0026(3)	0.0026(3)

Table 5.2b. Selected bond lengths and comparison with the sum of the ionic radii.[19]

bond	297.8K	2.7K	$r_B + r_O$ $r_{B'} + r_O$
Mo-O x6 (Å)	1.969(3)	1.963(2)	1.96
Y-O x6 (Å)	2.227(3)	2.226(2)	2.25

This compound has a charge difference of 2 for the B site ions which differ by 0.29Å in ionic radius [12], thus locating it near the B-site order/disorder boundary in the phase diagram of Anderson et al. [15] and the issue of Y/Mo site disorder should be investigated. This discussion follows closely that already presented for Ba_2YRuO_6.[6] Woodward et al[19] have studied B-site ordering in a number of double perovskites of the type $A_2BB'O_6$ with the combination B^{3+}/B'^{5+} which is relevant here. [20] The extent of B/B' site order was determined quantitatively by a constrained refinement of neutron powder diffraction data and by monitoring the relative widths of the hkl all-odd supercell reflections to the hkl all-even subcell reflections. In all cases of partial B-site order, the hkl all-odd reflections were significantly broader than the hkl all-even reflections. To summarize some of their findings, for $\Delta r > 0.260$ Å, 100% B/B' -site order is always found. For example, among the Fm3m phases studied, Ba_2YNbO_6 is judged to be 100% ordered, $\Delta r = 0.260$ Å, while Ba_2ScNbO_6 and Ba_2ScTaO_6, with $\Delta r = 0.105$ Å, show only about 50% order. Thus, one would expect 100% B-site order in Ba_2YMoO_6.

First, the neutron diffraction data were examined. The contrast in neutron scattering lengths between Mo(6.715fm) and Y(7.75fm) is ~ 15%, about twice the contrast for x-ray scattering. There is no indication from the atomic displacement parameters, U, Table 5.2, for obvious Y/Mo site disorder nor from the derived interatomic Y-O and Mo-O distances, which agree well with those of Cussen et al.[8] and the sum of the ionic radii.[16] As well, the full width at half maximum (FWHM) of several hkl-odd/hkl-even pairs were examined and no significant differences were found. For example the odd/even width ratio for the (551,711)/(624) pair is 1.04(8) and that for the (553,731)/(642) pair is 1.01(8). Thus, from the neutron powder diffraction data, there is no detectable Y/Mo site disorder.

Hence, ^{89}Y MAS NMR data were collected for this compound. Previous studies on Ba_2YRuO_6 which also showed no evidence for B-site disorder from neutron data disclosed a ~ 1% Y/Ru mixing.[6] Figure 5.9 shows the spectrum obtained for

Ba_2YMoO_6 at 288K and there are two distinct peaks located at -1391 ppm and -1334ppm with an area ratio of 81%/19%, respectively. The uncertainty in these areas is +/- 3%. This is a considerably greater site mixing than found in Ba_2YRuO_6 or Ba_2YReO_6.[6,7] Following the previous analysis [6] the more negatively shifted peak is assigned to a Y-$(O\text{-}Mo)_6$ local environment and the other to Y-$(O\text{-}Mo)_5(O\text{-}Y)$. Taking into account the coordination number of six at the Y-site, an estimate of the mixing level is ~ 3%, too small to be detected in the neutron diffraction data.[6] Note that these results imply that a finite concentration of "defect" clusters of composition [Mo-$(O\text{-}Mo)_6$] will exist and this will likely be reflected in both the bulk and especially the local susceptibility.

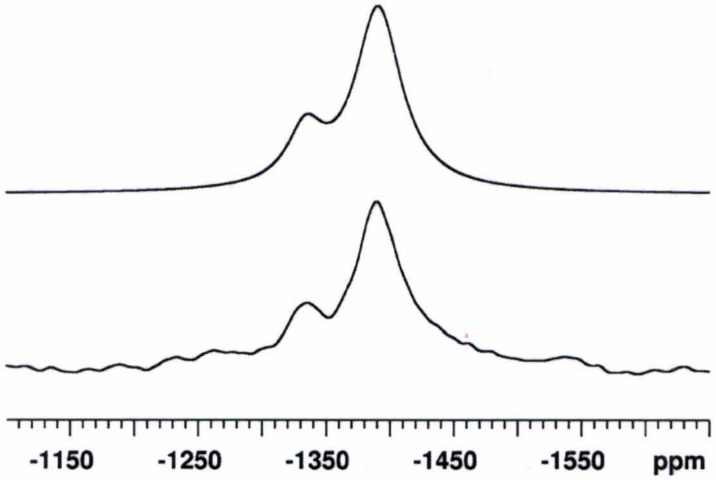

Figure 5.9. ^{89}Y MAS(magic angle spinning) NMR of Ba_2YMoO_6 at 288K. The top is a simulation and the bottom are the data. The relative intensities of the two peaks is 19%/81% with an error of +/- 3%.

Magnetic properties

Ba_2YMoO_6 shows only apparent bulk paramagnetic behavior down to 2K, Figure 5.10, which is consistent with the result previously reported by Cussen et al. [8]. The result of Curie-Weiss fitting above 150K shows θ = - 219(1) K, and an effective moment of 1.72(1)μ_B which is essentially the spin only value for S=1/2 (1.73μ_B). These values are somewhat larger than those reported by Cussen et al. The frustration index, $f = |\theta_{cw}|/T_N$ for this compound is thus > 100, indicative of extremely frustrated behavior. In order to verify any ordering/ spin dynamics, we have conducted low temperature neutron diffraction, heat capacity, muon spin relaxation and ^{89}Y NMR investigations.

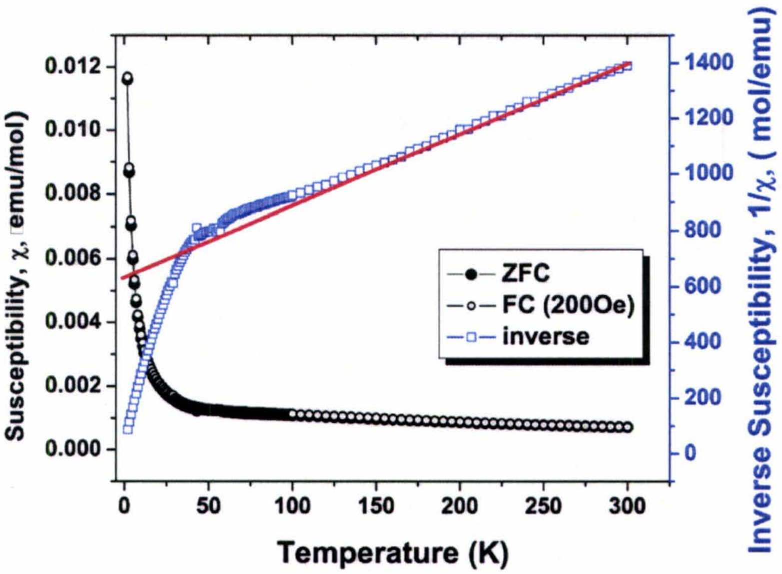

Figure 5.10. The susceptibility and inverse susceptibility of Ba_2YMoO_6 at an applied field of 200 Oe.

Magnetic Neutron Diffraction.

From the difference powder neutron diffraction pattern (2.8K – 297.8K), Fig. 5.11, no magnetic Bragg peaks were detected in the diffraction pattern. As in the case for La_2LiMoO_6, while this observation is evidence against long range magnetic order in this system, it is not necessarily conclusive given the small S value and other corroborating data are needed.

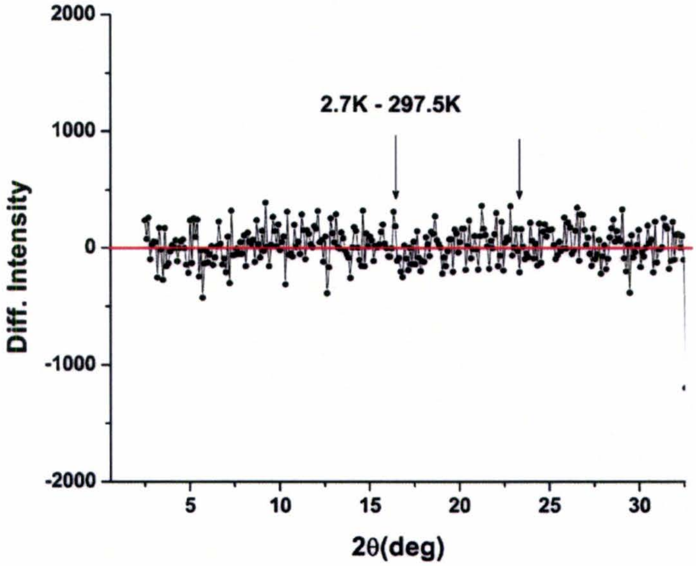

Figure 5.11. Neutron diffraction difference pattern, 2.7K – 297.5K for Ba_2YMoO_6. The arrows show the expected positions of magnetic reflections assuming a Type 1 fcc magnetic structure as found for Ba_2YRuO_6.[6]

Heat Capacity.

Heat capacity data for Ba_2YMoO_6 and Ba_2YNbO_6, the lattice match phase, are shown in Figure 5.12. Note the absence of a λ-type peak which again is evidence against long range order. The magnetic heat capacity shows very broad peak around 50K. The entropy lost in this temperature range (<50K) was calculated to be 51.9% of the theoretical value (R ln 2).

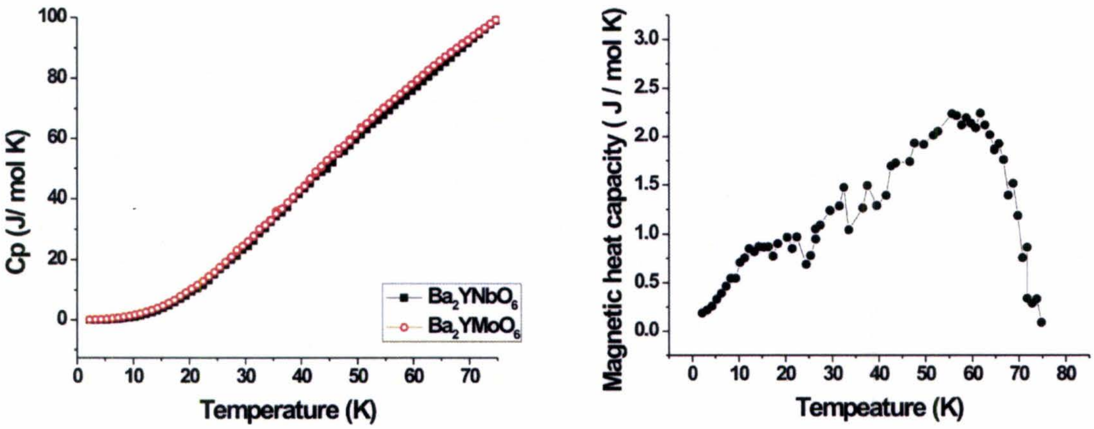

Figure 5.12. (a.) (Left) The heat capacity of Ba_2YMoO_6 and Ba_2YNbO_6. (b.) (Right) Magnetic heat capacity of Ba_2YMoO_6.

μSR.

μSR data, collected at various temperatures, are shown in Fig. 5.13. One can see that the relaxation functions indicate dynamic spin behavior down to 2K with a weak slowing down at 2K but no indication of spin freezing or order on any length scale. The relaxation functions were fitted with the equation for dynamic behavior, $P(t) = A \exp(-\lambda t)$. Overall, the spins in this compound show persistent fluctuating spin behavior within μSR time window.

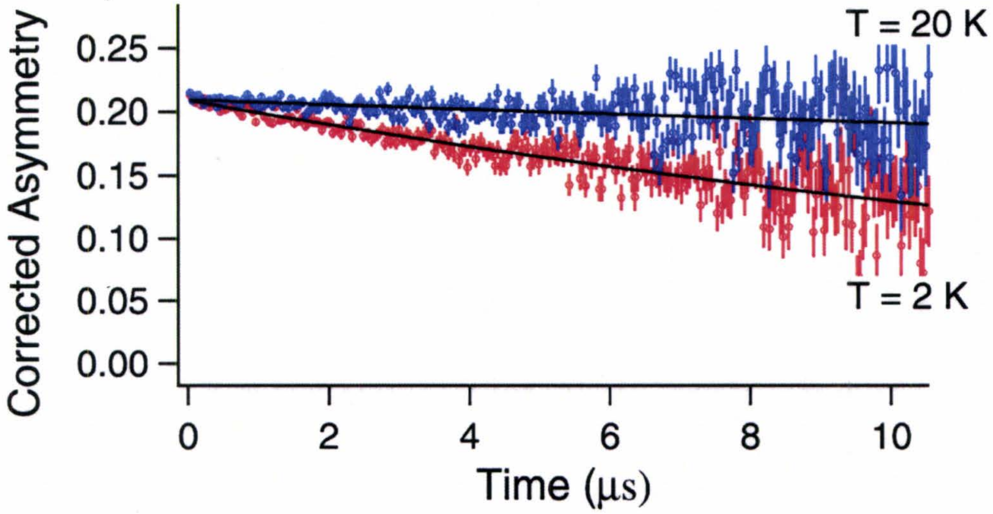

Figure 5.13. Zero Field (ZF) muon spin relaxation (μ SR) data for Ba_2YMoO_6 for two temperatures. The lines are fits to a single exponential relaxation function, see text.(Color online)

^{89}Y NMR.

Ba_2YMoO_6 magnetic properties and spin dynamics were also studied through ^{89}Y NMR, measuring the linewidth of resonance peaks and paramagnetic Knight shifts. NMR is an extremely useful probe to uncover the distinctive temperature dependences of the local magnetic susceptibility which is different from the overall bulk average. For example earlier ^{35}Cl and ^{17}O NMR measurements uncovered the presence of vanishingly small spin susceptibility in a Kagome antiferromagnet $ZuCu_3(OH)_6Cl_2$, although the bulk susceptibility data grows monotonically down to 2 K.[21,22] In Figure 5.14(a), representative ^{89}Y NMR lineshapes at 295 , 185 , and 75 K are presented. A sharp peak with FWHM (Full Width at Half Maximum) less than 10 kHz is evident near 295 K with however, a broad hump at the higher frequency side, and hence the overall lineshape is tapered toward higher frequency. In addition, a small side peak on the higher frequency side of the main peak is observed which is most distinctly visible at 185 K near 16.03 MHz. The main sharp peak broadens gradually with decreasing temperature and masks the presence of this side peak which is no longer distinguishable at 75 K. The entire lineshape is shifted to the lower frequency side compared with the expected position of the resonance in 7.7 Tesla, ${}^{89}f_o = {}^{89}\gamma_n B = 16.061$ MHz (shown by grey dotted line). For example, the peak frequency at 295 K, ${}^{89}f = 16.041$ MHz, is shifted from ${}^{89}f_o$ by $\Delta f = {}^{89}f - {}^{89}f_o = -0.020$ MHz. This shift Δf is caused by the paramagnetic *Knight shift*, as defined by

$$ {}^{89}K = \Delta f \;/\; {}^{89}f_o. \qquad (5.1)$$

${}^{89}K$ is represented in terms of %, by applying a factor of 100, following the common convention in condensed matter physics. (Note that 0.01% of the Knight shift corresponds to 100 ppm.) ${}^{89}K$ is related to the paramagnetic susceptibility of Mo magnetic moments χ by

$$ {}^{89}K = A\,\chi + K_{\mathrm{chem}}, \qquad (5.2)$$

where A is the hyperfine coupling constant, and K_{chem} is a small chemical shift (typically, $|\,K_{\mathrm{chem}}\,| < 0.02$ %, or equivalently, < 200 ppm).

Upon cooling, the overall lineshape shifts further to lower frequency. In view of the observed increase of the bulk susceptibility data χ at lower temperatures presented earlier in Figure 5.10, we can understand the observed temperature dependent shift of the NMR lineshapes as the consequence of a negative hyperfine coupling with magnetic moments, *i.e.* $A < 0$. The observed linewidth at 75 K, FWHM ~ 9 kHz, is typical for a paramagnetic insulator of a large bulk magnetic susceptibility. However, below ~75 K, qualitatively different NMR lineshapes emerge, as shown in Fig.5.14(b) in the form of two distinct peaks, clearly seen at 50K, with one shifted to higher frequency. At 50 K the main peak is narrower than the higher frequency component only by a factor of ~2 and below 50K the low frequency component becomes very broad with decreasing temperature while shifting dramatically to lower frequencies. The proximity between the two peaks and the asymmetric lineshape makes it difficult to estimate the intensity ratio accurately. Recalling that the hyperfine coupling constant $A < 0$, the ^{89}Y nuclear spins represented by the low frequency peak sense a growing hyperfine field with decreasing temperature. In contrast the broader peak at the higher frequency shifts to *higher* frequency with decreasing temperature reaching a constant value at ~ 40K. Thus, the local magnetic susceptibility near these ^{89}Y nuclear spins *decreases* with decreasing temperature.

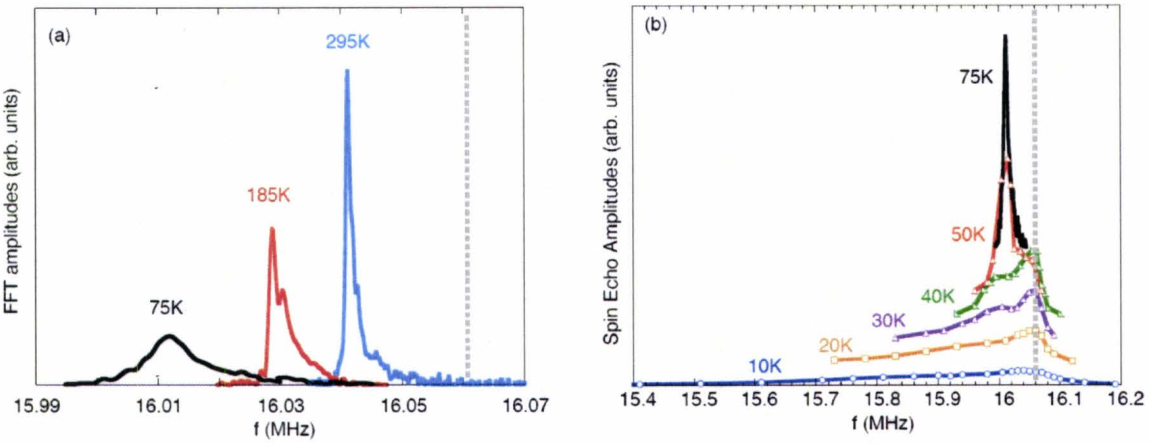

Figure 5.14. ^{89}Y NMR lineshape at various temperatures. (a.) (Left) Representative line shapes at selected temperatures for Ba_2YMoO_6. (b.) (Right) Evolution of the line shape below 75K. (Color online)

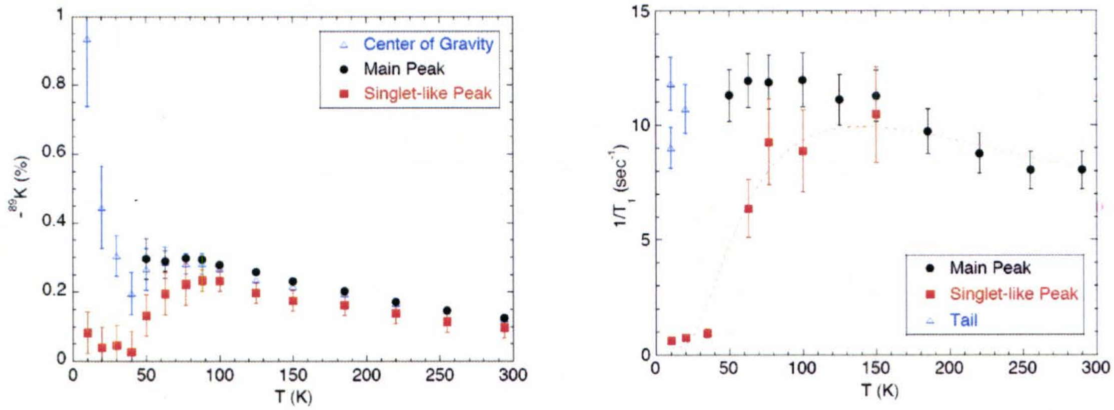

Figure 5.15. Temperature dependence of the paramagnetic Knight shift, $-^{89}K$,(Left) and the relaxation rate, $1/T_1$ (Right) for the "main" (lower frequency) peak and the singlet-like (higher frequency) peak of Fig.5.14(b). The dotted line is an empirical fit $1/T_1 \sim C/T \exp(-\Delta/k_BT)$ with $\Delta/k_B \sim$ 140K. Integrated intensities of the two are roughly equal.(Color online)

In Fig.5.15,(left panel) the contrasting behavior of local magnetic susceptibility for the two distinctive ^{89}Y environments in the sample is demonstrated by plotting the temperature dependence of ^{89}K, plotted as -^{89}K to reflect the fact that $A < 0$, defined for different components of the NMR lineshape. First, consider -$^{89}K_{CG}$, defined for the center of gravity of the whole lineshape (open triangles). In essence, -$^{89}K_{CG}$ is a bulk average of local magnetic susceptibility at the nuclear spin of each ^{89}Y site, although the non-local nature of the hyperfine coupling makes the direct comparison somewhat non-trivial. Nonetheless, notice that the observed temperature dependence of -$^{89}K_{CG}$ is qualitatively similar to the SQUID data in Figure 5.10. -$^{89}K_{CG}$, monotonically increases from 295 K to ~100 K, levels off, then increases rapidly as T → 0. The Knight shift -$^{89}K_{Main}$ defined for the low frequency peak exhibits analogous behavior down to ~ 50 K, where the sharp feature becomes no longer observable in the NMR lineshape. In contrast, the local magnetic susceptibility at the location of ^{89}Y nuclear spins involved in the higher frequency peak, as represented by -$^{89}K_{Singlet}$, begins to decrease below ~ 100 K down to ~ 40 K. The very small magnitude, -$^{89}K \sim 0.02$ %, observed at 40 K suggests that the *local magnetic susceptibility is vanishingly small at these sites*. Recalling that the integrated intensity of the higher frequency peak is roughly half of the overall NMR lineshape, we conclude that about half of the magnetic moments at Mo sites become vanishingly small.

Further analysis of the -^{89}K data can yield values of the hyperfine coupling constant, A, and an estimate of the separate contributions to the bulk susceptibility, $\chi = \chi_{spin} + \chi_{VV} + \chi_{dia}$, where χ_{VV} and χ_{dia} are the van Vleck and diamagnetic contributions, respectively.

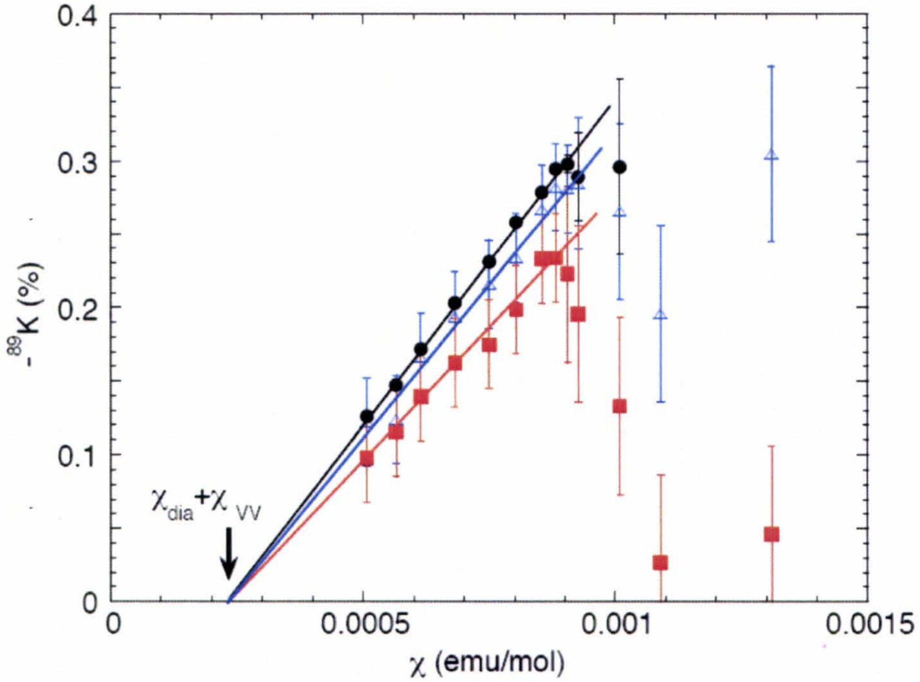

Figure 5.16. Scaling of the paramagnetic Knight shift (-^{89}K) with the bulk susceptibility for Ba_2YMoO_6. The derived hyperfine coupling constant, A = -23.4kOe/μ_B . The intercept gives the sum of the van Vleck and diamagnetic susceptibility components. (Color online)

In Fig.5.16, -^{89}K is plotted as a function of the bulk-averaged SQUID susceptibility, χ, by choosing temperature as the implicit parameter. Note the linear relations between -^{89}K and χ above ~ 100 K. From the slope, one obtains the hyperfine coupling constant A = -23.4 kOe/μ_B using the results of -$^{89}K_{CG}$. The magnitude of A is ~ 5% greater (smaller) for -$^{89}K_{Main}$ (-$^{89}K_{Singlet}$). By extrapolating the linear fit to -$^{89}K_{CG}$ = 0, we find that $\chi_{VV} + \chi_{dia} \sim 2.2 \times 10^{-4}$ emu/mol in the temperature range above ~ 100 K.

Finally, the nuclear spin-lattice relaxation rate $1/T_1$ in Fig.15 (right panel) provides additional evidence for the presence of a collective singlet-like ground state of Mo magnetic moments. $1/T_1$ measures the spectral weight at the NMR frequency ^{89}f of the fluctuating hyperfine magnetic fields at the location of nuclear spins, and may be written

as $$\frac{1}{T_1} \propto T \sum_{\vec{q} \in 1stB.Z.} \left|A(\vec{q})\right|^2 \chi''(\vec{q}, f) \qquad (5.3)$$

where χ” is the imaginary part of the dynamical susceptibility, **q** is the wave vector, f (~16 MHz) is the resonance frequency, *A*(**q**) is the hyperfine form factor, and the summation over **q** should be taken over the first Brillouin zone..

If $1/T_1$ is dominated by fluctuating hyperfine magnetic fields from localized magnetic moments at temperatures much greater than the energy scales of interactions between themselves, we expect $1/T_1$ ~ constant [23]. On the other hand, if the magnetic moments develop short-range order, $1/T_1$ generally increases with decreasing temperature near a magnetic instability. These results for $1/T_1$ measured at the main sharp peak show only a mild increase from 295 K down to ~50 K. The absence of a pronounced peak or divergent behavior rules out the presence of any magnetic long-range order. However, $1/T_1$ measured at the singlet-like peak begins to deviate from the behavior of the main sharp peak below ~100 K, and rapidly tends toward zero. This implies that the low energy excitations of magnetic moments are nearly non-existent, as expected for a collective singlet ground state. In order to characterize this singlet like spin state, we model the overall temperature dependence as $1/T_1 \sim C/T \exp(-\Delta/k_BT)$, where C is a constant. We found that the behaviors of the singlet-like peak below 150K as well as the main peak above 150K can be reproduced well by choosing the gap size as $\Delta/k_B \sim$ 140K. Recall, however, that the singlet-like peak accounts for only about a half of all ^{89}Y nuclear spins in the sample the other half being in the broad tail of the NMR lineshape below ~50 K, as shown in Fig.5.14(b). $1/T_1$ measured for these ^{89}Y nuclear spins does *not* show any suppression below ~50 K, as shown by data points represented by open triangles. In other words, approximately half of ^{89}Y nuclear spins continue to sense the same level of fluctuating hyperfine magnetic fields arising from low energy excitations of magnetic moments even below 50 K.

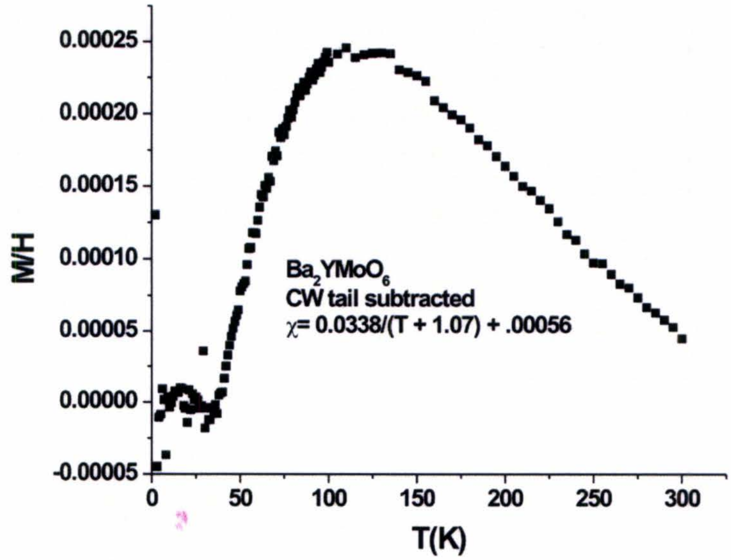

Figure 5.17. The Curie-tail subtracted bulk susceptibility of Ba_2YMoO_6.

It is of considerable interest to return to the bulk susceptibility at this stage, to look for evidence for the singlet state. In Figure 5.17, the bulk data are plotted following the subtraction of a Curie-Weiss plus TIP tail obtained by fitting the data below 40K. The constants for this fit are: C = 0.0338 emu-K/mol, θ = -1.07 K and χ(TIP) = 5.6 x 10^{-4} emu/mol. Note the similarity to the data of either Fig. 5.15 or Fig. 5.17, bringing the bulk and local susceptibility results into at least qualitative agreement. However, the Curie constant for the tail part of the bulk data, 0.0338 emu-K/mol, is much smaller than that found from fitting the high temperature bulk data, C = 0.36 emu-K/mol, and does not approach 50% as might be expected from the analysis of the local susceptibility via NMR.

Before continuing, it is important to consider a possible role for single ion physics in this system, as the Mo^{5+} ion, $5d^1$, $t_{2g}{}^1$, has been shown to reside at a site of rigorously octahedral symmetry. This problem was first addressed by Kotani[24] and a detailed discussion can be found as well from other sources.[25] The basic result is that the perturbation of spin-orbit coupling on the $^2T_2$ crystal field term of the $t_{2g}{}^1$ configuration results in an unusual "non-magnetic quartet" (NMQ) ground state which arises due to an accidental cancellation of the spin moment by the unquenched orbital moment. This is not a singlet state in the sense that this term is normally used, but the result is that the ground state magnetic moment is in fact zero. This NMQ state is separated from a magnetic doublet by an energy gap $\Delta = 3\lambda/2$, where λ is the single ion spin-orbit coupling constant. For Mo^{5+}, λ = 1030 cm^{-1} or 1481 K, thus, a gap of $\Delta/k_B \sim$ 2200 K would be expected on this basis. Even considering a reduction in λ due to orbital delocalization effects of 20- 30 % or even more, the single ion energy scale is more than one order of magnitude larger than anything seen in the data presented above. Thus, while the single ion effects should be considered in any detailed theory for this material, it seems highly doubtful that the observed singlet state is of single ion origin and strengthens the case for a collective singlet state.

Summary and Comparison with other S=3/2, S=1 and S = 1/2 systems.

This is the third part of a systematic study of the ground states of geometrically frustrated B-site ordered double perovskites. Beginning with the monoclinic phases, the S=3/2 compound, La_2LiRuO_6 shows antiferromagnetic long range ordering[6], while the S=1 compound, La_2LiReO_6, finds a collective singlet ground state with a finite concentration of defects which can be polarized in applied fields, indicating a role for the reduced spin quantum number in ground state determination. [7] Remarkably, the S = ½ analog, La_2LiMoO_6, is nearly long range ordered, showing at least short range order in both the heat capacity and μSR behavior. This is somewhat surprising as, normally, one expects unconventional behavior for S = 1/2 due to the enhanced importance of quantum fluctuations. This observation is especially puzzling when compared to the isostructural, iso-spin material, Sr_2CaReO_6, which has a spin frozen ground state.[10]

A possible explanation of this apparent paradox is provided by consideration of the role of the local environment of the S = 1/2 magnetic ion in the two compounds. As already mentioned, the Mo – O coordination is octahedral with a weak tetragonal compression. In contrast the Re – O octahedron shows a weak tetragonal elongation. [10] Thus, in La_2LiMoO_6 one expects an isolated d_{xy} ground state with nearly degenerate d_{xz} and d_{yz} at higher energies. Just the opposite level ordering will occur in Sr_2CaReO_6. This should give rise to a significant difference in the relative magnitudes of the various exchange pathways in the two materials. To test this hypothesis a spin dimer analysis was undertaken. [26,27] There are four such exchange pathways J_1 to J_4 as shown in Figure 5.18. Calculations were carried out assuming occupation of only the d_{xy} orbital for La_2LiMoO_6 and equal occupation of d_{xz} and d_{yz} for Sr_2CaReO_6 and the results are displayed in Table 5.3. Note that for La_2LiMoO_6 the J_4 pathway exceeds the other three by at least an order of magnitude, while for Sr_2CaReO_6 there are three interactions of comparable magnitude, perhaps all four. Thus, these results suggest that a low dimensional model is more appropriate for the Mo phase while a geometrically frustrated model is better for the Re material. This is consistent with the observations, as, for a low dimensional magnet, strong, short range spin-spin correlations can develop which will be detected by a local probe such as μSR (Mo case), while geometric frustration is favored when the exchange pathways are of roughly equal strength (Re-case).

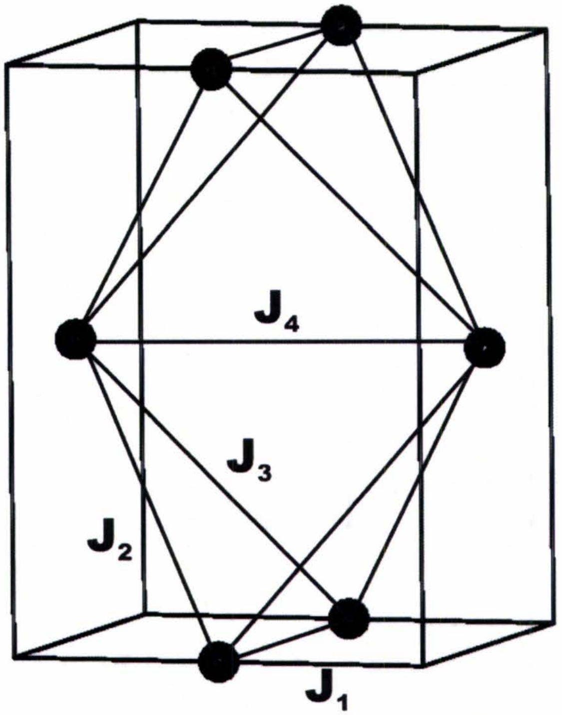

Figure 5.18. Mo^{5+}(Re^{6+}) sites in La_2LiMoO_6 (Sr_2CaReO_6) showing two edge-sharing tetrahedra within the monoclinic unit cell. The four exchange pathways calculated in Table 3 are indicated.

Table 5.3. Comparison of relative exchange pathway (Figure 18) strengths in La_2LiMoO_6 and Sr_2CaReO_6.

Pathway	La_2LiMoO_6 (d_{xy})	Sr_2CaReO_6 (d_{xz}, d_{yz})
J_1	0.14	1.0
J_2	0.014	0.16
J_3	4.3×10^{-4}	0.25
J_4	1.0	0.87

Turning to the cubic materials, Ba_2YRuO_6 ($S = 3/2$) shows a large frustration index, $f \sim 18$, but, in spite of detectable Y/Ru site mixing at the 1% level, is long range AF ordered below 36K.[6] Cubic Ba_2YReO_6($S = 1$) is also highly frustrated, $f > 12$, with no detectable Y/Re site disorder, yet, it shows spin freezing behavior with an ill defined freezing temperature. On the other hand, cubic Ba_2YMoO_6 ($S = ½$) exhibits a most unusual heterogeneous ground state comprised, roughly equally, of gapped, collective spin singlet and paramagnetic components. In spite of a ~ 3% Y/Mo site mixing there is no sign of spin freezing on any time scale investigated to 2K. A singlet/triplet gap, $\Delta/k_B \sim 140K$ was inferred from NMR data. Neutron inelastic scattering experiments are currently underway to investigate further the nature of the gap. Among these three iso-structural compounds, the enhanced quantum fluctuations in the $S = 1$ and $S = ½$ materials appear to play an important role in suppression of long range order.

Comparing Ba_2YMoO_6 to other $S = ½$ cubic double perovskites, one notes immediately a sharp contrast with Ba_2LiOsO_6 and Ba_2NaOsO_6 (based on $Os^{7+)}$ which are antiferromagnetic and ferromagnetic, respectively, with minimal evidence for a role for geometric frustration. [11] This is a most puzzling situation as no clear pattern of behavior emerges for these iso-structural/iso-spin materials which indicates that a detailed understanding of these remarkable differences will not be easily gained.

Acknowledgements.

We thank Paul Dube for assistance with SQUID and heat capacity measurements and H.F. Gibbs for TGA data. Franco Ieropoli assisted with the early stages of this work. J.E.G, G.M.L. C.R.W, T.I. and S.K. thank NSERC of Canada for support of this research. S.K. thanks the Canadian Foundation for Innovation and G.M.L. and T.I. thank the Canadian Institute for Advanced Research. For work done at Florida State University, C.R.W. thanks the NSF for funding through grant number DMR-08-04173.

References

[1] A. P. Ramirez, Annu. Rev. Mater. Sci. **24**, 453 (1994), J. E. Greedan, J. Mater. Chem. **11**, 37 (2001)

[2] P. W. Anderson Mat. Res. Bull. Vol.8, 153 (1973)

[3] J. S. Gardner, S. R. Dunsiger, B. D. Gaulin, M. P. Gingras, J.E. Greedan, R. F. Kiefl, M. D. Lumsden, W. A. Macfarlane, M. P. Raju, J. E. Sonier, I. Swainson and Z. Tum, Phys. Rev. Lett., **82**,1012 (1999), J.S. Gardner, A. Keren, G. Ehlers, C. Stock, E. Segal, J. M. Roper, B Fak, M. B. Stone, P. R. Hammar, D H. Reich and B. D. Gaulin, Phys. Rev. B **68** 180401R (2003), J.S.Gardner, B. D. Gaulin, A. J. Berlinsky and P. Waldron, S. Dunsiger, N. P. Raju and J.E. Greedan, Phys. Rev. B **64** 224416 (2001)

[4] Y.J.Uemura, A. Keren, K. Kojima, L/P. Le, G. M. Luke, W.D.Wu, Y. Ajiro, T. asano, Y. Kuriyama, M. Mekata, H. Kikuchi, K. Kakurai Phys. Rev.Lett. **73**, 3306 (1994)

[5] Y. Okamoto, M. Nohara, H. Aruga-Katori and H. Takagi, Phys. Rev. Lett. **99** 137207 (2007)

[6] T. Aharen, J. E. Greedan, F. Ning, T. Imai, V. Michaelis, S. Kroeker, H. Zhou, C. R. Wiebe, L. M. D. Cranswick, Phys. Rev. B, **80** 134423 (2009)

[7] T. Aharen, J. E. Greedan, C. A. Bridges, A. A. Aczel, J. Rodriguez, G. MacDougall, G. M. Luke, V. K. Michaelis, S. Kroeker, C. R. Wiebe, H. Zhou, L.M.D. Cranswick, Phys. Rev. **B 81** 064436 (2010).

[8] E. J. Cussen, C. R. Lynham, J. Rogers, Chem. Mater. **18** 2855 (2006)

[9] J. Tortelier and P. Gougeon, Acta. Cryst. **C52** 500 (1996)

[10] C. R. Wiebe, J.E. Greedan, G. M. Luke and J. S. Gardner, Phys. Rev. B **65**, 144413 (2002)

[11] K. E. Stizler et al, Solid State Sci., **4** 311 (2002)

[12] B.H. Toby, J. Appl. Cryst. **34** 210 (2001); A.C. Larson and R. Von Dreele, Los Alamos National Laboratory Report No. LAUR 86-748, 2004 (unpublished).

[13] J. Rodriguez-Carvajal, Physica B **192,** 55 (1993).

[14] K. Hyashi, G. Demazeau, M. Pouchard, P. Hagenmuller, Mat. Res. Bull. **15** 461, (1980); J. Darriet, G. Demazeau, M. Pouchard, Mat. Res. Bull. **16** 1013 (1981).

[15] M. T. Anderson, K. B. Greenwood, G. A. Taylor, K. R. Poppelmeier, Prog. Solid State Chem., **22** 197 (1993)

[16] R. D. Shannon, Acta Crystallogr., **A32**, 751 (1976)

[17] P. D. Battle, C. P. Grey, M. Hervieu, C. Martin, C. A. Moore, and Y. Park, J. solid State Chem., **175**, 20 (2003)

[18] C. R. Wiebe, P. L. Russo, A. T. Savici, Y. J. Uemura, G. J. MacDougall, G. M. Luke, S. Kuchta, J. E. Greedan, J. Phys. Cond. Mater. **17** 6469 (2005).

[19] P. Woodward, R-D. Hoffman, A. W. Sleight, J. Mater. Res., **9**, 2118 (1994).

[20] P. W. Barnes, M. E. Lufaso, P. M. Woodward, Acta. Cryst. **B62**, 384 (2006).

[21] T. Imai, E.A. Nytko, B.M. Bartlett, M.P. Shores and D.G. Nocera, Phys.Rev.Lett.**100**, 077203 (2008).

[22] A. Olariu, P. Mendels, F. Bert, F. Duc, C. Trombe, M.A. de Vries and A. Harrison, Phys. Rev. Lett. **100**, 087202 (2008).

[23] T. Moriya Prog. of Theor. Physics (Kyoto) **16** 641 (1956).

[24] M. Kotani, J. Phys. Soc. Japan **4**, 293 (1949).

[25] F.E. Mabbs and D.J. Machin in "Magnetism and Transition Metal Complexes" Chapman and Hall, London, 1973, pp. 68-84.

[26] Whangbo, M. H.; Koo, H. J.; Dai, D. J.; *J. Solid state Chem.,* **2003,** *176*, 417.

[27] Ren, J.; Liang, W.; Whangbo, M. H. "*Crystal and Electronic Structure Analysis Using CAESAR*". http://www.primeC.com, 2005.

Chapter Six

Additional works on S=1/2 Mo analogues

The motivation of this extended investigation on S=1/2 Mo analogues originates in the observation of the difference in the magnetic ground states of previously reported S=1/2 Re and Os based f.c.c. compounds. The S=1/2 Re compounds, Sr_2CaReO_6 and Sr_2MgReO_6, show spin glass behaviours [1] while the S=1/2 Os based compounds, Ba_2LiOsO_6 and Ba_2NaOsO_6, shows antiferromagnetic and ferromagnetic behaviour, respectively [2]. Furthermore, the Re based compounds did not show B site dependence for their magnetic ground states as both of them show glassy behaviour. On the other hand, the Os based compounds show B site dependence as B=Li is antiferromagnetic and B=Na ferromagnetic.

Table 6.1 The crystal structures and magnetic ground states of S=1/2 B-site ordered double perovskites. AFLRO: Antiferromagnetic long range ordering, FLRO: ferromagnetic long range ordering, AFSRO: antiferromagnetic short range ordering

	Crystal structure	B′ site ion	Ground state	
Sr_2MgReO_6	tetragonal	5d	Spin glass	$T_G \approx 45K$
Sr_2CaReO_6	monoclinic	5d	Spin glass	$T_G \approx 14K$
Ba_2LiOsO_6	Cubic	5d	AFLRO	$T_N = 8K$
Ba_2NaOsO_6	Cubic	5d	FLRO	$T_C = 8K$
La_2LiMoO_6	monoclinic	4d	AF SRO	$T_{transition} \approx 18K$
Ba_2YMoO_6	Cubic	4d	Spin liquid	paramagnetic at 2K
Ba_2LuMoO_6	Cubic	4d	?	paramagnetic at 2K
Ba_2ScMoO_6	Cubic	4d	?	paramagnetic at 2K

Another interesting observation is that all the four 5d transition metal based S=1/2 compounds mentioned above show some static spin behaviours, glassy or ordered, while 4d transition metal based S=1/2 cubic Ba_2YMoO_6 shows spin liquid like dynamic spin behaviour [3]. This difference suggests that dynamic behaviour of spins actually has preference to be in 4d transition metal based S=1/2 f.c.c. cubic compounds. To investigate the B-site dependence of Mo compounds, Ba_2LuMoO_6 and Ba_2ScMoO_6 have been synthesized.

The synthesis procedure for Ba_2LuMoO_6 and Ba_2ScMoO_6 is basically same as for Ba_2YMoO_6. Stoichiometric mixtures of $BaCO_3$, Lu_2O_3 or Sc_2O_3, and MoO_3 were heated in air at 950°C for overnight (>16hours) then reground, sintered in 5% H_2/Ar at 1300°C for 48 hours. A second firing in 5% H_2/Ar was required to produce a single phase for Ba_2ScMoO_6. The phase purity of two compounds was tracked by x-ray diffraction. The magnetic susceptibility as a function of the temperature (2K-300K) of both samples was measured using a SQUID magnetometer with an applied field of 100 Oe. Figures 6.1 and 6.4 show the magnetic susceptibility as a function of temperature of the two Mo f.c.c. analogues.

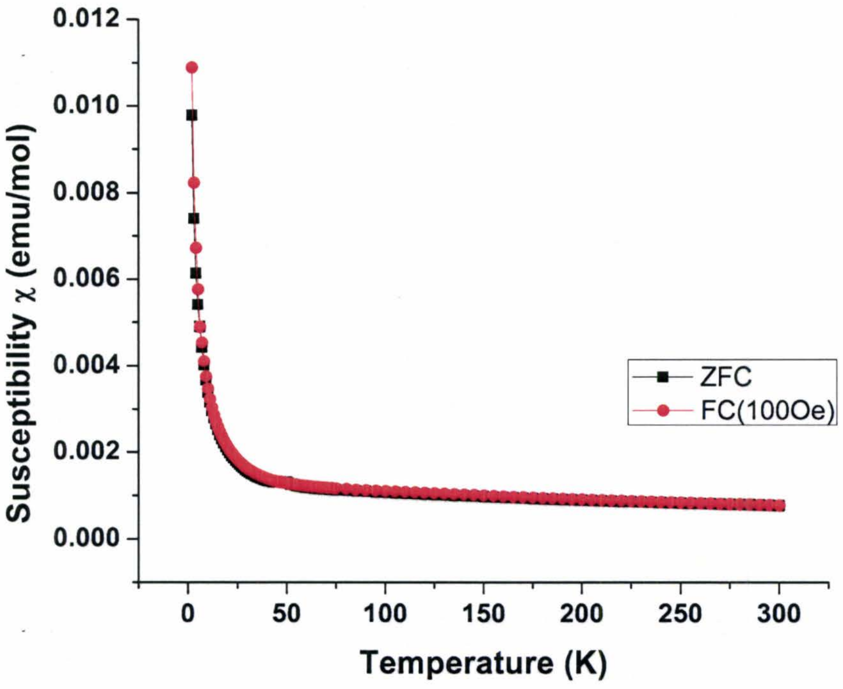

Figure 6.1 The temperature dependence of the magnetic susceptibility of Ba_2LuMoO_6

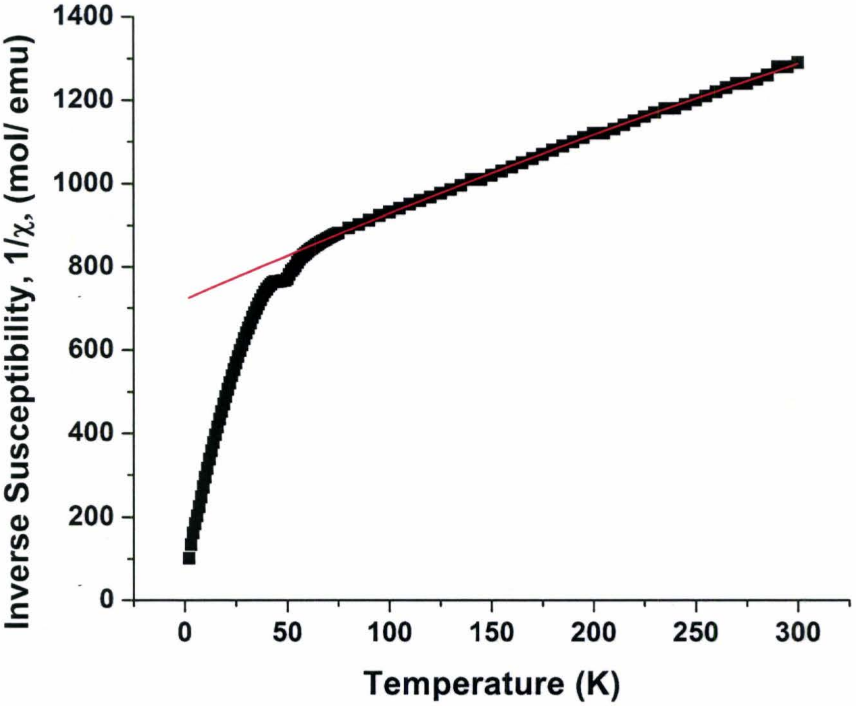

Figure 6.2 The inverse susceptibility as a function of temperature of Ba_2LuMoO_6 with the Curie-Weiss fitting line (Red color).

Ba_2LuMoO_6 shows paramagnetic behaviour at least down to 2K in common with Ba_2YMoO_6 as shown in Figure 6.1. The Curie-Weiss fit yielded the Curie constant C=0.33(1) emu-K/mol, the Weiss constant θ=-281(11)K and TIP=0.00021(2) emu/mol (Figure 6.2). According to the Curie constant, the effective magnetic moment is calculated to be $1.62\mu_B$, which is slightly smaller than the spin-only value ($1.73\mu_B$). It seems like that there is some orbital contribution. Clearly, a large degree of frustration is present, f > 140.

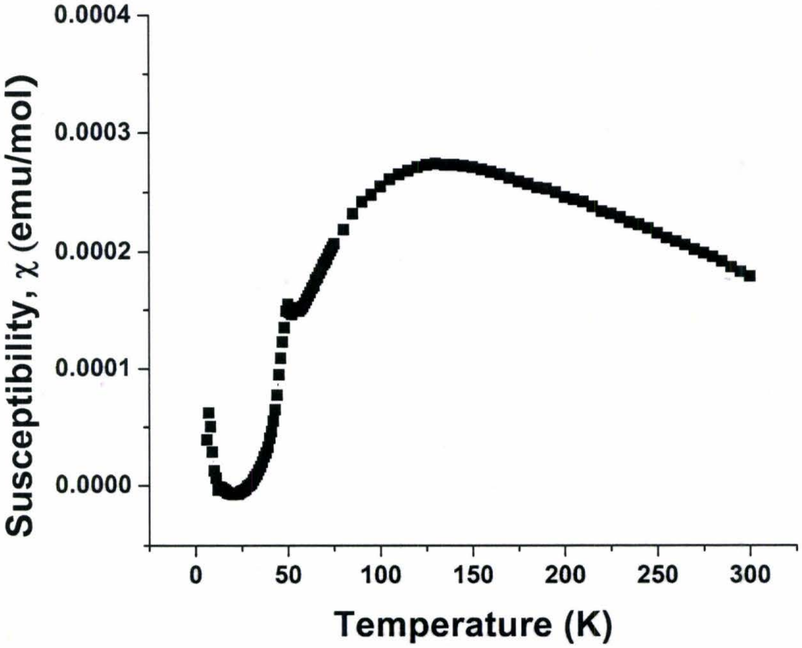

Figure 6.3 The Curie-tail subtracted bulk susceptibility of Ba_2LuMoO_6

It would be an interesting attempt of a Curie-tail subtraction of Ba_2LuMoO_6 as same as for Ba_2YMoO_6 (Figure 5.17). The Curie-Weiss fitting was performed on the inverse susceptibility below 30K and yielded the Curie constant C=0.0343(3) emu K/mol, the Weiss constant θ=-1.83(7)K and TIP=4.8(1)x10^{-4} emu/mol. Similarly to Ba_2YMoO_6, the subtracted bulk susceptibility decreases below 125K and becomes close to zero around 30K. The kink around 50K is due solid oxygen.

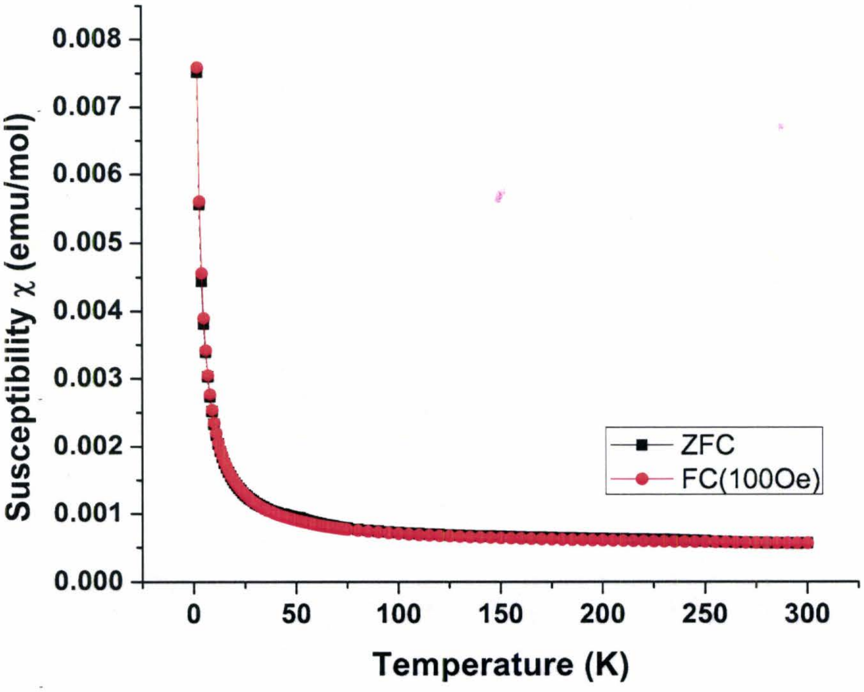

Figure 6.4 The temperature dependence of the magnetic susceptibility of Ba_2ScMoO_6

Ba_2ScMoO_6 also shows paramagnetic behaviour at least down to 2K as shown in Figure 6.4. A broad step was observed around 255K in the plot of the inverse susceptibility against the temperature (Figure 6.5). This broad step made it difficult for the Curie-Weiss fitting and may require high temperature region of the susceptibility for further analysis. The origin of this feature may signal a crystal structure distortion however, it requires a neutron diffraction measurement to prove.

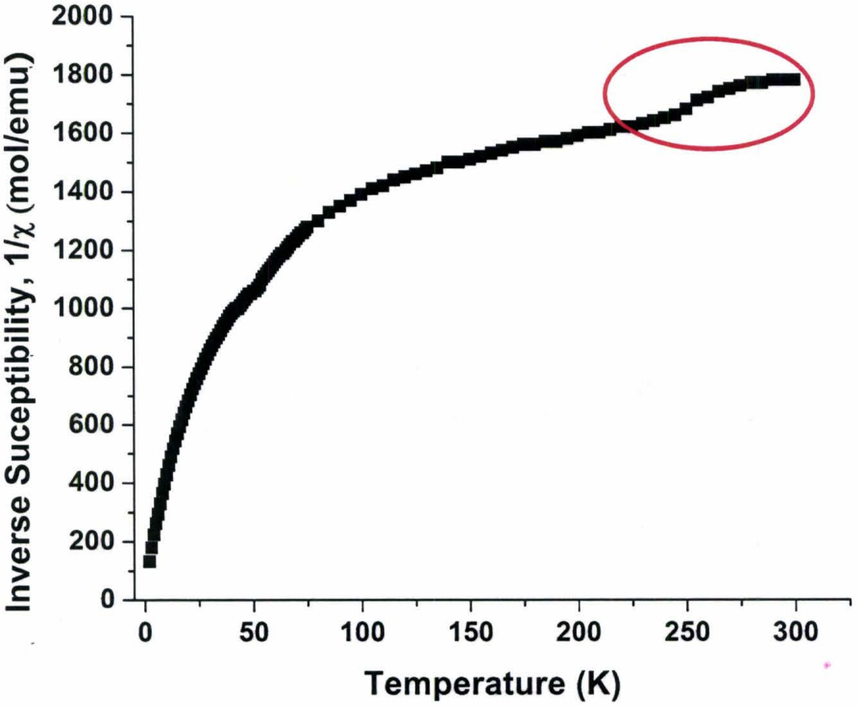

Figure 6.5 The inverse susceptibility as a function of temperature of Ba_2ScMoO_6

The possibility that B site disorder exists in these two analogues should be addressed here. The precise information about the disorder should be investigated using MAS NMR however the possibility of the disorder is evident via diffraction data. Figure 6.6 shows the contrast between the difference in ionic radii (Δr) in B site and the ratio of FWHM of all odd/all even peaks of the cubic f.c.c. compounds. The blue line is the criterion established by Barnes, Lufaso and Woodward [4] for 100% B/B' site order (Δr > 0.26Å). Both Ba_2LuMoO_6 (Δr =0.22 Å) and Ba_2ScMoO_6 (Δr =0.135Å) lie well to the left of the limit and therefore B site disorder should be more severe than the three cubic analogues studied in this thesis. Although the investigation of these additional two Mo analogues have not been completed yet, it is a remarkable point that none of the cubic Mo double perovskites presents any sign of spin glassy behaviour in spite of the presence of the B site mixing and severe frustration. This fact could be helpful for theoretical investigations on the origin of collective singlet ground state or non-spin glassy state of the geometrically frustrated f.c.c. materials.

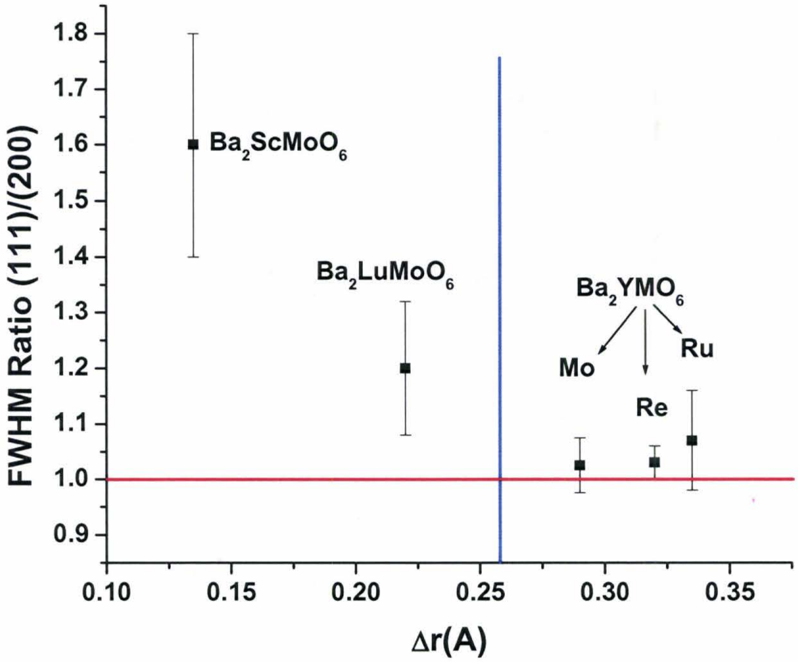

Figure 6.6 The ionic radii difference of selected cubic f.c.c. compounds and their FWHM ratio of all odd/all even reflection. The vertical blue line marks the limit for 100% B/B' site order according to Barnes et al.[4]

References

[1] C.R. Wiebe et al, Physical Review B 68, 134410 (2003); C. R. Wiebe et al, Physical Review B 65, 144413 (2002)

[2] K. E. Stitzer et al, Solid State Science, 4, 311 (2002)

[3] T. Aharen et al, Physical Review B81, 224409 (2010)

[4] P. W. Barnes, M. W. Lufaso and P. M. Woodward, Acta Crystallographica B62, 384-396 (2006)

Chapter Seven

Conclusion

The systematic study of crystal structures and magnetic properties of geometrically frustrated f.c.c. double perovskites, monoclinic La_2LiMO_6 and cubic Ba_2YMO_6 (M= Mo, Re and Ru), and further investigation on S=1/2 Mo analogues have been presented in this thesis. The importance of the spin quantum number of the B' -site ion (Mo, Re and Ru) and the local symmetry of these ions on determination of the ground states of these geometrically frustrated f.c.c. double perovskites has been examined.

For S=3/2 Ru compounds, monoclinic La_2LiRuO_6 and cubic Ba_2YRuO_6 have been prepared [1]. In the previous work, the crystal structure of La_2LiRuO_6 was determined to be monoclinic by neutron diffraction data collected at 8 and 300K [2]. No Li/Ru site mixing was observed by ^{7}Li MAS NMR and a peak was observed at 30K in the magnetic susceptibility [2]. Our susceptibility data for La_2LiRuO_6 shows a maximum at 30K, which was assigned as the Neél temperature in the previous paper. We were able to show the true T_N is actually 24K from the heat capacity and the temperature dependence of the

^{7}Li NMR spin-lattice relaxation rate ($1/T_1$). For Ba_2YRuO_6, the magnetic susceptibility above 80K and neutron diffraction data at 4.2K and room temperature, which support cubic structure of this compound, were reported previously, however there was no direct determination of the transition temperature of this compound. Our magnetic susceptibility data for this compound show a very high frustration index of ~16, and two broad peaks at 37K and 47K, which were not reported previously. The transition temperature of Ba_2YRuO_6 was confirmed to be 36K based on magnetic heat capacity and temperature dependent neutron diffraction data. The B-site ordering of this compound, Y/Ru mixing, was tested using ^{89}Y MAS NMR and confirmed to be at the ~1 % level. The ground state of both S=3/2 compounds is antiferromagnetic long range ordered.

For the S=1 Re compounds, monoclinic La_2LiReO_6 and cubic Ba_2YReO_6 were prepared [4]. The synthetic methods were reinvented for both compounds, i.e. are different from the literature methods. The crystal structure of La_2LiReO_6 was reported previously as orthorhombic [5] however it is determined to be monoclinic based on the refinement of neutron diffraction data in this work. This is first time to report the details of magnetic properties of this compound. La_2LiReO_6 shows some orbital ordering and a possible 'collective singlet state' mainly according to the observation of zero magnetization below ~ 10K in the ZFC magnetic susceptibility and a diluted spin system behavior in μSR. Ba_2YReO_6 was previously reported as monoclinic by X-ray diffraction[6]. However it was determined from neutron diffraction data that Ba_2YReO_6 remains cubic within the resolution of the data between 300K and 4K in apparent violation of the Jahn-Teller theorem. No significant Y/Re mixing was observed in this compound (at most ~0.5%) by

^{89}Y MAS NMR. The previous work reported one broad peak around 50K in the susceptibility and one near 30K in the heat capacity. The ground state was unclear based on these data. Our investigation shows two broad peaks at 50K and 25K in the susceptibility, and corresponding peaks are observed in the heat capacity. It is confirmed that this compound surprisingly shows spin glass behavior according to the μSR measurement, in spite of the absence of site mixing disorder. Overall, the ground states of these S=1 compounds are quite different.

Monoclinic La_2LiMoO_6 and cubic Ba_2YMoO_6 were prepared as S=1/2 analogues [7]. La_2LiMoO_6 was reported to be monoclinic based on single crystal X-ray diffraction [8] and no magnetic properties were reported. Interestingly, this compound achieves at least short range ordered state (nearly long range ordered state) around 18K according to the heat capacity and μSR results. This compound has a frustration index of only ~2 when T=18K was used for the calculation of the index. La_2LiReO_6 is isostructural with the highly frustrated spin glass Sr_2CaReO_6 (f ~ 32, T_g ~ 14K) and the contrast in properties is remarkable. An attempt was made to understand this using spin dimer analysis, based on the difference in the local site geometry which leads to different orbital orderings for the two materials. Ba_2YMoO_6 remains cubic at 2.7K according to the neutron diffraction data in spite of the Jahn-Teller theorem. The Y/Mo mixing ratio was determined to be about ~3 % by ^{89}Y MAS NMR. Ba_2YMoO_6 shows paramagnetic behavior down to 2K as reported previously in the magnetic susceptibility [9] although the frustration index *f* of the compound is found to be >100, which is much larger than the previous work (*f* = 45). The dynamic behavior of this compound is supported by μSR results. Evidence for a collective singlet ground state was observed in the paramagnetic ^{89}Y NMR Knight shift. This is the first observation of such behavior in f.c.c. double perovskites.

Further investigations on Ba_2LuMoO_6 and Ba_2ScMoO_6 have commenced as extended research on S=1/2 Mo analogues, and both are paramagnetic down to 2K. It could be another example for collective singlet ground state however additional measurements such as NMR, neutron diffraction, are required to complete this investigation. The fact that none of cubic Mo-based double perovskites present any sign of glassy behavior is surprising given evidence for significant Y/Mo site mixing. Further studies would be helpful to understand the origin of spin dynamics in S=1/2 Mo analogues.

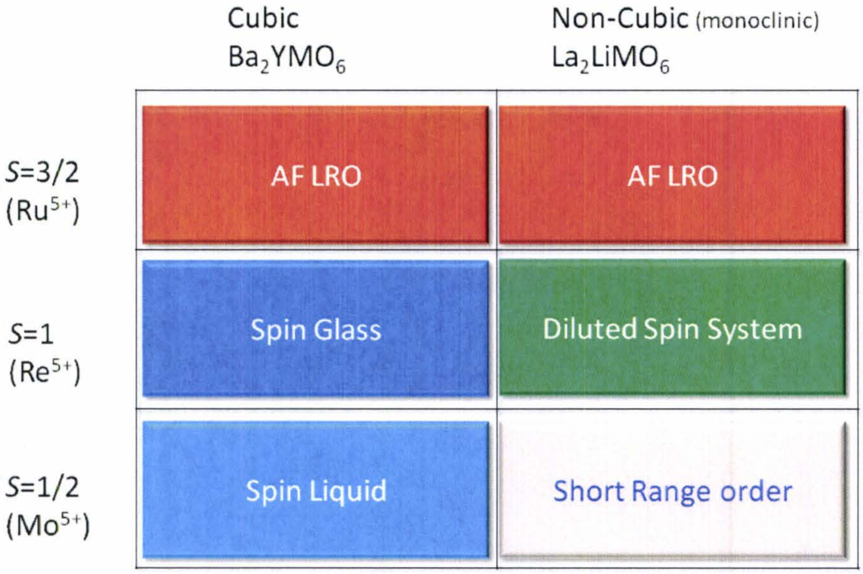

	Cubic Ba_2YMO_6	Non-Cubic (monoclinic) La_2LiMO_6
S=3/2 (Ru^{5+})	AF LRO	AF LRO
S=1 (Re^{5+})	Spin Glass	Diluted Spin System
S=1/2 (Mo^{5+})	Spin Liquid	Short Range order

Figure 7.1 Summary of the ground states found for the B-site ordered double perovskites, Ba_2YMO_6 and La_2LiMO_6 (M= Mo, Re and Ru)

Overall, the S=3/2 compounds show antiferromagnetic long range ordering while the compounds with lower spin quantum number mostly show disordered behavior with the exception of La_2LiMoO_6. This fact suggests that quantum fluctuation in the compounds with S=1 or 1/2 severely influence the ground states. Additionally, the difference in the ground states achieved in monoclinic and cubic series, and comparison with other f.c.c. double perovskite (Sr_2CaReO_6 and La_2LiMoO_6) suggests the importance of local symmetry on the determination of the ground state of f.c.c. materials[7].

The collective singlet, spin liquid ground state shown by the cubic S = ½ material Ba_2YMoO_6 would appear to match the theoretical study of Kuz'min [10] introduced in chapter one. However, there are many counter examples such as the cubic Os based double perovskites, $Ba_2Li(Na)OsO_6$ [11] and the monoclinic and tetragonal phases, La_2LiMoO_6 and $Sr_2Ca(Mg)ReO_6$ [7,12]. It has been argued that orbital ordering must be present in the S=1/2 Os compounds, although the crystal structure at low temperature is not known. Moreover, the S=1 monoclinic La_2LiReO_6 behaves unexpectedly in showing a spin singlet ground state at least in zero field which is beyond any published theory [4]. There is still much experimental and theoretical effort needed to develop a generalized and comprehensive understanding the origins/formations of the ground states of geometrically frustrated f.c.c. materials.

References

[1] T. Aharen et al, Physical Review B80, 134423 (2009)

[2] P.D. Battle et al, J. Solid State Chem., 175, 26 (2003)

[3] P. D. Battle and C. W. Jones, J. Solid State Chem., 78, 108 (1989)

[4] T. Aharen et al, physical Review B81, 064436 (2010)

[5] K. Hayashi et al, Mater. Res. Bull.,21, 401 (1986)

[6]Y. Sasaki et al, J. Mater. Chem., 12, 2361 (2002)

[7] T. Aharen et al, Physical Review B81, 224409 (2010)

[8] J. Tortelier and P. Gougeon, Acta Crystallogr., C52, 500 (1996)

[9] E. J. Cussen et al, Chem. Mater., 18, 2855 (2006)

[10] E. V. Kuz'min, J. Exp. Theo. Phys., 96(1), 129 (2003)

[11] Katharine E. Stizer et al, Solid State Sciences, 4, 311 (2002)

[12] C. R. Wiebe et al, Physical Review B 65, 144413 (2002)